

# **Bismutite-based cooperative catalysts – Efficient heterogeneous systems for heterocyclizations**

PhD Dissertation

**Marianna Kocsis**



Supervisors:           Prof. István Pálinkó<sup>†</sup>  
                                Prof. Pál Sipos

Consultants:           Gábor Varga, PhD  
                                Sándor Balázs Ötvös, PhD

Doctoral School of Chemistry  
Faculty of Science and Informatics  
University of Szeged

Szeged  
2023

## TABLE OF CONTENTS

<b>ABBREVIATIONS .....</b>	<b>4</b>
<b>1. INTRODUCTION .....</b>	<b>6</b>
<b>2. LITERATURE REVIEW .....</b>	<b>7</b>
2.1. MODERN CATALYSIS IN ORGANIC CHEMISTRY .....	7
2.1.1. Transition metal catalysis in heterocyclic chemistry .....	7
2.1.2. Heterogenization attempts and solid catalysts in heterocyclic chemistry .....	9
2.1.3. Lewis-acid catalysis in heterocyclic chemistry .....	11
2.1.4. Cooperative Catalysis .....	15
2.2. MULTI-SIDED BISMUTH .....	19
2.2.1. Bismuth salts and oxides in organic chemistry .....	20
2.2.2. Introduction to layered bismuth compounds .....	21
2.2.3. Bismutites .....	23
2.3. CATALYTIC APPLICATIONS .....	24
2.3.1. Catalytic synthesis of phenothiazine .....	24
2.3.2. Catalytic syntheses of 2-phenylbenzimidazole/ oxazole/ thiazole .....	25
2.3.3. Oxidative dehydrogenative coupling reactions of anilines .....	27
<b>3. THE MAIN AIMS OF THE DISSERTATION .....</b>	<b>30</b>
<b>4. EXPERIMENTAL PART .....</b>	<b>31</b>
4. 1. MATERIALS .....	31
4. 2. SYNTHESSES OF THE MODIFIED BISMUTITES .....	32
4. 3. INSTRUMENTATION AND CHARACTERIZATION METHODS .....	32
4.3.1. Powder X-ray diffractometry .....	32
4.3.2. Thermal analytical measurement .....	33
4.3.3. FT-IR spectroscopy .....	33
4.3.4. Raman spectroscopy .....	33
4.3.5. UV-Vis-NIR spectroscopy .....	33
4.3.6. XP spectroscopy .....	33
4.3.7. TEM-EDS microscopy .....	34
4.3.8. Adsorption measurements .....	34

4.3.9. ICP-MS measurements .....	34
4.3.10. Temperature programmed desorptions .....	34
4.3.11. GC-MS measurements .....	35
4.3.12. NMR spectroscopy.....	35
4.4. CATALYTIC REACTIONS.....	35
4.4.1. Optimal procedure for the synthesis of phenothiazine.....	35
4.4.2. Optimal procedure for the synthesis of 2-phenylbenzimidazole .....	36
4.4.3. Optimal procedure for oxidative azocoupling of anilines.....	36
4.4.4. Optimal procedure for synthesis of quinoline.....	37
4.4.5. Optimal procedure for synthesis of quinoxaline .....	37
4.4.6. Determination of catalytic indicators .....	37
<b>5. RESULTS AND DISCUSSION .....</b>	<b>39</b>
5.1. CHARACTERIZATION .....	39
5.1.1. Structural and analytical analysis of $\text{CuBi}_2\text{O}_2\text{CO}_3$ .....	42
5.1.2. Structural and analytical analysis of $\text{Mn/Co/NiBi}_2\text{O}_2\text{CO}_3$ .....	49
5.2. CATALYTIC STUDIES .....	60
5.2.1. Catalytic capability of $\text{CuBi}_2\text{O}_2\text{CO}_3$ as heterogeneous catalyst in the synthesis of phenothiazine and its derivatives .....	60
5.2.2. Catalytic capabilities of $\text{Mn/Co/NiBi}_2\text{O}_2\text{CO}_3$ as heterogeneous catalysts in the synthesis of 2-phenylbenzimidazole, its isosters and derivatives .....	69
5.2.3. Catalytic capabilities of $\text{Mn/Co/NiBi}_2\text{O}_2\text{CO}_3$ as heterogeneous catalysts in oxidative dehydrogenative couplings of anilines.....	82
<b>6. CONCLUSIONS.....</b>	<b>95</b>
<b>ACKNOWLEDGEMENT.....</b>	<b>99</b>
<b>REFERENCES.....</b>	<b>100</b>
<b>MAGYAR NYELVŰ ÖSSZEFOGLALÓ (SUMMARY IN HUNGARIAN) .....</b>	<b>107</b>
<b>APPENDIX .....</b>	<b>111</b>

## ABBREVIATIONS

2-MeTHF = 2-methyltetrahydrofuran

acac = acetylacetonate

Bi(OTf)<sub>3</sub> = bismuth(III) trifluoromethanesulfonate

COD = cyclooctadiene

dbbe = (diphenylphosphino)ethane

DMA = N,N-dimethylacetamide

DMSO = dimethyl sulfoxide

EDX = energy dispersive X-ray spectroscopy

EtOAc = ethyl acetate

HOMO = highest (energy) occupied molecular orbital

ICP-MS = inductively coupled plasma mass spectrometry

IR spectroscopy = infrared spectroscopy

LA = Lewis acid

LUMO = lowest (energy) unoccupied molecular orbital

MBi<sub>2</sub>O<sub>2</sub>CO<sub>3</sub> = transition metal-modified bismutite synthesized by co-precipitation, regardless of the oxidation state of the metallic components

M-Bi<sub>2</sub>O<sub>2</sub>CO<sub>3</sub> = impregnated reference compound to transition metal-modified bismutite

MeCN = methyl cyanide, acetonitrile

MEK = methyl-ethyl-ketone

MIR = mid infrared

MOF = metal-organic framework

NHC = N-heterocyclic carbene complex

NIR = near infrared

NMR = nuclear magnetic resonance spectroscopy

NP = nanoparticle

OAc = acetate

OTf = triflate, trifluoromethanesulfonate

PDF# = Powder diffraction file from the International Center for Diffraction Data (ICDD) database

TEM-EDS = transmission electron microscope coupled with energy-dispersive X-ray spectrometry

THF = tetrahydrofuran

TMC = transition metal catalysis

XPS = X-ray photoelectron spectroscopy

XRD = powder X-ray diffractometry

## 1. INTRODUCTION

Over the last 10 years, ca. a quarter of the 260.000 publication related to catalysis focused on the production and/or transformation of heterocycles.\* Their indisputable popularity and importance result from their prevalence (about one third of the known carbon compounds are heterocyclic compounds) and their broad applicability: they play an important role not only in life sciences, synthetic- and pharmaceutical chemistry, but also in agriculture, electronics, optical- and materials sciences<sup>1</sup>.

The beginnings of heterocyclic chemistry date back to the early 1800s. Initially, biologically active compounds were isolated from natural sources<sup>2</sup>, but due to the large amount of raw materials and solvents needed for these procedures, as well as the generally low achievable heterocyclic yield, many synthetic processes were also developed. Despite these already known and mostly well-established synthetic methods, the renewal of syntheses of heterocyclic compounds under modern (green) chemical aspects becomes more and more important.

With the present work we aimed at joining this field of research by presenting the syntheses, the characterization procedures and the catalytic capabilities of novel bismuth-based transition metal-containing catalysts. In the following, an attempt will be made to prove, that a very simple inorganic synthesis method is capable of yielding a catalyst which is suitable to readily combine the outstanding selectivity of the currently prevailing transition metal catalysis and the robustness of bismuth(III) (Lewis acid)-containing layered materials. By combining these features, efficient bimetallic and reusable systems for diverse heterocyclizations can be built up. In addition to the catalytic capabilities, the self-prepared catalysts were also comprehensively characterized from the materials science point of view by systematically combining different structural characterization means with analytical methods, thus the most likely structure, composition and the type of modification was identified for each catalyst.

---

\* A general search of Scifinder (<https://scifinder.cas.org>) on the 2<sup>nd</sup> of January, 2023 found 265,839 "catalysis"-related English-language journals published between 2012 and January 2023, of which 71,525 were for production and/or transformation of heterocycles.

## 2. LITERATURE REVIEW

### 2.1. Modern catalysis in Organic Chemistry

Modern industrial processes are now inconceivable without catalysis, as the alternative route or mechanism that they provide, is much more economical and competitive than non-catalyzed processes.<sup>3</sup> At least one catalytic process is certain to be found in any production of commercially produced chemicals, so various approaches to industrial catalysis have been developed. These include: transition metal catalysis, Lewis acid catalysis, organocatalysis, biocatalysis, phase transfer catalysis or electrocatalysis. To accurately assess the current work, we need to review the publications on transition metal and Lewis acid catalysis, the two main research areas in the field of heterocyclic chemistry.

#### 2.1.1. Transition metal catalysis in heterocyclic chemistry

Using transition metal catalysts, complex molecules can be constructed from simple starting materials. The entire d-field of the periodic table, including zinc, cadmium and mercury have already been studied and proved to be efficient in several chemical transformations under relatively mild reaction conditions. However, the best used and the most suitable metals are the expensive and rare noble metals.

The formation of heteroatom-containing backbones catalyzed by transition metals (hereafter abbreviated as TM -) include two fundamental steps: the formation of new carbon-carbon and new carbon-heteroatom bonds. **Table 1.** shows the typical reaction types and catalysts.

**Table 1.** Basic processes of transition metal catalyzed synthesis of heteroatom-containing backbone

FORMATION OF NEW C–C BOND	FORMATION OF NEW C–HETEROATOM BOND	FORMATION OF NEW C–C AND C–HETEROATOM BOND
<ul style="list-style-type: none"><li>olefin metathesis (ring closing metathesis, cyclisation metathesis)</li><li>cycloisomerization</li><li>cycloaddition</li></ul>	<ul style="list-style-type: none"><li>heterocyclization</li><li>cycloaddition</li><li>amino-Heck reaction</li><li>Sonogashira coupling</li></ul>	labelled processes in which the two processes occur together: <ul style="list-style-type: none"><li>intra- and intermolecular Heck-, Suzuki-, Stille reaction<sup>4</sup></li></ul>
<i>noble metal alkylidenes<sup>5,6</sup>, Ru-containing Grubb catalyst<sup>7</sup>, homogeneous complexes of Ru<sup>8</sup>, Ag<sup>9</sup> or Pd<sup>10,11</sup></i>	<i>higher valence metals Pd(II), Au(III) or Hg(II)<sup>12,13</sup>, Pd(0)<sup>12,13</sup>, Ru, Ti<sup>14</sup>, organolanthanides<sup>15,16</sup></i>	<i>classically Pd-catalyzed reactions</i>

**Table 2.** Catalytic heterocycle production by non-noble d-field metals

APPLIED D-FIELD METALS AS SUBSTITUTES OF NOBLE METALS		
Pauson-Khand cycloaddition	<i>organocobalt complexes</i> <sup>17</sup> , <i>Ti</i> <sup>18</sup> , <i>Zr</i> <sup>19</sup>	
cycloaddition reactions producing 6-membered rings	<i>nickel(COD)</i> <sub>2</sub> <sup>20</sup> , <i>mono- or multinuclear cobalt(I)/(II) complexes</i> <sup>21,22</sup> , <i>stoichiometric amounts of zirconium</i> <sup>23</sup> , <i>titanium</i> <sup>24</sup>	
8-membered heterocyclic enol ethers	<i>cobalt(III) carbene radical</i> <sup>25</sup>	
Sonogashira-coupling	<i>copper-iodine</i> <sup>26</sup>	
syntheses of 5-membered N-containing heterocycles	<i>MnO</i> <sub>2</sub> <sup>27</sup> and <i>CuBr-LiBr</i> <sup>28</sup> system	
asymmetric hetero-Diels-Alder reaction	<i>Ti, V, Mn, Cr, Co, Cu, Zn, Zr, Rh, Pd, La, Sm, Eu, and Yb, bearing a chiral ligand</i> <sup>29</sup>	
ADDITIONAL BENEFITS PROVIDED BY NON-NOBLE METALS		
dual functionalization of alkenes <sup>30</sup>	<i>copper-hexafluoroacetylacetone complexes</i>	carben/alkene metathesis reactions
enhanced selectivity <sup>31</sup>		
easy recyclability,		
excellent tolerance to various reaction protocols and functional groups, application in tandem reactions <sup>32</sup>	<i>copper-iodine</i>	Sonogashira-coupling
high enantioselectivity <sup>33,34</sup>	<i>zinc-complex, Ni(cod)</i> <sub>2</sub>	heteroaddition reactions
excellent robustness and reusaablity <sup>35</sup>	<i>copper-manganese bimetallic catalyst</i>	[3+2] cycloadditions
wide range of synthesizable materials <sup>36</sup>	<i>manganese-pincer complexes</i>	cross-dehydrogenative coupling
extensibility of the reaction to large scale <sup>37</sup>	<i>cobalt(III)-carbene radicals</i>	radical synthesis of 8-Membered Heterocyclic Enol Ethers
atom- and step-economical route by the activation of unreactive bonds <sup>38</sup>	<i>nickel-aluminium bimetal</i>	synthesis of tricyclic imidazoles
multicomponent reaction <sup>39</sup>	<i>nickel(COD)</i> <sub>2</sub>	syntheses of heterocycles with a larger number of members

Due to the achievable high chemo-, regio- and stereoselectivity and due to the broad raw material and substrate tolerance, noble metal-catalyzed reactions have formed the basis of heterocyclic chemistry from the 1970s until today. The benchmark studies focus on metals such as palladium, platinum, rhodium, iridium or gold. Depending on the starting material, nitrogen-, oxygen-, boron-, silicon-, phosphorus- and sulfur-containing heterocycles can be prepared in many different sizes and with different substituents. Moreover, they offer high efficiency under relatively mild reaction conditions. On the other hand, they have many obvious disadvantages, such as rare abundance, high cost and production of heavy metal contamination. As a result of



uses in homogeneous catalysis, the recyclability of TM salts or complexes is far from being resolved and is therefore considered as significant source of environmental pollution.<sup>40</sup>

Fortunately, many other d-field metal/metal ions can exhibit activity and adaptability similar to that of the noble metals listed in **Table 2**. However, it is important to mention that the non-commercial oxidation state of metal ions often needs to be stabilized with special ligands or conditions for maintaining their catalytic efficiency. On the other hand, using non-noble metals, such as copper, cobalt, manganese or nickel, additional benefits can be offered in addition to the elimination of the disadvantages mentioned above, for example enhanced selectivity, easy recyclability or excellent tolerance to different reaction protocols and functional groups.

#### 2.1.2. *Heterogenization attempts and solid catalysts in heterocyclic chemistry*

In the previous section, some examples of transition metals that can be used in the syntheses of heterocycles were presented. These transition metals are generally used in the form of their salts or complexes and are therefore suitable for homogeneous catalytic applications too. The advantage of a well-chosen homogeneous catalyst is not only the high activity, but also the high achievable selectivity with which chemo-, stereo- and enantioselective syntheses can be carried out under relatively mild conditions. Nowadays, the reusability of catalysts is becoming increasingly important from an ecological point of view, not only because of heavy metal pollution, but also for financial reasons. Based on these difficulties for their practical use, the need of heterogenization emerged.

There are several methods to solve this problem, but in general, heterogenization can often lead to a decrease in activity and/or selectivity due to the poorer accessibility of the active centers. Therefore, the synthesis of catalysts whose catalytic properties are not greatly affected by heterogenization, but which are reusable, is still a leading area of research in heterogeneous catalysis.

Heterogenization of homogeneous catalytic systems can be defined as the modification of homogeneous catalysts to resolve the uniformity between the molecules of the catalyst and the product(s) into separable phases. Two liquid phases with no, limited, or temperature controlled miscibility<sup>41</sup> or a solid phase and a liquid phase with no, limited, or temperature regulated solubility of the component(s) of the solid phase in the liquid phase<sup>42</sup> are the most common variants.

The simplest solid–liquid immobilization method is to use the solid form of a homogeneous catalyst, that has no or temperature-dependent solubility in the reaction media.

One such example is the application of copper(I)isonitrile complex for azyde-alkyne cycloaddition in water.<sup>43</sup>

The most commonly used and therefore most diverse heterogenization method is ionic or covalent bonding.<sup>44</sup> The catalytically active component is anchored *via* ionic or covalent interactions on the surface of a support, which is generally considered to be chemically inert. Organic functionalized materials, *e.g.*, polymers, copolymers, solid-phase peptides, or oxide surfaces (typically silica, alumina, ceria or titania) can be modified by covalent functionalization. Charged clays (natural or synthetic), zeolites or mesoporous materials can be functionalized by using ion exchange methods.<sup>45</sup>

There are two main methods to prepare supported catalysts. During the impregnation method a suspension of the solid support is treated with a solution of the active component, then the solid phase is separated by filtration and then dried. The material obtained may need to be further activated, for example by thermal treatment. With the co-precipitation method, covalently bonded supported catalysts can be prepared from (generally) aqueous solutions containing all components.

**Table 3.** Heterogeneous copper/manganese/cobalt/nickel-containing catalysts

<b>HETEROGENIZED COPPER, MANGANESE, COBALT AND NICKEL CATALYSTS</b>	
ACTIVE COMPONENT	CARRIER
<i>ethylenediamine–copper(II) complex</i>	PVC <sup>46</sup>
<i>Cu(II)</i>	chelate resin <sup>47</sup> , L-histidine functionalized multi-walled carbon nanotubes <sup>46</sup> , ionic liquid <sup>48</sup>
<i>copper-Schiff base complex</i>	silica-coated Fe <sub>3</sub> O <sub>4</sub> NPs <sup>49</sup>
<i>mesoporous MnO<sub>2</sub></i> <sup>50</sup>	
<i>copper</i> <sup>-51</sup> <i>or cobalt-containing modified MnO<sub>2</sub></i> <sup>52</sup>	
<i>manganese(II)-salen complex</i>	zeolite <sup>53</sup> , MOF <sup>54</sup>
<i>MOF derived Co(II)</i>	N,P co-doped porous carbon <sup>55</sup>
<i>N-doped C-supported cobalt NPs</i> <sup>56</sup>	
<i>Ni(II)MOF</i> <sup>57</sup>	
<i>CuNiFeO NPs</i> <sup>58</sup>	
<i>imine/thiophene-nickel (II) complex</i>	magnetic Fe <sub>3</sub> O <sub>4</sub> NPs <sup>59</sup>

As copper catalyzed transformations are widely accepted among synthetic reactions, there are several attempts for heterogenized copper catalysts from the simplest supported catalyst, to quite complex systems as shown in **Table 3**. Although, there are some publications about organic transformations and heterocyclization catalyzed by manganese complexes (porphyrin<sup>60</sup>, pincer<sup>61,62</sup>), heterogeneous examples are hard to locate. Likewise, homogeneous catalytic systems predominate in the preparation of heterocycles from nickel and cobalt, and the catalytically active forms are generally Ni(0), Ni(II) and Co(III)<sup>63,64</sup>.

Another important corner of heterogeneous catalysis is the use of bulk catalysts. Metal oxides and silica are often used because of their durability, environmental safety, ease of use, accessibility and inexpensiveness.<sup>65</sup> In syntheses of five- and six-membered heterocycles, CoO, In<sub>2</sub>O<sub>3</sub>, CuO, MgO, Al<sub>2</sub>O<sub>3</sub>, CaO, SnO<sub>2</sub>, ZnO and BaO are the most commonly used metal oxides as Lewis acids. In addition, mixed oxides-/supported oxides, such as Al<sub>2</sub>O<sub>3</sub>–Fe<sub>2</sub>O<sub>3</sub>/V<sub>2</sub>O<sub>5</sub>/CuO, MgO–La<sub>2</sub>O<sub>3</sub>/SnO<sub>2</sub>/Al<sub>2</sub>O<sub>3</sub> or MoO<sub>3</sub>–ZrO<sub>2</sub> and CuFe<sub>2</sub>O<sub>4</sub> are also quite common<sup>66</sup>. As TM oxide catalysts CuO<sup>67</sup> (co-catalyst alongside palladium<sup>68</sup>), Co<sub>2</sub>O<sub>3</sub>,<sup>52</sup> MnO<sub>2</sub>,<sup>50,51</sup> NiO,<sup>66</sup> their surface functionalized forms and combinations are used most often.

The catalytic features of the bulk catalyst depend on their specific surface area and the active site (Brønsted and/or Lewis, number and activity). The concentration and strength of acidic sites can be modified by adding other metal oxides (mixed oxides, supported catalysts) or by chemical treatments such as fluorination or sulfonation.<sup>69</sup> The number of active sites can increase as the surface area of the catalyst increases by increasing the porosity or decreasing the particle size (nanoscale oxides). For functionalized surface, impregnation, ion exchange, precipitation–calcination,<sup>65</sup> mechanochemical methods<sup>70</sup> and the sol–gel method<sup>71</sup> are the most commonly used.

The use of layered materials as catalysts, in addition to the advantageous properties of bulk catalysts, can offer a kind of shape selectivity due to the constraints introduced by the space of the interlamellar galleries. The first application of layered structures as catalysts was a petrochemical one in the 1980s.<sup>72</sup> In layered materials additional charge selectivity is also possible through charged layers. Moreover, the modification of the original structure by anchoring other catalytically active molecules (metal ions/complexes, organic molecules) can create efficient catalytic systems that can provide increased selectivity and multifunctionality through the contribution between the carrier/host and the guest. This interfacial effect is discussed in more detail in the chapter concerned with cooperative catalysis.

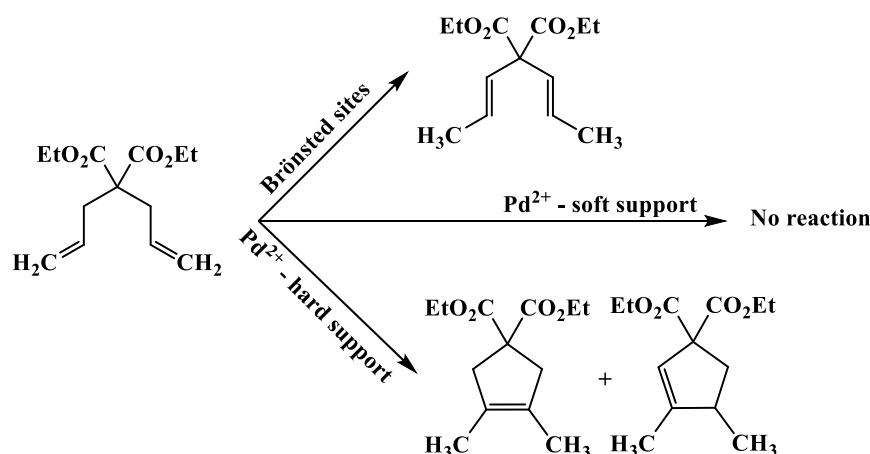
### 2.1.3. *Lewis-acid catalysis in heterocyclic chemistry*

The concept of Lewis acidity, according to which “the acid is an electron pair acceptor”, is derived from Lewis in 1923.<sup>73</sup> It is a more general and therefore more comprehensive definition of acids than that of Brønsted: “An acid is a molecule which is able to give proton(s)”. Lewis's definition covers practically all acid-base processes.

The concept of hard and soft acids and bases (HSAB), introduced by Pearson in 1963, explains the different affinities between acids and bases that do not depend on electronegativity or other associated macroscopic properties.<sup>74</sup> He stated that hard acids are more likely to be

associated with hard bases, and soft acids are more likely to be associated with soft bases, and that hard acids react easily with hard bases and soft acids with soft bases. He defined hard acids as small, strongly positively charged, and not easily polarizable electron acceptors, while soft acids were defined as larger, less positively charged acceptors with easily removable valence electrons. However, the concept of HSAB for solid acids has rarely been discussed because solids can contain Brønsted and Lewis sites simultaneously, which makes it considerably more difficult to address the hardness-softness issue. Furthermore, addressing the Brønsted or Lewis nature of an acid site needs a special concern, because new Brønsted acid sites can be generated from Lewis acid sites *via* hydrolysis in the presence of water, according to the  $LA + H_2O \rightarrow H^+ + LA(OH)^-$  equation.

Since the existence of a reaction catalyzed exclusively by Brønsted acids has not been demonstrated yet, it can be generally stated, that acid-catalyzed reactions can also be carried out with Lewis acids. However, this will lead to a different activity and/or selectivity in the product distribution. Furthermore, the type of Lewis acid can also influence the activity and selectivity values. While in TM-catalyzed reactions the activity of the homogeneous complex depend strongly on the nature of the coordinating ligands, it can be interpreted as the modifying effect of the ligand on the metal center's softness or hardness. The same phenomenon can be induced by binding metal ions to a solid support. (**Scheme 1.**)



**Scheme 1.** Modifying effect of Brønsted and Lewis sites to palladium(II)-catalyzed cyclization of diethyl-2,2-diallylmalonates

During the cyclization reaction of diethyl-2,2-diallylmalonate, adsorption of palladium(II) salts on the surface of zeolite (hard support) can provide an active heterogeneous catalyst for the preparation of cyclopentenes, while a gradual loss of activity is observed with increasing softness of the support. On the other hand, Brønsted acid sites give a different

product from a C=C bond isomerization without a cyclized product.<sup>75</sup> This example illustrates an important difficulty in heterogenization attempts: a well-chosen support can strongly contribute to the enhancement of the catalytic activity, while with an unsuitable carrier, activity and selectivity can be destroyed, even totally extinguished or, alternatively, it may redirect the reaction to another pathway.

The "effectiveness" of any Lewis acid, *i.e.*, its ability to catalyze a given reaction, depends on several factors that define its ultimate hard-soft nature. In general, the coordination of electron-withdrawing ligands increases the Lewis acidity of the central metal. On the other hand, strong back electron donation by the coordinating atoms may decrease the availability of the original empty metal orbital to accept an electron pair from a base<sup>76</sup>. The hard-soft character is also determined by the available empty metal orbital. Tin and organotin derivatives with empty 5d orbital, for example, are softer Lewis acids than aluminum with empty 3p orbital. Analogous to electron-withdrawing ligands, electron-donating ligands such as alkoxy substituents generally reduce the Lewis acidity. In tetrahedral titanium(IV) compounds, for example, acidity can be tuned with the number of halide and alkoxy coordinating groups. The more the alkoxy ligand, the softer the titanium salt. Furthermore, from titanium mono- to trialkoxy halides, acidity depends on steric hindrance as well.

Several metal salts and oxides have been used as Lewis acids for an enormous variety of organic reactions. The most typical salts are AlCl<sub>3</sub>, ZnCl<sub>2</sub>, FeCl<sub>3</sub>, SnCl<sub>4</sub>, TiCl<sub>4</sub>, LiCl, typically for Friedel-Crafts reactions, TiCl<sub>4</sub> for Aldol reaction and rearrangements with BF<sub>3</sub>·Et<sub>2</sub>O, TiCl<sub>4</sub>, and its alkoxy homologues (TiCl<sub>3</sub>(OiPr), TiCl<sub>2</sub>(OiPr)<sub>2</sub>) for Diels-Alder cycloadditions, or BF<sub>3</sub>/Et<sub>2</sub>OTiCl<sub>4</sub>, SnCl<sub>4</sub>, BF<sub>3</sub> for oxidation reactions<sup>77</sup>. The other important group of typical Lewis-acids are metal oxides, such as Al<sub>2</sub>O<sub>3</sub>, Bi<sub>2</sub>O<sub>3</sub>, CeO<sub>2</sub>, TiO<sub>2</sub>, MoO<sub>3</sub>, ZnO, SnO<sub>2</sub> and La<sub>2</sub>O<sub>3</sub>.<sup>77</sup> Various solutions have been also used to make Lewis acid catalysis more environmentally friendly, such a two phase liquid system, in which the Lewis acid remains dissolved in one of the solvents, while the products can be extracted by another immiscible liquid. Supercritical CO<sub>2</sub>, biphasic fluoro systems, or ionic liquids have been used for this.<sup>77</sup>

#### Lewis acid-catalyzed reactions in water

Although water might be the perfect solvent for green chemical methods, it is unfortunately widely accepted that Lewis acid-catalyzed reactions must be carried out under strictly anhydrous conditions, as any traces of water can decompose the Lewis acid catalysts instantaneously or gradually. The formation of hydroxides or oxides can lead to the immediate or gradual loss of Lewis acid activity. While the hydrolysis of anhydrous metal halides such as

$\text{AlCl}_3$ ,  $\text{TiCl}_4$ , and  $\text{BCl}_3$  are typical examples of the dramatic adverse effect of the presence of water, some other studies have been reported on metal salts that do not undergo immediate hydrolysis. These salts are mainly rare earth triflates ( $\text{La}(\text{OTf})_3$ ,  $\text{Yb}(\text{OTf})_3$ ,  $\text{Sc}(\text{OTf})_3$ ,  $\text{Ge}(\text{OTf})_3$ ),<sup>78</sup> and heterogenized metal compounds, such as Sn-, Ti- or Al-containing zeolites.<sup>79</sup>

An interesting phenomenon is seen in the aldol reaction of silyl enol ether with aldehydes in a mixture of tetrahydrofuran (THF) and water catalyzed by  $\text{La}(\text{OTf})_3$ , which may nuance the “water disinclination” of Lewis-acid catalysis. The amount of water in the reaction medium strongly influences the yield of aldol products and there is an optimal concentration for the process. Smaller or larger water content can significantly reduce the product yield. For example, the reaction of cyclohexanone trimethylsilyl ether with benzaldehyde gives an aldol yield of 80% if the medium contains 10-20% water, while in pure THF or water it is reduced to only 10 and 18%, respectively<sup>80</sup>. Based on the proposed mechanism, it was suggested that the catalyst is immediately hydrated upon dissolution and the water molecules are continuously exchanged in the coordination sphere of the metal. If an aldehyde molecule is nearby, it can coordinate to the metal center and activate it, and the silyl enol ether can already attack this Lewis adduct. However, according to this model, it should be possible to quantitatively predict the precise activity of a given metal salt as a Lewis acid in aqueous media, which is not supported by the experimental observations. On the other hand, the formation of Brønsted acid from the interaction of metal triflate and water cannot be completely excluded, so that a considerable amount of hydroxonium ion can be generated, which can also be an important component of the actual catalyst. Consequently, this catalyst is not only compatible with water but is also activated by water.

#### Lewis acids supported on solids

While strong Lewis acids are very corrosive on their own, they can be made more environmentally friendly *via* heterogenization on high-surface-area solids, such as  $\text{Al}_2\text{O}_3$ ,  $\text{SiO}_2$ , zeolites or clays<sup>77</sup>. Conventional Lewis acids can be physisorbed, chemisorbed, or anchored on inorganic supports<sup>81</sup> or can be intercalated, for example with  $\text{FeCl}_3$ ,  $\text{SbF}_5$ , or aluminum halides between the layers of graphite, increasing the interlaminar spacing and yielding strong acid catalysts.<sup>82</sup> The catalytic activity of the supported system can be enhanced if the preparation is carried out in the presence of Brønsted acid, fluorine or some kind of transition metal compound.

Alumina can be a popular carrier, such as  $\text{AlCl}_3$  on alumina, which is one of the most studied supported Lewis-acid catalyst. According to a publication reported in 1980,<sup>83</sup> the Lewis

acid can strongly interact with hydroxyl or even oxide groups at the surface of the alumina, and thus new active sites can be formed with the possible alumina local structures. This results in the complete disappearance of surface hydroxyls and therefore the absence of Brønsted acid sites.

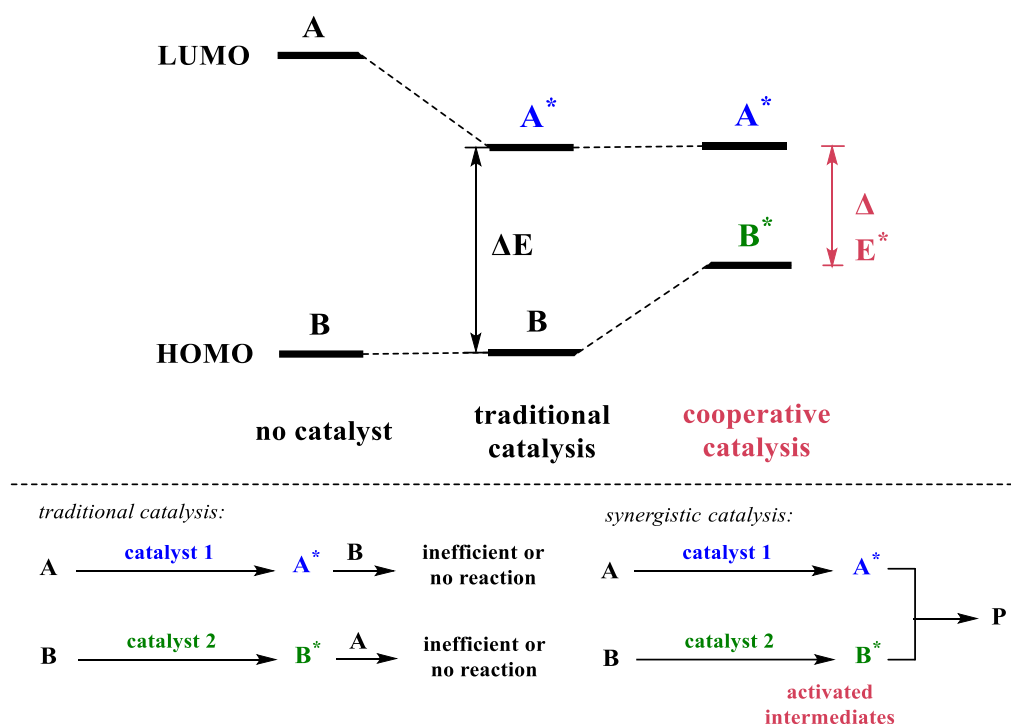
Fluorination and chlorination, may also promote the acidity of alumina, for example in alumina-supported group VIII metals (Fe, Co, *etc.*).<sup>84</sup> The chlorination of  $\text{Al}_2\text{O}_3$  with  $\text{CCl}_4$  was proposed to occur in two steps. In the first stage the surface Al-O-Al species and isolated hydroxyl groups react with  $\text{CCl}_4$ , increasing the chlorine content, then the number of surface OH groups decreases even further, and the Cl content increases to *ca.* 14%. It is accepted that this phenomenon is originated from the inductive effect of chlorine atoms on acid sites in the neighborhood.

Acid-treated clays, amorphous or mesoporous silica, titanium- and other metal oxides, molecular sieves, polymers, ion-exchange resin or graphite are also preferred carriers for supported Lewis acid catalysts.<sup>77</sup> They can be prepared by a variety of synthetic methods, such as impregnation-, precipitation-, reductive-, or colloidal methods.<sup>85</sup>

#### 2.1.4. *Cooperative Catalysis*

By definition “catalysts are substances that increase the reaction rate by forming intermediates but are not consumed in the reaction and remain unchanged after the intermediate decomposes into the final product and the catalyst molecule”.<sup>86</sup> In conventional catalysis, an activated reagent reacts with another non-activated molecule (reagent 2), with the reduction of the total reaction energy being carried out by a unique catalyst.

In multi-catalytic mechanisms, such as cooperative catalysis, both reagents are activated simultaneously by a catalyst or catalysts. Increasing the energy level of the highest occupied molecular orbital (HOMO) of reagent1 and decreasing the energy level of the lowest unoccupied molecular orbital (LUMO) of reagent2 can lead to highly efficient systems (**Scheme 2.**).



**Scheme 2.** Schematic energy diagram of traditional- and cooperative catalysis.

However, the concept of cooperative catalysis cannot be consistently delineated in the literature for two reasons. One is that different authors prefer to use different terms to describe the same principle, such as synergistic catalysis by McMillen,<sup>87</sup> cooperative double catalysis by Jacobsen,<sup>88</sup> or contemporaneous dual catalysis by Trost.<sup>89</sup> The other reason is that the distinction between the very similar multi-catalytic mechanisms is not uniform either, such as bifunctional catalysis versus synergistic catalysis.<sup>87</sup>

In heterogeneous catalysis, the question of the supporting active component can also overshadow the overall picture. The minor component(s) of these systems, usually present in negligible amounts relative to the overall catalyst, are presumed to be responsible for this induced catalytic activity. The mayor component(s) is/are readily regarded as chemically inert, playing no role in the catalytic cycle. However, in many cases this is not simple. The simplest eventuality corresponds to the scenario described above, where the mayor component(s) actually act as an inert scaffold and their function is merely the “solidifying” of the active components. The second possibility is a group of the so-called promoter molecules, which themselves have little or no catalytic effect, but when added to catalytically active components, they can improve the final catalytic performance. Finally, the mayor component(s) may contribute significantly to the catalytic activity of the solid, which may already correspond to the concept of cooperative catalysis. (Axiomatically, cooperative catalysis means that “two catalysts and two catalytic cycles work together to form a new bond”, *i.e.* “a single chemical



transformation is achieved by activating both the nucleophile and the electrophile by two different catalysts”).<sup>87</sup> In special cases, the combination of two efficient catalysts can create a system so powerful whose final catalytic activity is stronger than the sum of the effects of the building blocks, a phenomenon known as the interface effect.

There is a growing need for clarification of the concept of cooperative catalysis, as the use of complex supported systems overwhelms the literature. While from a practical point of view, knowledge of the final capabilities of the catalytic systems is usually sufficient, clarification of the contribution of the individual components would be useful. Therefore, knowledge of possible interface effects in multicomponent- and cooperative systems can provide useful knowledge for catalyst development in the future. This can also serve the increased demand for efficacy and sustainable development.

In recent years, many combinations have been investigated for cooperative systems, which can be divided into different groups. (**Table 4.**) The first is the group of metal complexes with which enantio- and diastereoselective processes can be carried out.<sup>90,91</sup> The second interesting group is the combination of different Lewis acids.<sup>92–94</sup> The third group is the combination of Brønsted base/acid with Lewis acid/base.<sup>95,96</sup> And finally, the last is metal–support cooperative catalysts<sup>97,98</sup> which group is the most related to the current work.

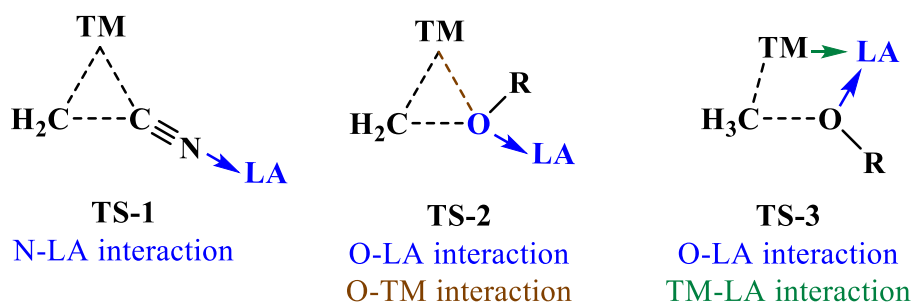
**Table 4.** Cooperative combinations of catalysts

COMBINATION OF			
METAL COMPLEXES	LEWIS ACIDS	BRØNSTED BASE/ACID AND LEWIS ACID/BASE	METAL AND SUPPORT
<i>Co(II)-phosphinoamido half-sandwich complex</i> <sup>90</sup>	<i>Co(salen) complex - achiral Ti(IV)</i> <sup>92</sup>	<i>phosphoric acid triphenyl ester and triphenylphosphine sulfide</i> <sup>95</sup>	<i>Au and Ag NPs - hydrotalcite</i> <sup>97</sup>
<i>rare earth-alkali metal heterobimetallic complexes</i> <sup>91</sup>	<i>Ir photocatalyst-CoBr<sub>2</sub></i> <sup>93</sup>	<i>CuOTf and 9-amino-9-deoxyepicinchona-derived urea</i> <sup>96</sup>	<i>MoO<sub>3</sub> - SiO<sub>2</sub></i> <sup>98</sup>
	<i>AgOTf-Cu(OAc)<sub>2</sub></i> <sup>94</sup>		

Most publications have described the role of the metal and acid domains in this class of bifunctional catalysts.<sup>99</sup> The final performance of the catalyst is rarely a simple overlap of the reactions promoted by the isolated metal and acid sites, as the presence of the metal can significantly affect the strength of the acid and the acid centers can exert synergistic or antagonistic effects on the catalytic activity of the supported metal. Therefore, the systematic design of bifunctional solid catalysts is difficult, because the identification of the active centers

can be more complicated, than on traditional solid surfaces (which is also not straightforward). Moreover, the stability and reusability of the catalyst, the leaching of metals, and formation of byproducts can also be problematic. For these reasons the use of bifunctional solid catalysts in industrial processes is still limited, despite the fact that they can clearly offer advantages over the corresponding homogeneous phase-catalyzed processes. Higher productivity is an obvious advantage, but these processes can be cleaner, safer and cheaper compared to the corresponding sequential processes using monofunctional catalysts. Cooperative catalysts can be extremely versatile, they can be used in a wide range of processes, their operation can be broken down into elementary reaction steps and overall, they can be extremely useful in creating more sustainable processes on a larger scale.

#### Cooperative interactions between Lewis acids and transition metals



**Scheme 3.** – Possible Lewis acidic interactions with the substrates or TM catalysts.

Lewis acids are often used as co-catalysts in transition metal catalyzed reactions because they can increase reactivity and/or selectivity via  $\sigma$ -coordination, but the explanation of the acceleration effect of Lewis acids is not yet fully understood. The usually proposed mechanism is enhanced charge transfer from the transition metal to the electron-deficient substrate due to  $\sigma$ -donation, but the catalyst-substrate interaction can also be influenced by other factors such as Pauli repulsion, electrostatics, polarization and dispersion.

**Scheme 3.** shows three types of transition states between substrate, transition metal (TM) and Lewis-acid (LA) centers in Ni-catalyzed C–X (X = H, C, O) bond cleavage by oxidative addition, which were quantitatively described by Gao and co-workers using energy decomposition approach.<sup>100</sup> They found, that the elucidation of enhanced charge transfer from metal to substrate can only be applied for those transition states that exhibit only heteroatom–Lewis acid interactions (*e.g.*, C–H, C–CN and C(acyl)–O oxidative additions (TS-I type transition state)). In contrast, Pauli repulsion and electrostatics/polarization are the decisive

factors in the TS-II and TS-III types. For example, TS-II type transition state is the transition state of C–O oxidative addition when the oxygen atom of the substrates interacts with both TM and LAs with O–LA and O–TM interactions (*e.g.*, C(benzyl)–O and C(aryl)–O oxidative additions). The decisive factor for their improved reactivity is attributed to the reduced Pauli repulsion between the occupied orbitals. In TS-III, LAs serve as a bridge to connect the TM center and the oxygen atom and form O–LA and TM–LA interactions (*e.g.*, C(benzyl)–O oxidative addition). The reaction is facilitated by greater charge separation and electron delocalization effects by strengthening electrostatics and polarization.

## 2.2. Multi-sided bismuth

Bismuth is a soft gray naturally occurring metal and the heaviest known member of Group 15. The most common forms are bismite ( $\text{Bi}_2\text{O}_3$ ), bismutite ( $\text{Bi}_2\text{O}_2\text{CO}_3$ ), or bismuthinite ( $\text{Bi}_2\text{S}_3$ ) and is obtained as a by-product of copper and lead smelting. Bismuth and its compounds have several interesting properties that can be exploited in many different areas. For example the low melting point, high boiling point, and low neutron absorption cross-section allow lead-bismuth eutectic alloy as a coolant in nuclear reactors<sup>101</sup> or the expansion on solidification is a useful property used in the printing industry. It is the most diamagnetic element, has the second lowest thermal conductivity after mercury, and is popular in electronics and photovoltaic applications, such as solar cells, light emitting diodes<sup>102</sup>, semiconductors<sup>103</sup> or photocatalysts<sup>104</sup> because of its high absorption coefficients, charge carrier mobilities, defect tolerances, and photoluminescence efficiencies.

Bismuth-containing compounds, *e.g.* Bi NPs, bismuth subnitrate or bismuth subcarbonate, are widely used as medicines for the treatment of gastrointestinal disorders such as dyspepsia, gastric ulcers or *H. pylori* infections, and more recently in the treatments of viral infections, multidrug resistant microbial infections or cancer. In addition, they are also popular in imaging, drug delivery or biosensing.<sup>105</sup> Due to the low solubility of bismuth salts on physiological conditions, the high chemical stability and (not least) affordability, they are becoming an increasingly attractive alternative for many synthetic transformations.<sup>106</sup>

Compared to the lighter members of group 15, the +5 oxidation state is less common in organobismuth compounds due to the increasing diffusivity of the  $s^2$  electrons and is less stable than in P, As and Sb, so that the most common oxidation state of bismuth is +3. The elemental metal, the bismuth complexes with inorganic substituents and the organo analogues are Lewis acids due to, bismuth has a tendency to extend the coordination around bismuth center, because of the availability of unoccupied orbitals (d and/or  $\text{BiX } \sigma^*$ ).<sup>107</sup> The Lewis acid property can be

enhanced by the presence of electronegative ligands ( $X = \text{OTf}$ ), making the bismuth centers more electropositive, so that the appropriately chosen chemical environment can increase the activity of bismuth-based catalysts.

#### 2.2.1. *Bismuth salts and oxides in organic chemistry*

In the last decade, the chemical community has finally explored the hitherto underutilized bismuth chemistry, which is capable of substituting noble metals to promote a variety of organic reactions, thus signifying a bypass route to perform synthetic organic transformations in a more sustainable manner.

The foundations of this field date back to the early 1850s when Löwig and Schweizer investigated the synthesis of trivalent and pentavalent organic bismuth derivatives.<sup>108</sup> This was followed by the work of Michaelis and Polis, which was very important for the development of bismuth chemistry, as the first organobismuth compounds were spontaneously flammable upon contact with air. The synthesis of triphenyl bismuthine, which was stable in air, in 1887 therefore marked the beginning of the actual development of bismuth organic chemistry.<sup>109</sup>

Further studies of Gilman in the late 1930s and early 1940s, concerning the reactivity of organobismuth compounds with alkali metals<sup>110</sup> and the synthesis of triaryl derivatives of bismuth<sup>110</sup> were inspired by the seminal work of Michaelis. Wittig and Clauss also worked on the synthesis of pentaaryl derivatives of Group V elements, such as bismuth in the 1950s.<sup>111</sup> In further studies, Suzuki and Matano investigated the synthesis of organobismuth(V) derivatives and bismuthonium salts.<sup>112</sup> Then in 2006–2007, Mukaiyama and co-workers demonstrated the utility of organobismuth(V) derivatives as very efficient reagents for various phenylations and oxidation.<sup>113</sup>

The use of bismuth(III) salts as Lewis acids has only been studied since the late 1990s with the pioneering work of Dubac,<sup>114</sup> Wada<sup>115,116</sup> and others, who paved the way for broad and general methods using bismuth(III) catalysts. The increasing number of publications in the field has clearly highlighted the versatile use of bismuth salts in various syntheses. The low toxicity and low cost of bismuth salts make them an attractive and practical alternative. The discovery that bismuth-triflate ( $\text{Bi}(\text{OTf})_3$ ) can be used as “water-proof” Lewis acid under aqueous conditions, because it exists in an equilibrium of  $\text{Bi}(\text{OTf})_3$  with bismuth hydroxide and trifluoric acid in water, finally opened the door to the development of bismuth-containing catalysts and proved the concept of water-compatible Lewis acids, which has since been applied to various types of green reaction. Beside the triflate salt, other bismuth(III) salts have also been used in various transformations, such as  $\text{BiCl}_3$ ,  $\text{BiBr}_3$ , or  $\text{Bi}(\text{OH})_3$ .<sup>106</sup> On contrary, the catalytically

active forms of bismuth halides are very often bismuth oxyhalides, *e.g.*, the elegant stereo-selective intramolecular etherification reactions of d-trialkylsilyloxyaldehydes and ketones, using a catalytic amount of BiBr<sub>3</sub>.<sup>117</sup>

The various reviews published in the last 10 years demonstrate that bismuth chemistry is truly an emerging field. The transformations using bismuth salts are definitively high potential processes from bulk chemicals to steroid and terpene chemistry, which encompass C–C and C–heteroatom bond formation, oxidations, polymerizations, syntheses of heterocycles, cyclization, allylation and catalytic alkylation reactions, multicomponent reactions or asymmetric catalysis using chiral bismuth(III) complexes.<sup>106</sup> In contrast, the very simple, but easy-to-use, solid-state bismuth oxides are underused in synthetic organic chemistry (photochemical applications are the main focus). After a longer search, some reactions with small molecules could be found, such as acylation of aromatic compounds,<sup>118</sup> oxidation reactions of hydroxyketones<sup>119</sup> or aldehydes<sup>120</sup> with Bi<sub>2</sub>O<sub>3</sub>. To the best of our knowledge, Bi<sub>2</sub>O<sub>2</sub>CO<sub>3</sub> has not yet been used for organic transformations.

### 2.2.2. *Introduction to layered bismuth compounds*

From the point of view of layered materials' applicability, bismuth species represent a very important and versatile group. The layered bismuth compounds are one of the focal points of research in the field of photochemistry,<sup>121</sup> electrochemistry<sup>122</sup> as well as in energy storage.<sup>123</sup> The tunable width of the band gap by different anions and cations,<sup>124</sup> the possible high dispersity of the band structure by *p* and *s-p* hybrid states,<sup>125</sup> and the stable skeletal structure with large interlamellar gallery<sup>126</sup> are the interesting properties that make bismuth-based materials applicable in solar cells, thermo- and optoelectrical devices or in ion batteries.

These layered materials are classified into four categories based on their composition: unitary, binary, ternary and multinary 2D bismuth-based materials. Unitary 2D bismuth consists of rhombohedral bismuth layers with a relatively large vertical gap.<sup>127</sup> Guest ions or coordinatively unsaturated bismuth atoms embedded between the layers provide good opportunities for catalytic application.

Binary 2D bismuth-based layered materials are mainly constructed from bismuth with halogen or chalcogen elements (**Fig. 1. A**). Since both bismuth and the halogen or chalcogen are p-block elements, binary 2D bismuth-based layered materials belong to p-block semiconductors with ultra-narrow band gaps and ultra-high charge carriers. Their main field of application are therefore the photo- and thermoelectric applications.

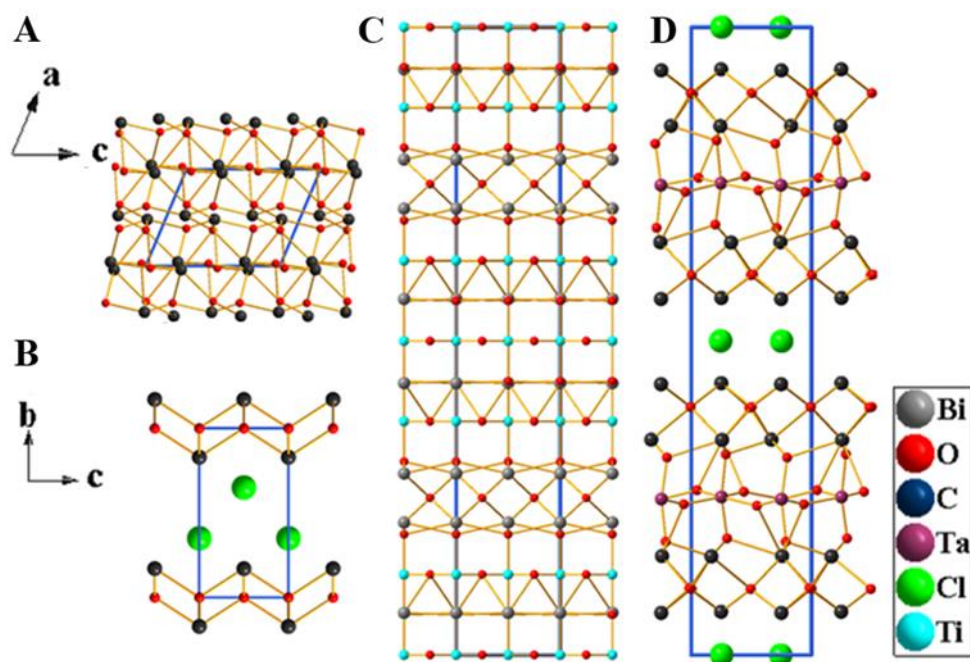


**Figure 1.** Classification of 2D bismuth-based layered materials: A – binary ( $\alpha$ - $\text{Bi}_2\text{O}_3$ ), B – ternary (Sillén-type  $\text{BiOCl}$ ), C and D – multinary (Aurivillius-type  $\text{Bi}_4\text{Ti}_3\text{O}_{12}$  and Sillén-Aurivillius-type  $\text{Bi}_4\text{TaO}_8\text{Cl}$ ).

The structure of ternary 2D bismuth-based layered materials consists of  $[\text{Bi}_2\text{O}_2]^{2+}$ -based frameworks into which simple or oxyacid anionic groups are inserted (**Fig. 1. B**). The interactions between positively charged bismuth-containing layers and anionic layers are van der Waals forces or weak electrostatic forces<sup>128</sup>. In simpler cases, non-metal oxyacid anions (*e.g.*,  $\text{CO}_3^{2-}$ ,  $\text{SiO}_3^{2-}$ ,  $\text{IO}_3^-$ ) can be introduced into the layers (**Fig. 2. A**). By introducing halogen anions into the fluorite-like  $[\text{Bi}_2\text{O}_2]^{2+}$  layers like in bismuth oxyhalides ( $\text{BiOX}$ ,  $\text{X} = \text{Cl}$ ,  $\text{Br}$ , and  $\text{I}$ , **Fig. 1. B**), an interesting superstructure is constructed, it is the so-called Sillén-type superstructure<sup>123</sup>. By inserting more complex, transition metal-based oxyacid anions, another superstructure can be constructed, called simple Aurivillius phase (general formula of  $(\text{Bi}_2\text{O}_2)(\text{TM})\text{O}_x$  ( $\text{TM} = \text{Mo}$ ,  $\text{W}$ ,  $\text{Sn}$ ,  $\text{Nb}$ ,  $\text{Ta}$ ,  $\text{Ti}$ , *etc.*) (**Fig. 1. C**). In this composition, corner-sharing connected  $(\text{TM})\text{O}_x$  octahedral layers are sandwiched between the  $[\text{Bi}_2\text{O}_2]$ -based layers<sup>129</sup>. Due to these typical structures, ternary bismuth-based p-block semiconductors can be designed with high chemical and thermal stabilities.

Finally, multinary 2D bismuth-based layered materials often have very complicated compositions that are not easy to define. As an example, the complex Aurivillius-phase<sup>130</sup> and Aurivillius-Sillén compounds can be mentioned. This latter is built up alternately from Aurivillius- and Sillén-phase structures (general formula of  $[(\text{Bi}_2\text{O}_2)_2\text{X}]^{3+}[\text{A}_{n-1}\text{B}_n\text{O}_{3n+1}]^{3-}$  ( $\text{X}$  is a halogen element,  $n = 1, 2, 3$ , *etc.*, Aurivillius  $[\text{A}_{n-1}\text{B}_n\text{O}_{3n+1}]$ -based perovskite and Sillén  $(\text{Bi}_2\text{O}_2)_2\text{X}$  layers, **Fig. 1. D**).<sup>131</sup> On the other hand, there are some simpler examples among

multinary 2D bismuth-based compounds, such as bismuthoxyhalides partially substituted with Ca, Sr, or Ba<sup>132</sup> (**Fig. 2. B**). Complex, multinary bismuth-based compounds possess the advantages of Aurivillius-phase and Sillén-phase semiconductors in terms of light absorption, charge separation and transfer, as well as photo-stability, suggesting their potential applications in photocatalysis.

### 2.2.3. Bismutites

An important representative of the layered bismuth compounds is the mineral family of bismutites. According to the classification based on their structure and composition, they belong to ternary or multinary 2D bismuth-based compounds with Sillén-type superstructure. In general, the positively charged  $\text{Bi}_2\text{O}_2^{2+}$  layers of bismutites are compensated by carbonate anions, incorporated into the interlayer space. The ternary or multinary classification depend on the complexity of the carbonate-based anion. Their simplest representative of bismutites is the also called bismutite with the formula of  $\text{Bi}_2\text{O}_2\text{CO}_3$ , in which carbonate anions are embedded between the layers. (**Fig. 2. A**). In coordination with carbonate ions, other metals can also be part of the anionic building block, such as calcium(II) ions in the naturally occurring mineral called beyerite ( $\text{CaBi}_2\text{O}_2(\text{CO}_3)_2$ ), **Fig. 2. B**.

Similar to other bismuth oxides, the main application field of bismutites is also photochemistry and photovoltaics, but compared to bismuth oxyhalides, bismutites are more stable photocatalysts.<sup>133</sup>

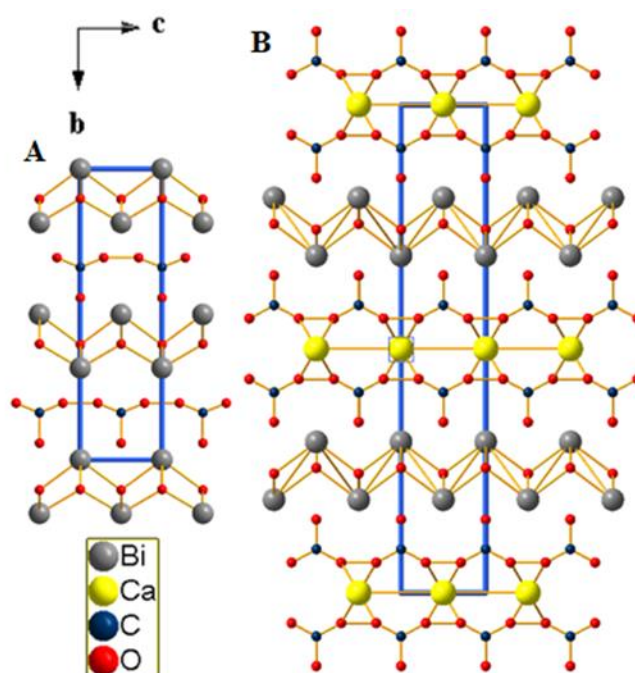


**Figure 2.** – Layered structure of bismutites: A – Bismutite:  $\text{Bi}_2\text{O}_2\text{CO}_3$ , B – Beyerite:  $\text{CaBi}_2\text{O}_2(\text{CO}_3)_2$

In several previous works, we have successfully synthesized and used the artificial silver analogue of this compound. The Sill  n-type bismutite framework was applied as a host, providing a strong anchorage for the guest silver(I) cations, thus these works can be considered as forerunners of the present dissertation.<sup>134–137</sup> Nevertheless, the active role of bismuth centers as Lewis acids, proving the bifunctionality of the as-prepared bismutite analogues, has not yet been harnessed.

## 2.3. Catalytic applications

### 2.3.1. Catalytic synthesis of phenothiazine

Phenothiazines and their derivatives are representative examples of N-heterocyclic structures with C–N and C–S moieties. These compounds possess a very diverse range of applications. From electrogenerated chemiluminescence emitters<sup>138</sup> to chemosensors,<sup>139</sup> as molecular wires,<sup>140</sup> or the backbone with various side chains can be used in psychotropic-, antituberculous or antifungal drugs.<sup>141–143</sup> Although the family of the compound has been known for a long time, the actuality of them is unquestionable, considering their novel applications are being continuously reported, such as piperazinyl phenothiazine which was recently investigated as an antipsychotic agent against SARS-CoV-2.<sup>144</sup>

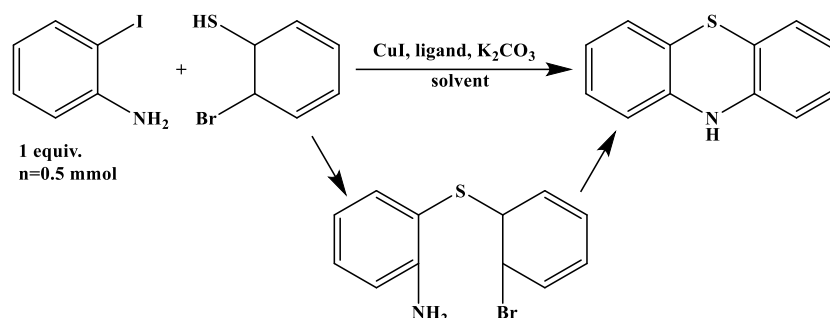
Numerous different synthesis strategies of phenothiazines were elaborated over the past decades (**Table 5**).<sup>145–147</sup> However, the heterocyclization step is still insufficient, thus the most important challenge on this highlighted point is to achieve a step-economical N–H/S–H functionalization cascade. Despite the fact of the notable progress that has been made on C–N couplings, many defects can be identified in the strategies shown in **Table 5**.

<b>Table 5.</b> Synthesis strategies of phenothiazines and their defects	
<b>SYNTHESIS STRATEGIES OF PHENOTHIAZINES</b>	<b>DISADVANTAGES AND DEFECTS</b>
heat treatment of diphenylamines and sulfur at high temperature <sup>145</sup>	large amount of added base (10–30 mol %) is required very long reaction time (48–96 h)
four-step route <i>via</i> Smiles rearrangement <sup>146</sup>	high reaction temperature (110–150 °C) sequential control of reaction conditions
C–N couplings <sup>147</sup>	high catalyst loading (10–20 mol %)

Of these reactions, really few elegant, cascade processes were reported; however, using organic additives and/or high catalyst loading (30 mol %) is necessary to provide good yields



(70–85%).<sup>147</sup> One of the most effective example for this is the cascade-like N-arylation and S-arylation-containing heterocyclization of 2-iodoanilines and 2-bromobenzenethiol<sup>148</sup> (**Scheme 4**, **Table 6**).



**Scheme 4.** Sequentially controlled CuI/ligand-catalyzed cascade N-arylation and S-arylation of 2-iodoanilines and 2-bromobenzenethiol yielding phenothiazines *via* heterocyclization.<sup>148</sup>

This reaction sequence formed one of the small molecule test reactions of the present work, with the addition that no relevant progress has been achieved for producing phenothiazine in a heterogeneous catalytic manner. Additionally, contrary to noble metals and copper-based systems, capabilities of Lewis acids are mainly untapped.

**Table 6.** Reaction conditions of sequentially controlled CuI/ligand-catalyzed cascade N-arylation and S-arylation of 2-iodoanilines and 2-bromobenzenethiol yielding phenothiazines *via* heterocyclization<sup>148</sup>

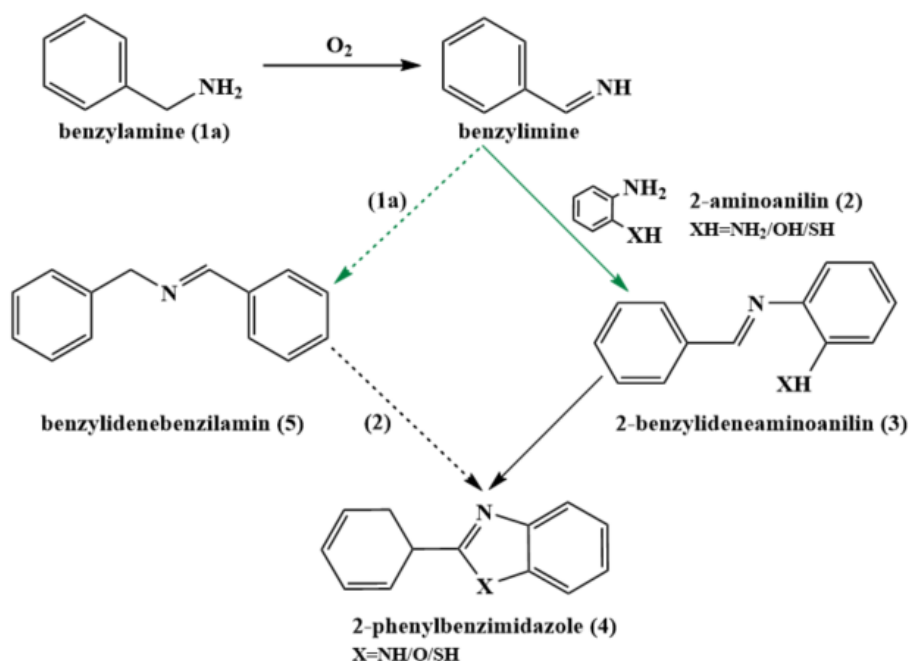
Temperature	90 °C (1 <sup>st</sup> step), 110 °C (2 <sup>nd</sup> step)
Reaction time	48h (1 <sup>st</sup> step), 72h (2 <sup>nd</sup> step)
Ligand	0.2 mmol L-proline (0.4 equiv.)
Solvent	2 mL 2-methoxyethanol
Catalyst loading	0.1 mmol CuI (20 mol%)
Base	2.5 mmol K <sub>2</sub> CO <sub>3</sub> (5 equiv.)
Yield of phenothiazine	<b>77 %</b>

### 2.3.2. Catalytic syntheses of 2-phenylbenzimidazole/ oxazole/ thiazole

Oxidative cross couplings and oxidative annulations of anilines and amines are among the key processes both in the industrial and academic production of nitrogen-containing heterocyclic compounds. Pharmaceuticals,<sup>149</sup> functional materials<sup>150</sup> or chemical sensors<sup>151</sup> can also be produced *via* these reactions.

For annulations, the most efficient catalysts are typically Brønsted and Lewis acids,<sup>152,153</sup> on contrary, promising Lewis acids such as Bi-compounds did not occur as yet. Due to the

extreme likelihood of homocoupling of amines, (aromatic) alcohols are more often used as reaction partners with anilines. However, dimer imines can also be useful products, providing that the reaction sequence can be controlled, and thus the product distribution depends on the reaction conditions. Oxidative cross couplings of anilines and amines toward imines could be catalyzed by non-noble metal ions such as Co(II),<sup>154</sup> Fe(II)<sup>155</sup>/Fe(III)<sup>156</sup> and Cu(I)<sup>157</sup>/Cu(II)<sup>158</sup> salts. Nevertheless, the widespread use of these valuable metals as catalysts in these annulations/couplings are severely limited by the fact that non-commercial oxidation state of the metal ions must be maintained for catalytic efficacy<sup>159</sup>.



**Scheme 5.** FeBr<sub>2</sub> catalyzed reaction sequence for benzimidazole/oxazole/thiazole production *via* oxidative coupling reaction of benzylamine and 2-amino/hydroxy/mercaptoaniline.<sup>155</sup>

Such an example is the work of Gopalaiah and Chandrudu, who used iron(II)bromide to catalyze the oxidative annulation of benzylamine and 2-aminoaniline producing 2-phenylbenzimidazole.<sup>155</sup> What they gain with the simplicity and cheapness of the catalyst, they lose with the impossibility of recyclability after the first reaction cycle. The reaction sequence and the reaction conditions are shown in **Scheme 5.** and **Table 7.**

**Table 7.** Reaction conditions of FeBr<sub>2</sub> catalyzed reaction sequence for 2-phenylbenzimidazole production *via* oxidative coupling reaction of benzylamine and 2-aminoaniline<sup>155</sup>

Temperature	110 °C
Reaction time	4h
Additive	molecular O <sub>2</sub> (balloon)
Solvent	2 mL chlorobenzene
Catalyst loading	0.1 mmol FeBr <sub>2</sub> (5 mol%)
Yield of 2-phenylbenzimidazole	<b>92%</b>

Since the control of the two reaction pathways was not attempted, this reaction sequence was chosen as the second test reaction for the present work.

### 2.3.3. *Oxidative dehydrogenative coupling reactions of anilines*

Quinolines and quinoxalines are important intermediates in many industrial processes, such as in the synthesis of polymers<sup>160</sup>, dyes<sup>161</sup>, pharmaceuticals<sup>162</sup> or pesticides<sup>163</sup>. Despite the well-known disadvantages of the industrial-scale syntheses such as environmentally unreliable reagents, high solvent requirements, harsh reaction conditions, or limited substrate scope, the vapor phase double condensation of ethylenediamine derivatives with 1,2-dicarbonyl compounds<sup>164</sup> and the Lewis acid-mediated Skraup synthesis are still the most widely used profitable and technically feasible methods.<sup>165</sup> On the other hand, oxidative and acceptorless dehydrogenation couplings are today's most advanced methods in scientific life and in terms of sustainability. **Table 8.** compares the advantages and disadvantages of the oxidative and acceptorless types of these couplings.

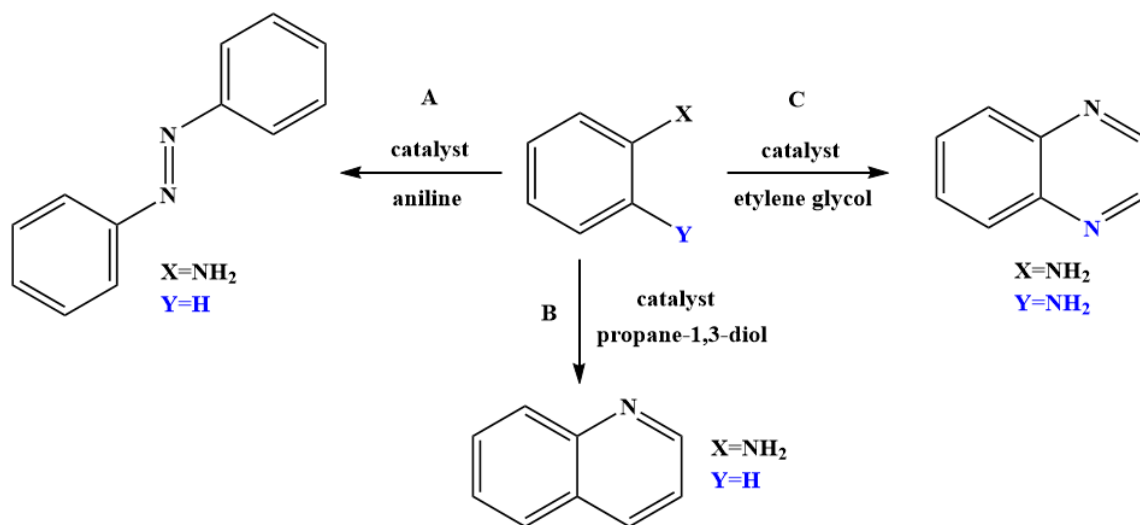
Beyond the listed examples, some paper can also be found in the literature about the combination of the simplicity of oxidative conversions and the efficiency of acceptorless dehydrogenative couplings. For example Corma *et al.* successfully published an elegant one-pot synthesis of quinoxalines, in which the oxidation of biomass-derived vicinal diols yields the corresponding dicarbonyls first, than the cyclic condensation with 2-aminoaniline and its derivatives to provide the final product.<sup>166</sup> For this a noble metal based Au/CeO<sub>2</sub> catalyst was used, which however was also be able to promote the formation of C-C bond cleaved by-product.

**Table 8.** Reaction conditions of FeBr<sub>2</sub> catalyzed reaction sequence for 2-phenylbenzimidazole production *via* oxidative coupling reaction of benzylamine and 2-aminoaniline

DEHYDROGENATIVE COUPLING			
ACCEPTORLESS		OXYDATIVE	
for quinolines: mono coupling of 2-aminobenzyl alcohols with ketones <sup>167</sup> or double coupling of secondary alcohols with 2-aminobenzyl alcohol <sup>168</sup> in modified Friedländer syntheses diols with aniline derivative <sup>169</sup> for quinoxalines: non-symmetric 1,2-diols and 2-nitroanilines or o-phenylenediamines <sup>170</sup>		the oxidation trap of $\alpha$ -hydroxycarbonyl compounds with 1,2-diamines <sup>171</sup> or the bismuth-mediated oxidative coupling of epoxides with ene-1,2-diamines <sup>172</sup>	
<i>PROs</i>	<i>CONTRA</i> s	<i>PROs</i>	<i>CONTRA</i> s
no overoxidized or C–C bond-cleaved by-product	non-efficient Michael addition step	mild reaction conditions, easy-to-perform	appearance of overoxidization and/or C–C bond cleavage
high selectivity	expensive and chemically sensitive 4d and 5d (noble) metal catalyst (Ir, Ru)	simplier transition metal salts (beside the also popular noble metals) as the actual catalysts, even in heterogeneous phase	lower versatility and selectivity
no need of halogenated or pre-functionalized starting material	use of special ligand, additives and/or stoichiometric amounts of base, inert atmosphere, non-green solvents (e.g., toluene)		requirement of pre-functionalization of the starting material

As there are some examples in the literature that the usage of bismuth or lead promoters beside noble metal catalysts can help to avoid overoxidatization<sup>173</sup>, and because some other reports have shown that TM containing heterogeneous catalysts, even cooperating with Lewis acids, are able to show promising catalytic abilities in oxidative dehydrogenative transformations,<sup>174</sup> the main aim of the final part of the current work was to investigate the applicability of the bimetallic, cooperative catalysts in oxidative dehydrogenative (self-)couplings without the application of any additive or special oxygen resource. **Scheme 6.** shows the investigated reactions. In azo coupling, reaction A, new N=N bond is formatting between two aniline. In the synthesis of quinoline, reaction B, aniline is coupled with propan-1,3-diol for creating new C=N and C–C bonds. Reaction C shows the coupling reaction of 2-aminoaniline and ethylene glycol producing quinoxaline *via* new C=N bonds formations and

reaction D shows the homocoupling of 2-aminobenzylamine with new C=N and N=N bonds formations.



**Scheme 6.** Catalytic oxidative coupling reactions of anilines

### 3. THE MAIN AIMS OF THE DISSERTATION

The present work is related to heterogenization methodologies of TMs with the primary goal of preparing copper, manganese, cobalt and nickel modified bismuth-based solid phase catalysts. First, attempts were made to anchor copper(II), manganese(II), cobalt(II) and nickel(II) cations. After the successful syntheses, the characterization of the catalyst candidates were also attempted by systematically combined analytical and spectroscopic methods to interpret structure-activity-selectivity-reusability relationships. To have deep knowledge about the as-prepared structures, the following analytical and spectroscopic methods were applied: powder X-ray diffractometry (XRD), infrared (IR) and Raman spectroscopy, near-infrared (NIR), UV-Vis and X-ray photoelectron (XPS) spectroscopy, transmission electron microscope with energy-dispersive X-ray spectroscopy (TEM-EDS), inductively coupled plasma mass spectrometry (ICP-MS), thermogravimetry (TG) with evolved gas analysis (EGA) and surface adsorption measurements. In addition to the structural information, the determination of the most probable compositions and structures as an additional goal was also set.

After reviewing the literature, it was hypothesized, that self-made catalysts will be applicable in organic reactions of small molecules as cooperative or (at least) bifunctional catalysts. Moreover, it was assumed, that the original reaction sequence, the activity and selectivity values, and/or the reaction conditions can be improved by the new, heterogeneous catalysts. In case of positive results, the feasibility of the concept can be verified. For this reason, the following catalytic cyclisation reaction have been chosen as tests: oxidative coupling of 2-iodoaniline and 2-bromobenzenethiol, oxidative annulation of benzylamine and 2-aminoaniline, oxidative coupling of aniline and propane-1,3-diol, oxidative coupling of 2-aminoaniline and ethylene glycol and oxidative homocoupling of 2-aminobenzylamine.

## 4. EXPERIMENTAL PART

### 4.1. Materials

All chemicals used for catalyst syntheses were of analytical grade Sigma-Aldrich products and were used without further purification. Bismuth(III)nitrate-pentahydrate ( $\text{Bi}(\text{NO}_3)_3 \times 5\text{H}_2\text{O}$ ); copper(II)nitrate-trihydrate ( $\text{Cu}(\text{NO}_3)_2 \times 3\text{H}_2\text{O}$ ); manganese(II)nitrate-hydrate ( $\text{Mn}(\text{NO}_3)_2 \times \text{H}_2\text{O}$ ); cobalt(II)nitrate-hexahydrate ( $\text{Co}(\text{NO}_3)_2 \times 6\text{H}_2\text{O}$ ); ammonia solution (25%;  $\text{NH}_4\text{OH}$ ); sodium carbonate anhydrous ( $\text{Na}_2\text{CO}_3$ ); concentrated nitric acid (cc.  $\text{HNO}_3$ ); copper(II)-oxide ( $\text{CuO}$ ); Manganese(IV)oxide ( $\text{MnO}_2$ ); cobalt hydroxide ( $\text{Co}(\text{OH})_2$ ) was precipitated from an aqueous solution of cobalt(II)nitrate-trihydrate using the appropriate amount of 3M sodium hydroxide solution.

The reagents and bases used for the catalytic reactions: 2-iodoaniline ( $\text{IC}_6\text{H}_4\text{NH}_2$ ); 2-bromothiophenol ( $\text{BrC}_6\text{H}_4\text{SH}$ ); 4-amino-3-iodobenzonitrile ( $\text{IC}_6\text{H}_3(\text{NH}_2)\text{CN}$ ); 2-iodo-4-nitroaniline ( $\text{IC}_6\text{H}_3(\text{NO}_2)\text{NH}_2$ ); 4-chloro-2-iodoaniline ( $\text{ClC}_6\text{H}_3(\text{I})\text{NH}_2$ ); 2,4-dichloro-6-iodoaniline ( $\text{Cl}_2\text{C}_6\text{H}_3(\text{I})\text{NH}_2$ ); 4-chloro-2-fluoro-6-iodoaniline ( $((\text{Cl})(\text{F})\text{C}_6\text{H}_3(\text{I})\text{NH}_2$ ); 2-iodo-4,6-dimethylaniline ( $\text{I}(\text{CH}_3)_2(\text{C}_6\text{H}_3)\text{NH}_2$ ); potassium carbonate ( $\text{K}_2\text{CO}_3$ ); benzylamine ( $\text{C}_6\text{H}_5\text{CH}_2\text{NH}_2$ ), 2-aminoaniline ( $\text{C}_6\text{H}_4(\text{NH}_2)_2$ ), 2-aminophenol ( $\text{C}_6\text{H}_4\text{NH}_2\text{OH}$ ); 2-aminothiophenol ( $\text{C}_6\text{H}_4\text{NH}_2\text{SH}$ ); 4-methoxybenzylamine ( $\text{CH}_3\text{OC}_6\text{H}_4\text{CH}_2\text{NH}_2$ ); 2-methoxybenzylamine ( $\text{C}_6\text{H}_4\text{CH}_2\text{NH}_2\text{OCH}_3$ ); 4-chlorobenzylamine ( $\text{ClC}_6\text{H}_4\text{CH}_2\text{NH}_2$ ); 2-chlorobenzylamine ( $\text{C}_6\text{H}_4\text{CH}_2\text{NH}_2\text{Cl}$ ); 3-nitrobenzylamine hydrochloride ( $\text{O}_2\text{NC}_6\text{H}_4\text{CH}_2\text{NH}_2 \times \text{HCl}$ ); aniline ( $\text{C}_6\text{H}_5\text{NH}_2$ ); *o*-anisidine ( $\text{CH}_3\text{OC}_6\text{H}_4\text{NH}_2$ ); *p*-anisidine ( $4-(\text{CH}_3\text{O})\text{C}_6\text{H}_4\text{NH}_2$ ); 3-nitroaniline ( $\text{O}_2\text{NC}_6\text{H}_4\text{NH}_2$ ); 4-bromoaniline ( $\text{BrC}_6\text{H}_4\text{NH}_2$ ); 4-chloroaniline ( $\text{ClC}_6\text{H}_4\text{NH}_2$ ); *o*-toluidine ( $\text{CH}_3\text{C}_6\text{H}_4\text{NH}_2$ ); *p*-toluidine ( $4-(\text{CH}_3)\text{C}_6\text{H}_4\text{NH}_2$ ); 4-aminobenzonitrile ( $\text{H}_2\text{NC}_6\text{H}_4\text{CN}$ ); 1,3-propanediol ( $\text{HO}(\text{CH}_2)_3\text{OH}$ ); 2-aminoaniline ( $\text{C}_6\text{H}_4(\text{NH}_2)_2$ ); ethan-1,2-diol ( $\text{HOCH}_2\text{CH}_2\text{OH}$ , ethylene-glycol); 4-bromo-1,2-diaminobenzene ( $\text{C}_6\text{H}_3(\text{NH}_2)_2\text{Br}$ ); 4-chloro-1,2-diaminobenzene ( $\text{C}_6\text{H}_3(\text{NH}_2)_2\text{Cl}$ ); 4-nitro-1,2-diaminobenzene ( $\text{C}_6\text{H}_3(\text{NH}_2)_2\text{NO}_2$ ); 3,4-diaminobenzoic acid ( $((\text{H}_2\text{N})_2\text{C}_6\text{H}_3\text{CO}_2\text{H})$ ); 3,4-diaminotoluene ( $\text{CH}_3\text{C}_6\text{H}_3(\text{NH}_2)_2$ ); 2-aminobenzylamine ( $\text{H}_2\text{NC}_6\text{H}_4\text{CH}_2\text{NH}_2$ ); sodium sulfate anhydrous ( $\text{Na}_2\text{SO}_4$ ) and brine, and the solvents: dimethyl sulfoxide ( $\text{C}_2\text{H}_6\text{OS}$ ); ethyl acetate ( $\text{CH}_3\text{COOCH}_2\text{CH}_3$ ); ethylene glycol ( $((\text{CH}_2\text{OH})_2$ ); 5-methyloxolan-2-one ( $\gamma$ -valerolactone,  $\text{C}_5\text{H}_8\text{O}_2$ ); pentane-2,4-dione (acetylacetone,  $\text{C}_5\text{H}_8\text{O}_2$ ); N,N-dimethylacetamide ( $\text{CH}_3\text{CON}(\text{CH}_3)_2$ ); N,N-dimethylformamide ( $\text{HCON}(\text{CH}_3)_2$ ); 2-butanone ( $\text{CH}_3\text{C}(\text{O})\text{CH}_2\text{CH}_3$ ); butanone (methylethylketone,  $\text{CH}_3\text{CCH}_2\text{CH}_3$ ); toluene ( $\text{C}_6\text{H}_5\text{CH}_3$ ); acetonitrile ( $\text{C}_2\text{H}_3\text{N}$ ); methanol ( $\text{CH}_3\text{OH}$ ) were also Sigma-Aldrich products which were of analytical grade and were

used without further purification except the liquid anilines, which were freshly distilled, and 3-nitrobenzylamine hydrochloride, which was liberated from its salt with 1M HCl before use.

## 4. 2. Syntheses of the modified bismutites

In a typical synthesis, performed by a modified co-precipitation method, appropriate amounts of  $\text{Bi}(\text{NO}_3)_3 \times 5\text{H}_2\text{O}$ , considered as 1 equivalent (3.75 mmol), and the related transition metal nitrate salt,  $\text{Cu}(\text{NO}_3)_2 \times 3\text{H}_2\text{O}$  (3.75 mmol)/  $\text{Mn}(\text{NO}_3)_2 \times 6\text{H}_2\text{O}$  (3.75 mmol)/  $\text{Co}(\text{NO}_3)_2 \times 6\text{H}_2\text{O}$  (3.75 mmol)/  $\text{Ni}(\text{NO}_3)_2 \times 6\text{H}_2\text{O}$  (3.75 mmol), were dissolved in 25 mL of 5 wt % aqueous nitric acid solution. After dissolution, 40–40 mL of 0.6–0.6 M ammonia and sodium carbonate solutions were added to the nitric acid solution containing the reagent salts followed by continuous stirring for 24 hours at 80 °C for  $\text{CuBi}_2\text{O}_2\text{CO}_3$  and at 100°C for Co-, Mn-,  $\text{NiBi}_2\text{O}_2\text{CO}_3$ . The obtained, colored products ( $\text{MBi}_2\text{O}_2\text{CO}_3$ ) were filtered, washed with distilled water several times, and dried at 60 °C overnight. With the exception of  $\text{CuBi}_2\text{O}_2\text{CO}_3$ , the finely powdered solids were treated with further heat treatment for 3 hours under 290 ° C to remove remained water traces before catalytic use.

The transition metal-free bismutite ( $\text{Bi}_2\text{O}_2\text{CO}_3$ ) was synthesized under identical conditions both at 80 and 100 °C but without loading the TM salt.

The bismutite-supported transition metal oxide composites ( $\text{M-Bi}_2\text{O}_2\text{CO}_3$ ) were synthesized by wet impregnation and were used for comparison. 1 equivalent (3.75 mmol) of the as-synthesized  $\text{Bi}_2\text{O}_2\text{CO}_3$  and 7.5 mmol of  $\text{CuO}$ /  $\text{MnO}_2$ / *in situ* precipitated  $\text{Co}(\text{OH})_2$ /  $\text{Ni}(\text{OH})_2$  were suspended in 50 ml ethanol. After sonicated for 2h at room temperature, solvent was evaporated.

## 4. 3. Instrumentation and characterization methods

### 4.3.1. Powder X-ray diffractometry

The XRD patterns were recorded on a Rigaku XRD MiniFlex II instrument by applying  $\text{CuK}\alpha$  radiation ( $\lambda = 0.15418 \text{ nm}$ ) and 40 kV accelerating voltage at 30 mA.

The interlayer distance (the interlayer space and the thickness of one layer) was calculated by Bragg's law:

$$n\lambda = 2d_{hkl} \sin \Theta.$$

where  $n$  is an integer;  $\lambda$  is the wavelength of the incident light,  $d_{hkl}$  is the lattice spacing and  $\theta$  is the angle of incidence.

The primer crystallite size was calculated by Scherrer equation:



$$D = \frac{K\lambda}{\beta \cos \theta}$$

where  $D$  is the average crystallite size,  $\beta$  is the line broadening in radians while  $\theta$  is the Bragg angle as well as  $\lambda$  is the wavelength of the incident light.

#### 4.3.2. *Thermal analytical measurement*

The thermal behavior of the as-prepared transition metal containing composites was studied on a Setaram Labsys derivatograph, employed under constant air flow conditions with 1 °C/min heating rate. The samples (30-35 mg) were placed into high-purity  $\alpha$ -Al<sub>2</sub>O<sub>3</sub> crucibles. For evolved gas analysis (EGA) a Pfeiffer QMS 200 mass spectrometer was used under oxygen flow (40 mL/min) with a 5 °C/min heating rate using *ca.* 100 mg of the samples.

#### 4.3.3. *FT-IR spectroscopy*

To take the FT-IR spectra, a Bio-Rad Digilab Division FTS-65A/896 (mid-range spectra) instrument was used with 4 cm<sup>-1</sup> resolution. The 4000–600 cm<sup>-1</sup> wavenumber range were recorded with 256 scans for each spectrum, in ATR mode by utilizing a Harrick's single reflection diamond ATR accessory.

#### 4.3.4. *Raman spectroscopy*

Raman spectra were also collected for the study of inorganic structural elements by a Raman Senterra II (Bruker) microscope at an excitation wavelength of 765nm. 12.5 mW laser power was applied and 20 spectra with an exposition time of 20 s were averaged.

#### 4.3.5. *UV-Vis-NIR spectroscopy*

NIR and UV-Vis spectra were recorded on a SHIMADZU UV-3600i Plus UV-Vis-NIR spectrophotometer equipped with photomultiplier tube, InGaAs, and PbS detectors in the 50,000–6000 cm<sup>-1</sup> wavenumber range with 4 cm<sup>-1</sup> resolution recorded in reflection mode.

#### 4.3.6. *XP spectroscopy*

The XPS measurements were carried out with a SPECS instrument equipped with a PHOIBOS 150 MCD 9 hemispherical analyzer, under a main-chamber pressure in the high vacuum range (10<sup>-9</sup>–10<sup>-10</sup> mbar). The analyzer was in fixed analyzer transmission mode with 40 eV pass energy for the survey scan and 20 eV pass energy for the high-resolution scans. The powdered sample was pressed into an indium foil and loaded into the chamber on a gold-coated sample holder. The Al K $\alpha$  X-ray source was used at 14 kV and at 150 W power. Charge referencing

was done to the adventitious carbon (284.8 eV) on the surface of the sample. XP spectra were evaluated by the CasaXPS commercial software package.

#### 4.3.7. *TEM-EDS microscopy*

High resolution images from the morphology of the samples were taken by a Philips CM20 instrument running at an acceleration voltage of 200 kV, and a Cs-corrected scanning/transmission electron microscope of Themis instrument was used. The EDS mapping was monitored by Super-X detectors of the Themis instrument at 200 kV. The SAED patterns were evaluated using ProcessDiffraction software.<sup>175</sup>

#### 4.3.8. *Adsorption measurements*

Porosity and surface area studies were performed on a NOVA3000 instrument (Quantachrome, USA) gas adsorption system using nitrogen gas as the adsorbate. Porosity data were calculated by the Barrett–Joyner–Halenda method in the 0.05-0.35 relative pressure range. Before adsorption measurements, all the samples were outgassed under vacuum for 16 h at 25 °C. The specific surface areas were measured by the BET method by adsorption of N<sub>2</sub> at -196 °C. To remove any adsorbents from the surface of the samples, the samples were flushed with N<sub>2</sub> at 100 °C for 5 hours.

#### 4.3.9. *ICP-MS measurements*

The ICP-MS measurements were performed on an Agilent 7700× instrument. During the sample preparation, a few milligrams of the samples measured by analytical accuracy were dissolved in 1.0 mL of concentrated nitric acid, and then they were diluted with distilled water to 50 mL and then filtered prior to the measurements. For the quantitative analyses, multielement standard was used (Sigma-Aldrich).

#### 4.3.10. *Temperature programmed desorptions*

The basic sites were also characterized by using CO<sub>2</sub>-temperature programmed desorption (TPD) technique, carried out on a Hewlett-Packard 5890 GC system equipped with a TCD detector. *Prior to* the measurements, a quartz tube was loaded with a portion of the sample (100 mg) followed by an initial purge in a He stream (50 mL/min) at room temperature for 10 min to remove impurities. The temperature was then raised to 650 K using the ramp rate of 10 K/min and then held for 1 hour to remove water and other impurities. The temperature was then lowered to 373 K. Finally, the gas was changed to CO<sub>2</sub> in He (30 mL/min CO<sub>2</sub>, 50 mL/min He)

and circulated over the sample for 1 h. The gas was then removed from the sample by systematically increasing the temperature.

The surface acidity of the catalysts was characterized by  $\text{NH}_3$ -TPD. The samples were pre-treated as above to remove impurities and water. Ammonia was then adsorbed for 30 minutes. Finally, the sample was heated from room temperature to 823 K at a rate of 10 K/min and the desorbed gases were analyzed with a TC detector.

#### 4.3.11. GC-MS measurements

During the synthesis of phenothiazines, gas chromatographic measurements were carried out with a Thermo Scientific Trace 1310 Gas Chromatograph coupled with a Thermo Scientific ISQ QD Single Quadrupole Mass Spectrometer using a Thermo Scientific TG-SQC column (15m $\times$ 0.25mm ID $\times$ 0.25 $\mu$ m film). The operational parameters were as follows: column oven temperature: from 50 to 300 °C at 15 °C min<sup>-1</sup>; injection temperature: 240 °C; ion source temperature: 200 °C; electrospray ionization: 70 eV; carrier gas: He at 1.5 mL min<sup>-1</sup>; injection volume: 2  $\mu$ L; split ratio: 1 to 33.3; and mass range: 25–500 m/z. The starting materials, the products, and the undesirable byproducts were identified using reference samples.

#### 4.3.12. NMR spectroscopy

NMR spectroscopic measurements were carried out by a Bruker DRX500 instrument 500 MHz NMR spectrometer. Samples were dissolved in 0.7 mL of DMSO- $d_6$  or chloroform- $d$ , and  $^1\text{H}$  and  $^{13}\text{C}$  spectra were taken at room temperature. Spectra were evaluated by MestReNova-14.1.0-24037 with fixing internally to the remaining resonance of the DMSO- $d_6$  ( $^1\text{H}$ : 2.50 ppm,  $^{13}\text{C}$ : 39.52 ppm) or chloroform- $d$  ( $^1\text{H}$ : 7.26 ppm,  $^{13}\text{C}$ : 77.16 ppm).

### 4. 4. Catalytic reactions

#### 4.4.1. Optimal procedure for the synthesis of phenothiazine

2 mL mixture of DMSO and distilled water in ration of 1:2, the corresponding 2-iodoaniline or its derivatives (0.5 mmol, 1.0 equiv.), 2-bromobenzenethiol (0.55 mmol, 1.1 equiv.),  $\text{K}_2\text{CO}_3$  as the base (2.5 equiv.), and copper-containing bismutite as the catalyst (19 mg, corresponding to 5 mol % metal ion loading) were combined in a nitrogen-flushed Schlenk-tube equipped with a magnetic stirrer bar and was stirred continuously at 90 °C for 15h. Then, the mixture was cooled to room temperature, and the resultant liquid was extracted with 3x15 mL brine and 10 mL ethyl acetate. The organic layer was dried over  $\text{Na}_2\text{SO}_4$  and concentrated under reduced pressure. In order to find the mildest reaction conditions, the solvent, the temperature, the reaction time, the amount of the added base, and the catalyst loading were altered. In the

reusability study, the solid catalyst was removed after the reaction by filtration for five identical rounds. The conversion and the selectivity values were determined after each reaction by using gas chromatography coupled with mass spectrometry (GC–MS) and by NMR spectroscopy. In the scope, 2-iodoniline derivatives with different electron donating and -withdrawing functional group were screened under the optimized reaction conditions.  $^1\text{H}$  and  $^{13}\text{C}$  NMR spectra of phenothiazine and its derivatives are included in the appendix (**Appendix S1.**).

#### 4.4.2. *Optimal procedure for the synthesis of 2-phenylbenzimidazole*

2 mL mixtures of DMSO and distilled water in ratio of 1:9, the corresponding benzylamine or its derivative (0.5 mmol, 1 equiv.) and 2-aminoaniline (0.6 mmol, 1.2 equiv.) were combined in round-bottomed flasks equipped with a magnetic stirrer bar and a reflux condenser. The reaction mixtures were stirred for 8h at 90 °C with 10 mol% of  $\text{MnBi}_2\text{O}_2\text{CO}_3$  and at 110 °C with 2.5 mol% of  $\text{CoBi}_2\text{O}_2\text{CO}_3$ . Then, as the mixtures were cooled to room temperature, the resultant liquids were each extracted with 3x15 mL brine (saturated sodium-chloride solution) and 10 mL ethyl acetate. The organic layers were dried over  $\text{Na}_2\text{SO}_4$  and concentrated under reduced pressure. To find the mildest reaction conditions for the maximum achievable product yield, the solvent, the temperature, the reaction time and the catalyst loading were altered for both catalysts. Afterwards, the reusability of the catalysts were investigated in a 5-rounded consecutive reaction series. Between the identical reactions, the catalysts were filtered from the reaction mixtures.

The extensibility of heterocyclization was investigated from both reagents under optimized reaction conditions: by systematic pairing of benzylamine derivatives and 2-aminoaniline, 2-aminophenol or 2-aminothiophenol, different N-, O- and S-containing heterocycles were prepared. The conversion (C) and the selectivity (S) values were determined after each reaction by using NMR spectroscopy.  $^1\text{H}$  and  $^{13}\text{C}$  NMR spectra of 2-phenyl benzimidazole/oxazole/thiazole and their derivatives are included in the appendix (**Appendix S2.**).

#### 4.4.3. *Optimal procedure for oxidative azocoupling of anilines*

Aniline of 0.5 mL as reagent and solvent and the transition metal-containing bismutite of 10 mol% metal ion loading were combined in a round-bottomed flask equipped with a magnetic stir bar using a reflux condenser. The reaction mixture was stirred at 150 °C for 72h, then, the mixture was cooled down to room temperature, and the resultant liquid was extracted with 2x15 mL distilled water, 1x15 mL brine and 10 mL portion of ethyl acetate. The organic layer was dried over  $\text{Na}_2\text{SO}_4$  and concentrated under reduced pressure. To find the highest azo-product

yield, different solvents and solvent-free condition were investigated. During the scope, the corresponding aniline derivative (0.25 mmol, 1.0 equivalent) and the transition metal-containing bismutite as catalyst were combined in 0.5 mL aniline. The catalytic indicators were determined after each reaction by NMR spectroscopy.  $^1\text{H}$  and  $^{13}\text{C}$  NMR spectra of azobenzene and its derivatives are included in the appendix (**Appendix S3**).

#### 4.4.4. *Optimal procedure for synthesis of quinoline*

In the procedure for quinoline synthesis, 1 equiv. (0.5 mmol) aniline and 2 mL propane-1,3-diol were mixed in a round-bottom flask equipped with a magnetic stir bar and a reflux condenser with the catalyst powders of 10 mol% metal ion loading. The reaction mixtures were stirred for 72h at 150 °C immersed in a silicon oil bath. After the reaction time was over, the mixture was cooled down to room temperature, and was extracted with 2x15 mL distilled water, 1x15 mL brine and 10 mL ethyl acetate. Then, the organic layer was dried over  $\text{Na}_2\text{SO}_4$  and concentrated under reduced pressure. During the scope, the corresponding aniline derivatives (0.25 mmol, 1.0 equivalent) and the transition metal-containing bismutite as catalyst were combined in propane-1,3-diol of 0.5 mL. The catalytic indicators were determined after each reaction by NMR spectroscopy.  $^1\text{H}$  and  $^{13}\text{C}$  NMR spectra of quinoline and its derivatives are included in the appendix. (**Appendix S4**).

#### 4.4.5. *Optimal procedure for synthesis of quinoxaline*

For producing quinoxaline, the round-bottom flask was filled with 1 equiv. (0.5 mmol) 2-aminoaniline, 2 mL ethylene glycol and the corresponding bismutite catalyst of 10 mol% metal ion loading. The reaction mixtures were stirred for 24h hours with a magnetic stir bar in an oil bath of 110 °C, then the extracted samples (2x15 mL distilled water + 1x15 mL brine and 10 mL ethyl acetate) were concentrated under reduced pressure and analyzed by NMR spectroscopy. In the versatility study, the corresponding 2-aminoaniline derivative (0.25 mmol, 1.0 equiv.) and the transition metal-containing bismutites as catalysts were combined in 0.5 mL ethylene glycol. The catalytic indicators were determined after each reaction by NMR spectroscopy.  $^1\text{H}$  and  $^{13}\text{C}$  NMR spectra of quinoxaline and its derivatives are included in the appendix (**Appendix S5**).

#### 4.4.6. *Determination of catalytic indicators*

The catalytic indicators were determined after each reaction by gas chromatography MS (GC-MS) or by NMR spectroscopy based on the following equations:

$$(1) \quad C_{\text{starting material}} = \frac{n_{(0)} \text{ starting material}}{n_{(0)} \text{ starting material} - n_{(t)} \text{ starting material}} \times 100$$

$$(2) \quad S_{\text{product}} = \frac{n_{(t)} \text{ product}}{n_{(t)} \text{ product} + n_{(t)} \text{ by-product(s)}} \times 100$$

$$(3) \quad Y_{\text{product}} = S_{\text{product}} \times C_{\text{product}}$$

where C is the conversion of the starting materials, S and Y are the selectivity and yield of the desired products,  $n_0$  is the corresponding initial volume of the reactants/products while  $n_t$  is the corresponding volume of the reactants or products at a given time.

## 5. RESULTS AND DISCUSSION

### 5.1. Characterization

The previously reported, new silver(I) modified Sill  n-type bismutite structural analog was synthesized with the urea hydrolysis method in which the amount of hydroxide and carbonate anions required for precipitation is provided by the controlled hydrolysis of urea.<sup>134</sup>

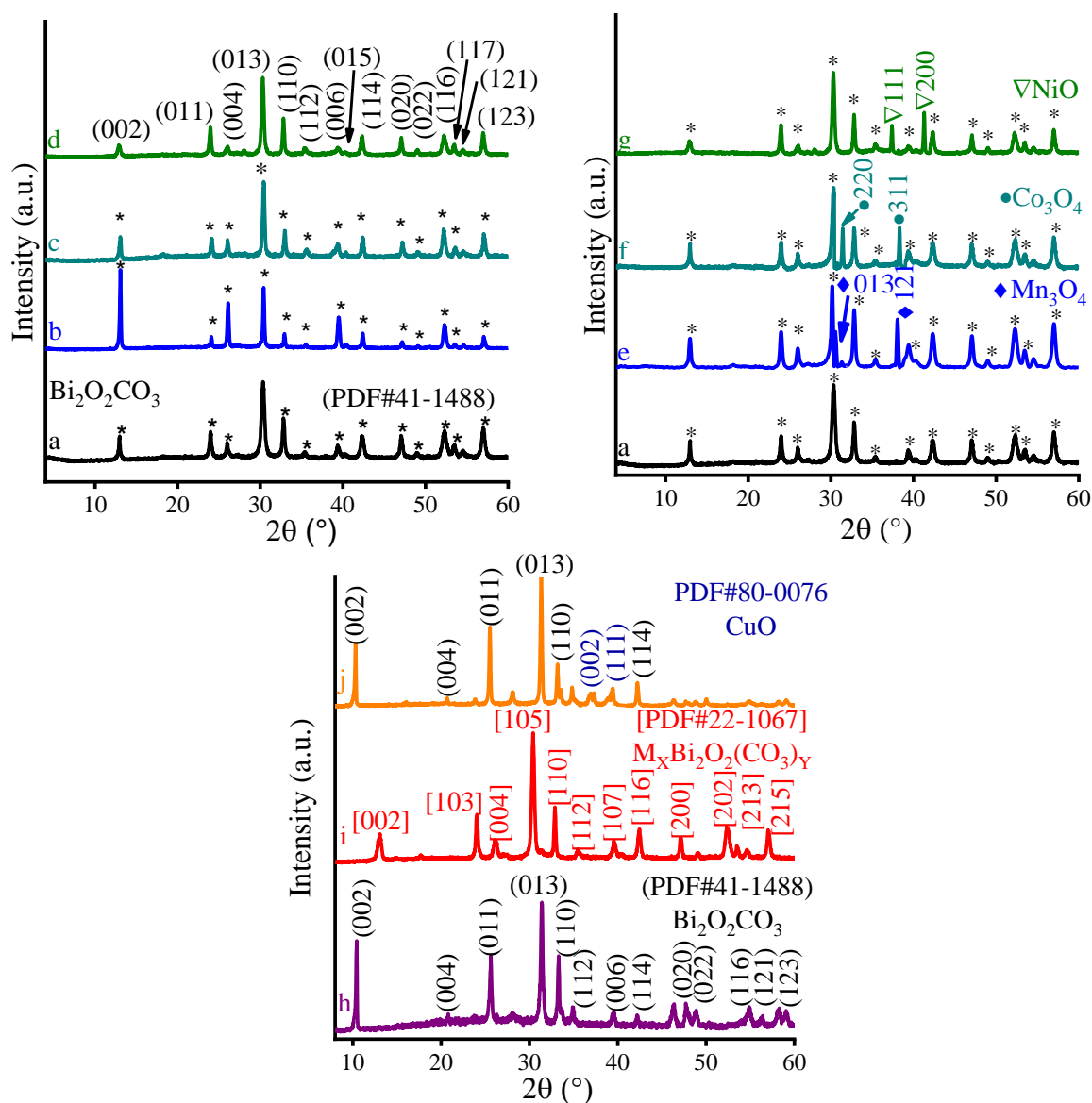


**Figure 3.** XRD patterns of  $\text{Bi}_2\text{O}_2\text{CO}_3$  (a),  $\text{MnBi}_2\text{O}_2\text{CO}_3$  (b),  $\text{CoBi}_2\text{O}_2\text{CO}_3$  (c),  $\text{NiBi}_2\text{O}_2\text{CO}_3$  (d),  $\text{Mn-Bi}_2\text{O}_2\text{CO}_3$  (e),  $\text{Co-Bi}_2\text{O}_2\text{CO}_3$  (f),  $\text{Ni-Bi}_2\text{O}_2\text{CO}_3$  (g),  $\text{Bi}_2\text{O}_2\text{CO}_3$  (80 C) (h),  $\text{CuBi}_2\text{O}_2\text{CO}_3$  (i),  $\text{Cu-Bi}_2\text{O}_2\text{CO}_3$  (j).<sup>176</sup>

Following the successful preliminary experiments with urea hydrolysis, the syntheses of copper-, manganese-, cobalt- and nickel modified structures were carried out directly with the addition of a specific concentration of ammonia and sodium-carbonate solutions in a modified co-precipitation method. Each co-precipitated sample was compared with an

impregnated reference sample prepared by wet impregnation of the corresponding TM salt solution and a bismutite support. (**Fig. 3.**) The exact reaction conditions of the syntheses are described in detail in the Experimental Part. Noteworthy, for reproducible synthesis of copper-containing samples, lower reaction temperature had to be used (80°C) than for other transition metal-containing samples (100°C). However, repeating the synthesis of pure bismutite at 80°C for comparison, this also led to the alteration of the structure of the pure bismutite, probably due to the changes generated in its water content. Accordingly, the analysis of copper-containing structures and the corresponding as-prepared bismutite can be found separately from others.

All of the obtained materials have the same, well-crystallized structure – except for the copper-impregnated bismutite and the as-prepared bismutite at 80°C – with a primary particle size of about 18.2–50.2 nm, as calculated by Scherrer equation. The diffraction peaks appeared at 13.1, 24.1, 26.1, 30.4 and 32.9° are related to the (002), (103), (004), (105) and (110) planes of the tetragonally structured bismuth–subcarbonate ( $\text{Bi}_2\text{O}_2\text{CO}_3$ ; PDF#41-1488)<sup>177</sup> (Powder Diffraction File from the International Center for Diffraction Data (ICDD) database). Moreover, these diffractograms are identical to the diffractogram of silver-containing bismutite.<sup>134,135</sup> Based on Bragg equation, the interlamellar distance between the layers in plane 002 is 0.68 nm. Diffraction peaks detected at 10.5, 25.6, 31.4 and 33.2° 2 $\theta$  positions (**Fig. 3. h, j**) indicating also the formation of bismutite structure but with expanded interlayer distance. On the basis of previous studies, it is known that carbonate ions and water molecules reside in the interlayer space resulting in increase of the interlayer distance.<sup>178</sup> (TG/DTG measurements on bismutite verified this, since 12.5% total weight loss was observed compared to a theoretical loss of 8.5%.<sup>178</sup>) Consequently, copper species could be intercalated into the interlamellar gallery of bismutite causing the distortion of its tetragonal structure that comes along with a shift of the characteristic reflections (**Fig. 3. I**).

For the impregnated reference, intense reflections of a separate crystallized phase that can be associated with the corresponding metal oxides ( $\text{CuO}$  (PDF#80-0076),<sup>179</sup>  $\text{Mn}_3\text{O}_4$  (PDF#24-0734)<sup>180</sup>,  $\text{Co}_3\text{O}_4$  (PDF#42-1467)<sup>181</sup> and  $\text{NiO}$  (PDF#47-1049)<sup>182</sup>) can also be identified in addition to the identified bismutite phase. On the contrary, for co-precipitated solids, no other crystalline phase could be detected which can be considered as evidence for the incorporation of the TM samples into the bismutite framework and/or the precipitation of oxide nanoparticles on the surface of the bismutite host. In the following, for the easier follow-up, the formula  $\text{MBi}_2\text{O}_2\text{CO}_3$  always denotes TM-containing samples synthesized by co-precipitation, regardless



of the oxidation state of the metallic components, while the formula  $M\text{-Bi}_2\text{O}_2\text{CO}_3$  refers to the impregnated reference compounds.

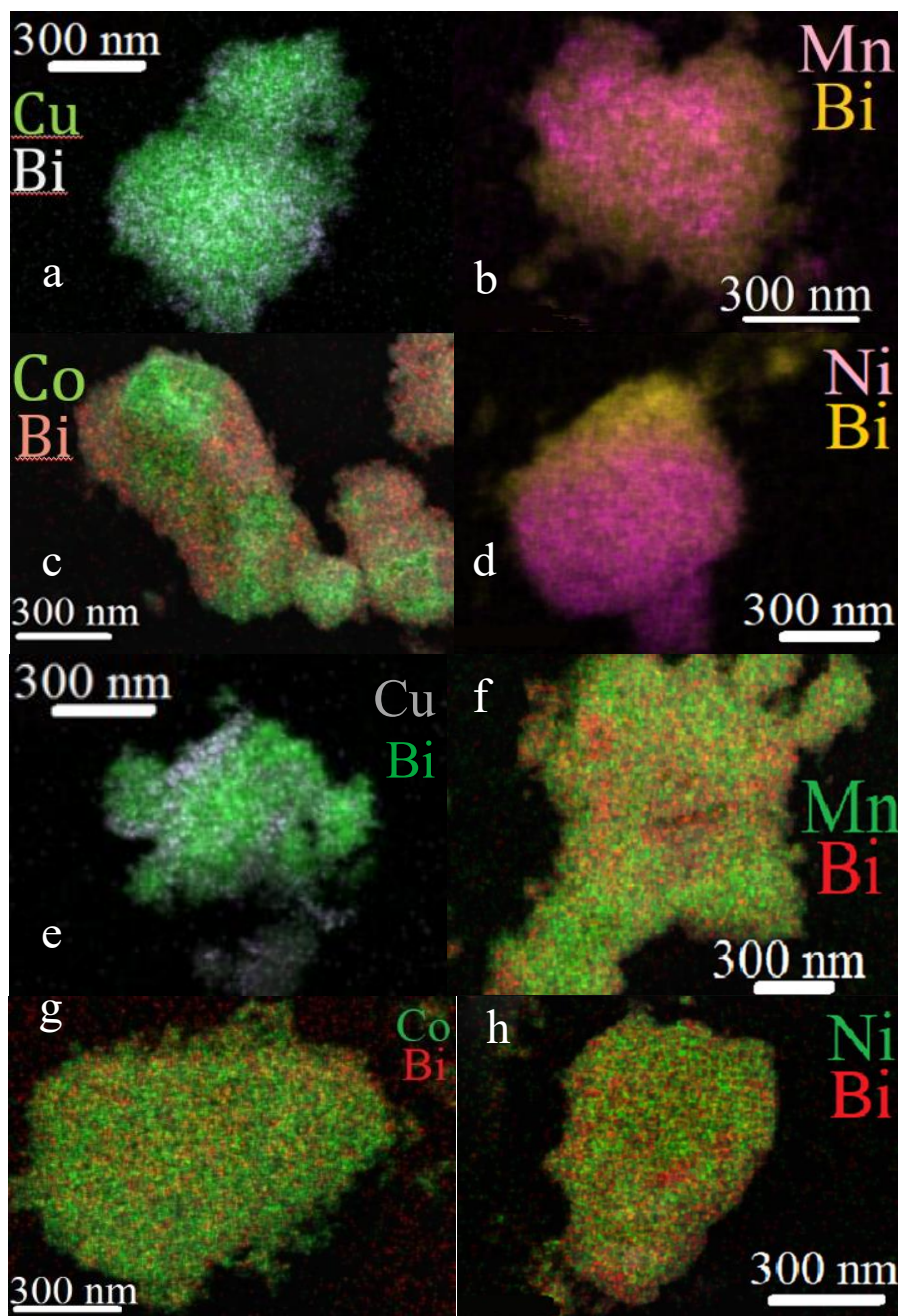


**Figure 4.** Elemental maps of  $\text{CuBi}_2\text{O}_2\text{CO}_3$  (a),  $\text{MnBi}_2\text{O}_2\text{CO}_3$  (b),  $\text{CoBi}_2\text{O}_2\text{CO}_3$  (c),  $\text{NiBi}_2\text{O}_2\text{CO}_3$  (d),  $\text{Mn-Bi}_2\text{O}_2\text{CO}_3$  (e),  $\text{Co-Bi}_2\text{O}_2\text{CO}_3$  (f),  $\text{Ni-Bi}_2\text{O}_2\text{CO}_3$  (g) detected by scanning electron microscope (co-precipitation: a–d, wet impregnation: e–h).<sup>176</sup>

Contrary to the optimistic assumption based on the XRD results, the energy dispersive X-ray fluorescence (**Fig. 4.**) did not confirm the basic hypothesis that the same structure differing in TM content was obtained after each synthesis. The corresponding elemental maps of the as-prepared solids showed a homogeneous spatial distribution for the copper ions, but a heterogeneous distribution for manganese, cobalt and nickel species. Besides, homogeneously

distributed TM and bismuth ions were found for the impregnated references. Consequently, the structural characterizations are presented in two parts: first, the structural features of copper-containing bismutite, then the characteristics of manganese-, cobalt-, and nickel-containing systems.

### 5.1.1. Structural and analytical analysis of $\text{CuBi}_2\text{O}_2\text{CO}_3$

To quantify the exact chemical composition of copper-modified bismutite, ICP-MS measurement was combined with TG/DTG analysis (**Fig. 5.** and **Table 9.**)

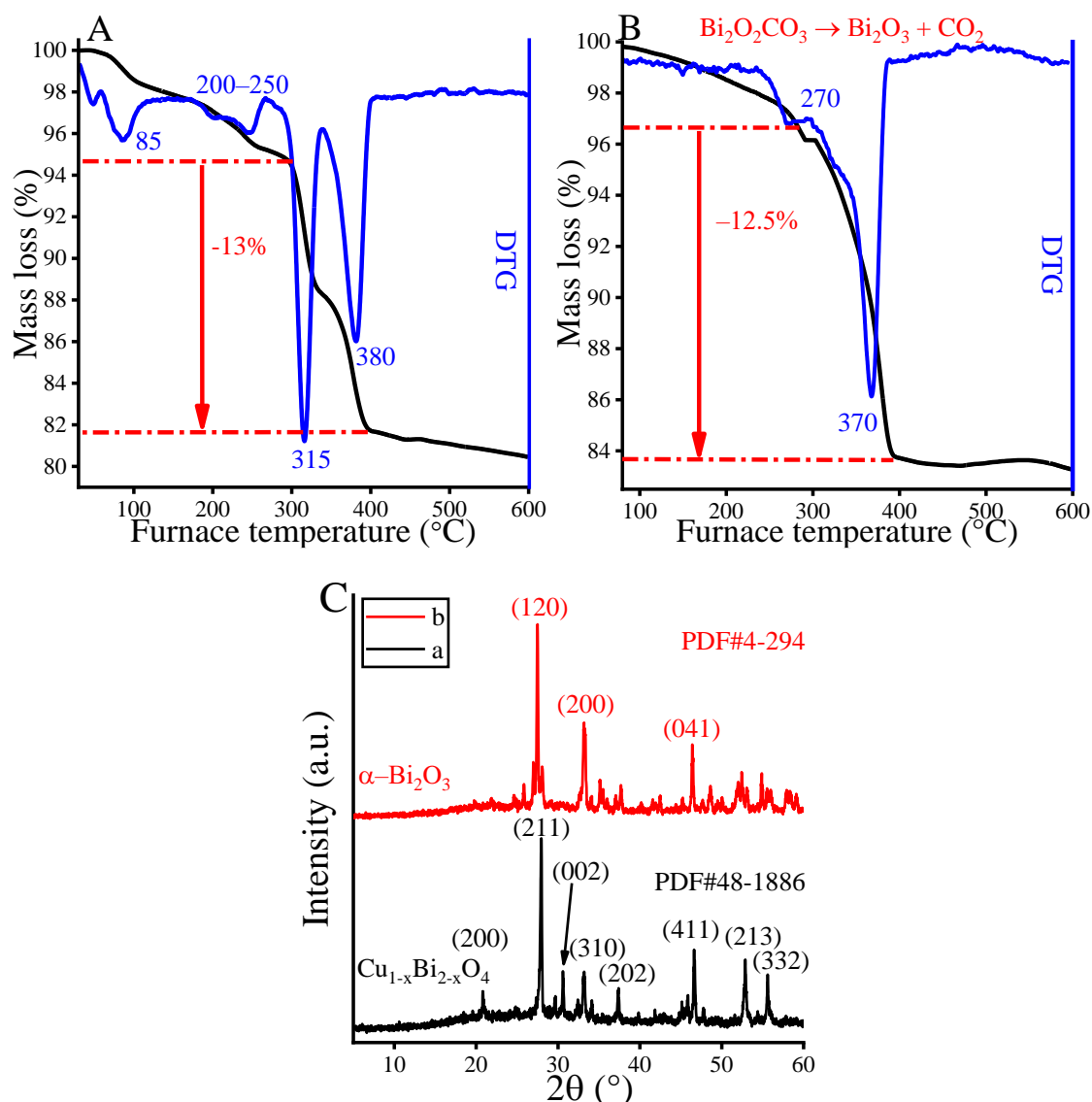


**Figure 5.** Thermogravimetric behavior of  $\text{CuBi}_2\text{O}_2\text{CO}_3$  (A) and  $\text{Bi}_2\text{O}_2\text{CO}_3$  (B) and XRD patterns (C) of  $\text{CuBi}_2\text{O}_2\text{CO}_3$  (a) and  $\text{Bi}_2\text{O}_2\text{CO}_3$  (b) after heating on 600 °C.<sup>176</sup>

Using ICP-MS, the actual Cu/Bi molar ratio was determined to be 0.25. The TG curves exhibited four well-separated weight losses. The first two (50–85 and 200–250 °C) were attributed to the removal of water molecules. The first loss corresponds to weakly adsorbed water molecules on the outer surface of the material, while the second loss is due to the removal

of interlayer water molecules, similar to what is observed in layered double hydroxides.<sup>183</sup> The incorporation of water molecules into the Sillén-type superstructure has not been reported so far, so their occurrence can be interpreted as evidence for the incorporation of copper ions into the framework. The other two weight losses can be attributed to the elimination of carbonate ions and/or the hydroxyl groups intercalated among the layers.

The observed thermogravimetric behavior is similar to that of malachite, a hydroxyl-carbonate double salt of copper(II). Above 300 °C, both the hydroxyl groups and the carbonate ions were lost, resulting in two mass losses in the narrow temperature range of 310–380 °C. This assumption was verified by evolved gas analysis (EGA) with a TG-MS instrument, as complete dehydroxylation of framework-modified bismutite occurred up to 350 °C, which is in good agreement with the weight loss for malachite.<sup>184</sup>

**Table 9.** Thermogravimetric analysis of  $\text{Bi}_2\text{O}_2\text{CO}_3$  and  $\text{CuBi}_2\text{O}_2\text{CO}_3$  structures.<sup>176</sup>

Sample	Original formula*	Temperature range (°C)	Leaving species	Mass loss (%)	Formula of the obtained solids
$\text{Bi}_2\text{O}_2\text{CO}_3$	$\text{Bi}_2\text{O}_2(\text{CO}_3)_x \times n \text{H}_2\text{O}$	25–300	$\text{H}_2\text{O}$	4	$\text{Bi}_2\text{O}_2(\text{CO}_3)_x$
		300–400	$\text{CO}_3^{2-}$	12.5	$\alpha\text{-Bi}_2\text{O}_3^2$
$\text{CuBi}_2\text{O}_2\text{CO}_3$	$\text{Cu}_{0.5}\text{Bi}_2\text{O}_2(\text{CO}_3)_{1.25}(\text{OH})_{0.5} \times n \text{H}_2\text{O}$	25–200	$\text{H}_2\text{O}$	2.5	$\text{Cu}_{0.5}\text{Bi}_2\text{O}_2(\text{CO}_3)_{1.25}(\text{OH})_{0.5}$
		200–280	$\text{H}_2\text{O}/\text{OH}$ –	2.8	$\text{Cu}_{0.5}\text{Bi}_2\text{O}_2(\text{CO}_3)_{1.25}(\text{OH})_{0.5-x}$
		290–350	$\text{OH}^-$		
		310–400	$\text{CO}_3^{2-}$	13	$\text{Cu}_2\text{Bi}_2\text{O}_5 + \text{Bi}_2\text{O}_3(\text{CO}_3)_x$
		400–600	$\text{CO}_3^{2-}$	1	$\text{Bi}_{2+x}\text{Cu}_{1-x}\text{O}_4^{**}$

\* Actual molar ratio of metal ions was determined by ICP–MS; \*\* confirmed by XRD

When the temperature was increased, phase-pure, non-stoichiometric copper-bismuth mixed oxide formed at 600 °C after the layered structure collapsed, as confirmed by XRD (**Fig. 5.**; PDF#48-1886).<sup>185</sup> The scale of mass loss showed significant differences between framework-modified bismuth and malachite, as the only significant weight loss of pure bismutite (**Fig. 5. B**)<sup>178</sup> overlapped with a two-step loss of malachite. Assuming a coordination sphere similar to the microstructure of malachite around the copper ions, corresponding to the measured actual molar ratio of the cations, the possible composition of the product could be offered as  $\text{Cu}_{0.5}\text{Bi}_2\text{O}_2(\text{CO}_3)_{1.25}(\text{OH})_{0.5} \times n \text{H}_2\text{O}$ . The theoretical weight loss of copper-bismutite based on this formula is 1.5% for the strongly bound OH units and 10% for the  $\text{CO}_2$ , giving a total loss of 11.5%. The measured actual weight loss of the composite, due to decomposition of the hydroxyl and carbonate groups at 300–400 °C, is 13%, which is very close to the theoretical values.

The Raman and UV-DR spectra of the as-prepared composites convincingly proved the incorporation of copper ions and their local structures (**Fig. 6**). In all Raman spectra, four relatively sharp, intense peaks can be related to the bismutite framework. Two of them, at  $71\text{ cm}^{-1}$  and  $162\text{ cm}^{-1}$ , can be attributed to the external vibrations of the  $[\text{Bi}_2\text{O}_2]^{2+}$  layer, one, at  $358\text{ cm}^{-1}$ , is from the Bi-anion stretching vibration mode, and the last one, at  $1060\text{ cm}^{-1}$ , is assigned to  $\nu_2$  out of plane bending mode vibration of the carbonate anions.<sup>186</sup>

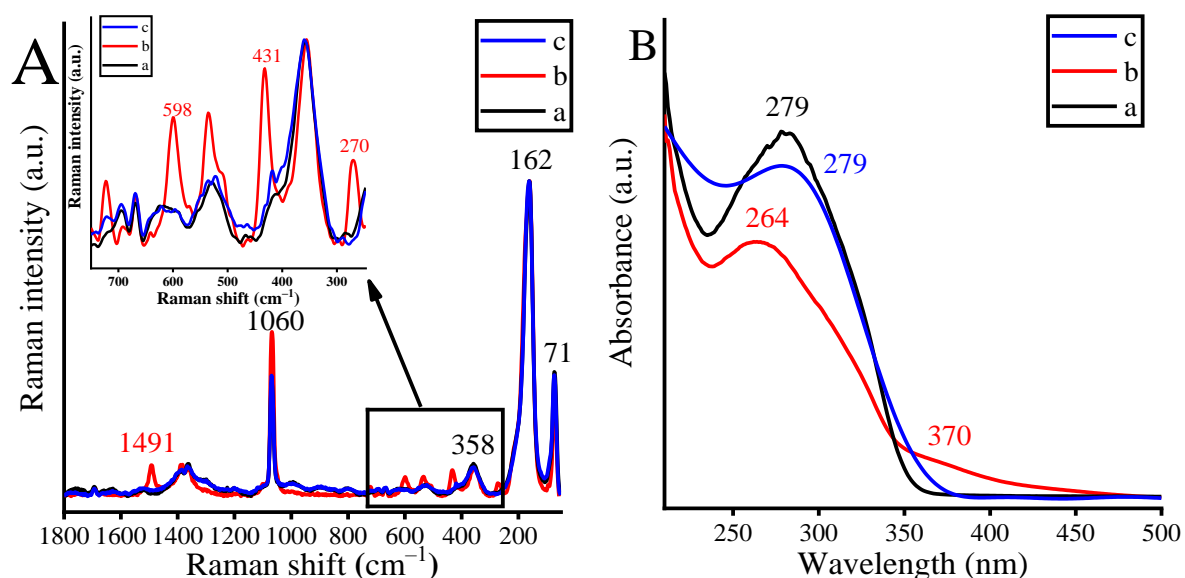


**Figure 6.** Raman (A) and UV-DRS (B) spectra of  $\text{Bi}_2\text{O}_2\text{CO}_3$  (a),  $\text{CuBi}_2\text{O}_2\text{CO}_3$  (b) and  $\text{Cu-Bi}_2\text{O}_2\text{CO}_3$  (c).<sup>176</sup>

No significant changes were observed in the Raman spectrum of the impregnated reference due to the absorption of 10% CuO on the surface of pure bismutite. However, after incorporation of copper ions into the framework, the Raman spectrum showed well-separated relatively intense peaks at 270, 431, 598 and  $1491\text{ cm}^{-1}$ , which can be considered as markers for the incorporation of copper ions with malachite-like microstructure. The vibration frequencies below  $600\text{ cm}^{-1}$  are related to the stretching vibration modes of Cu–O ( $598\text{ cm}^{-1}$ ) and Cu–OH ( $431\text{ cm}^{-1}$ ), and the bending vibration mode of the OCu–OH unit ( $270\text{ cm}^{-1}$ ) in a malachite-like structure, which were found at almost identical positions as in pure malachite<sup>187</sup>. The band at  $1491\text{ cm}^{-1}$  identified as the  $\nu_3$  vibration band of the carbonate group is shifted compared to  $\sim 1400\text{ cm}^{-1}$  detected in pure bismutite.

These assignments are further evidence that the first coordination sphere of the intercalated copper is similar to that of malachite. As with the Raman measurements, no remarkable changes in the optical properties of bismutite-supported CuO were observed at UV-DRS compared to pure bismutite. In contrast, the position of the absorption maximum in the UV range of the framework-modified bismutite is shifted to lower wavelengths ( $279\text{ nm} \rightarrow$

264 nm). In addition, a new absorption peak can be seen at 370 nm, which can probably be assigned to the d-d electron transition between Cu(II) cations and conduction band electrons of the bismuth subcarbonate.<sup>188</sup>

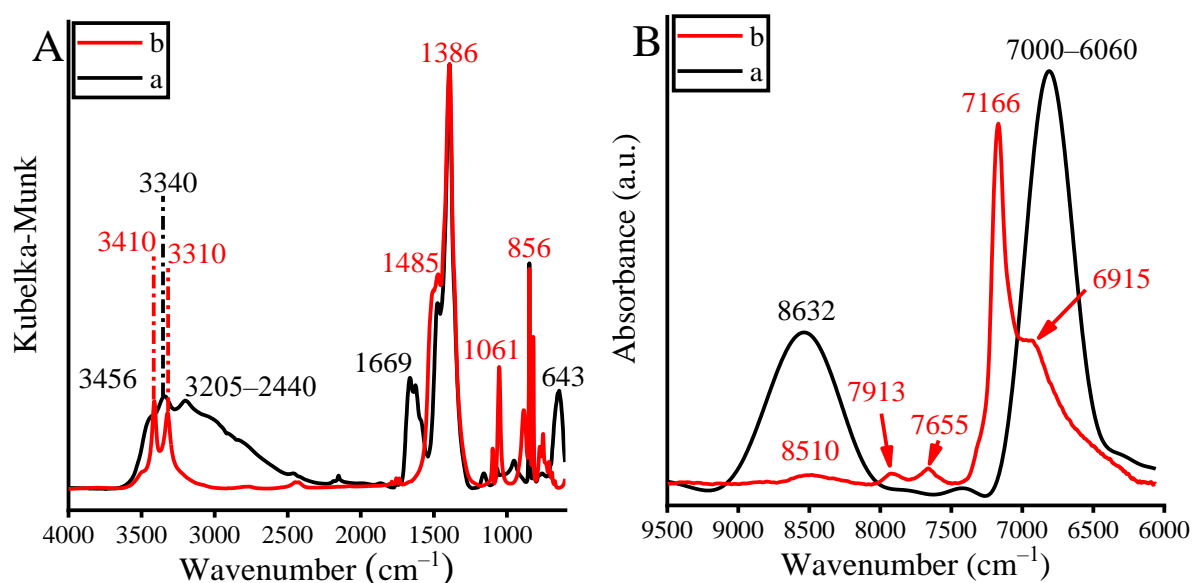


**Figure 7.** Comparison of mid- (A) and near- (B) infrared spectra of Bi<sub>2</sub>O<sub>2</sub>CO<sub>3</sub> (a) and CuBi<sub>2</sub>O<sub>2</sub>CO<sub>3</sub> (b).<sup>176</sup>

The mid and near-infrared spectra of the pristine and the framework-modified bismutite (**Fig. 7.**) demonstrate the different roles of the hydroxyl groups/water molecules in the structures. In the pure bismutite, the water molecules are involved in a large-scale hydrogen bonding system, whereas in the framework-modified CuBi<sub>2</sub>O<sub>2</sub>CO<sub>3</sub>, coordinating hydroxide anions are more likely to be found.

Most of these intense absorption bands are seen in the mid-infrared region (4000 – 600 cm<sup>-1</sup>) and are mainly related to the stretching mode vibrations of the carbonate group ( $\nu_1$ : 836 cm<sup>-1</sup>;  $\nu_3$ (interlayer): 1386 cm<sup>-1</sup> and  $\nu_3$ (surface): 1485 cm<sup>-1</sup>), which is consistent with what was previously reported for pristine bismutite.<sup>186</sup> The appearance of the band at 1061 cm<sup>-1</sup>, attributed to the  $\nu_1$  stretching mode vibration of the carbonate ions is possible if the symmetry of the carbonate ions are D<sub>3h</sub>.<sup>189</sup> This condition can only be fulfilled if there is no interaction between (part of) the carbonate ions and the oxide layers. The absorption peak of this band is lost after the successful intercalation of the copper species, while a new absorption band appears at 643 cm<sup>-1</sup> attributed to the symmetric stretching mode vibration of the Cu–O bond.<sup>190</sup> Based on these results, the copper species most likely replaced the weakly bound carbonate ions among the layers.

The absorption peaks in the range 4000–2500 cm<sup>-1</sup> are assigned to the stretching mode vibrations of lattice water molecules and OH groups: The broad band around 3450 cm<sup>-1</sup> belongs



to free or defect water which can readily overlap with the bridging and H-bonded modes of water molecules at 3300 and 3200–2500  $\text{cm}^{-1}$ . This assignment fully describes the OH- region of the pristine bismutite, which reflects the adsorption of water molecules.<sup>186</sup> Absorption bands of the M–OH bond can be observed at 7166 and 6915  $\text{cm}^{-1}$  for the copper-modified sample. These vibrations are accompanied by the appearance of very sharp, well-localized bands around 3300–3400  $\text{cm}^{-1}$  with no significant broadening.<sup>190,191</sup> Investigating the spectral data in the wavenumber range of 9500–7300  $\text{cm}^{-1}$ , further significant spectral differences can be seen, which can be attributed to electron transitions between the composites. However, there is not yet enough information to interpret these differences.

In the transmission electron micrographs (**Fig. 8. A-C**), a typical Sill  n-like layered structure with regular nanoplate-like morphology can be seen for both the pristine bismutite and the copper-loaded material. The samples consisted of monodisperse nanospheres with uniform particle size of about 150 nm. The interlayer distances ( $d_{001}$ ) were estimated to be 0.661 and 0.785 nm for  $\text{CuBi}_2\text{O}_2\text{CO}_3$  and  $\text{Bi}_2\text{O}_2\text{CO}_3$ , respectively, which were in good agreement with the values calculated from the XRD results. The combined TEM/EDX analysis (**Fig. 8. D-F**) also confirmed the very homogeneous distribution of copper (and bismuth) without measurable clusters or non-integrated species.

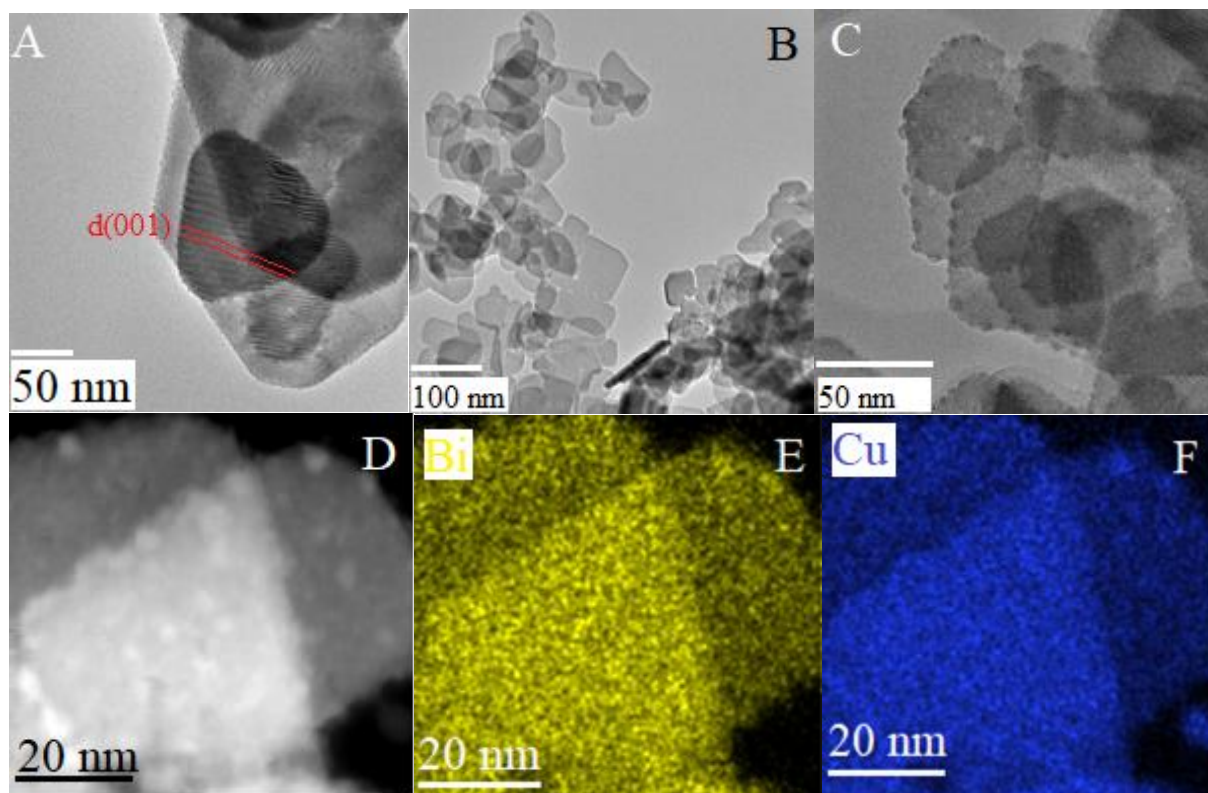


**Figure 8.** TEM images of (A)  $\text{Bi}_2\text{O}_2\text{CO}_3$  and (B, C)  $\text{CuBi}_2\text{O}_2\text{CO}_3$  and elemental maps of  $\text{CuBi}_2\text{O}_2\text{CO}_3$  (D–F).<sup>176</sup>

XPS studies carried out to validate the information on the copper microstructure and to determine the surface compositions and chemical states on the bismutite structures. The survey scans showed the incorporation of the expected elements (Bi, C, O and/or Cu) with a minor Na-contamination for  $\text{Bi}_2\text{O}_2\text{CO}_3$  (**Fig. 9**). Only one component was required in both samples to fit the Bi 4f spectra. The measured binding energies and the separation of the 4f bands verified the presence of Bi(III) ions on the surfaces of pristine and copper-loaded bismutite. It is worth noting that a higher binding energy was observed for the modified bismutite compared to the values reported for the pure bismutite.<sup>178,192</sup>

In addition, there were significant shifts in the binding energies following the incorporation of copper cations, suggesting that the copper was indeed incorporated into the framework. The C 1s spectra of the samples consisted mainly of three regions. In general, the binding energies around 285 eV accounted for hydrocarbons, while the peak with a binding energy above 286 eV was assigned to unidentified carbon–oxygen species. The peaks with a binding energy of ~288.5 eV indicate that carbonate ions from the subcarbonate were also inserted into the structures, and with copper insertion, remarkable shifts in the binding energy of the carbonate–C 1s transition could be detected in the copper-modified sample. In contrast to the literature data, only two components should be used to fit the O 1s region of the samples.

One of them has the characteristic binding energy for the Bi–O bond, while the other could be attributed to the Bi–CO<sub>3</sub> linkage. The Cu 2p region of  $\text{CuBiO}_2\text{CO}_3$  could be fitted with a  $2p_{3/2}$  peak at 933.53 eV, and a strong satellite feature at 941.42 eV. Accordingly, the presence of Cu(II) ions near the surface could be detected in the same chemical environment. Overall, the surface analysis confirmed all the above-mentioned structural features associated with bismutite analogue structures, clearly demonstrating the success of Cu(II) incorporation.<sup>193</sup>

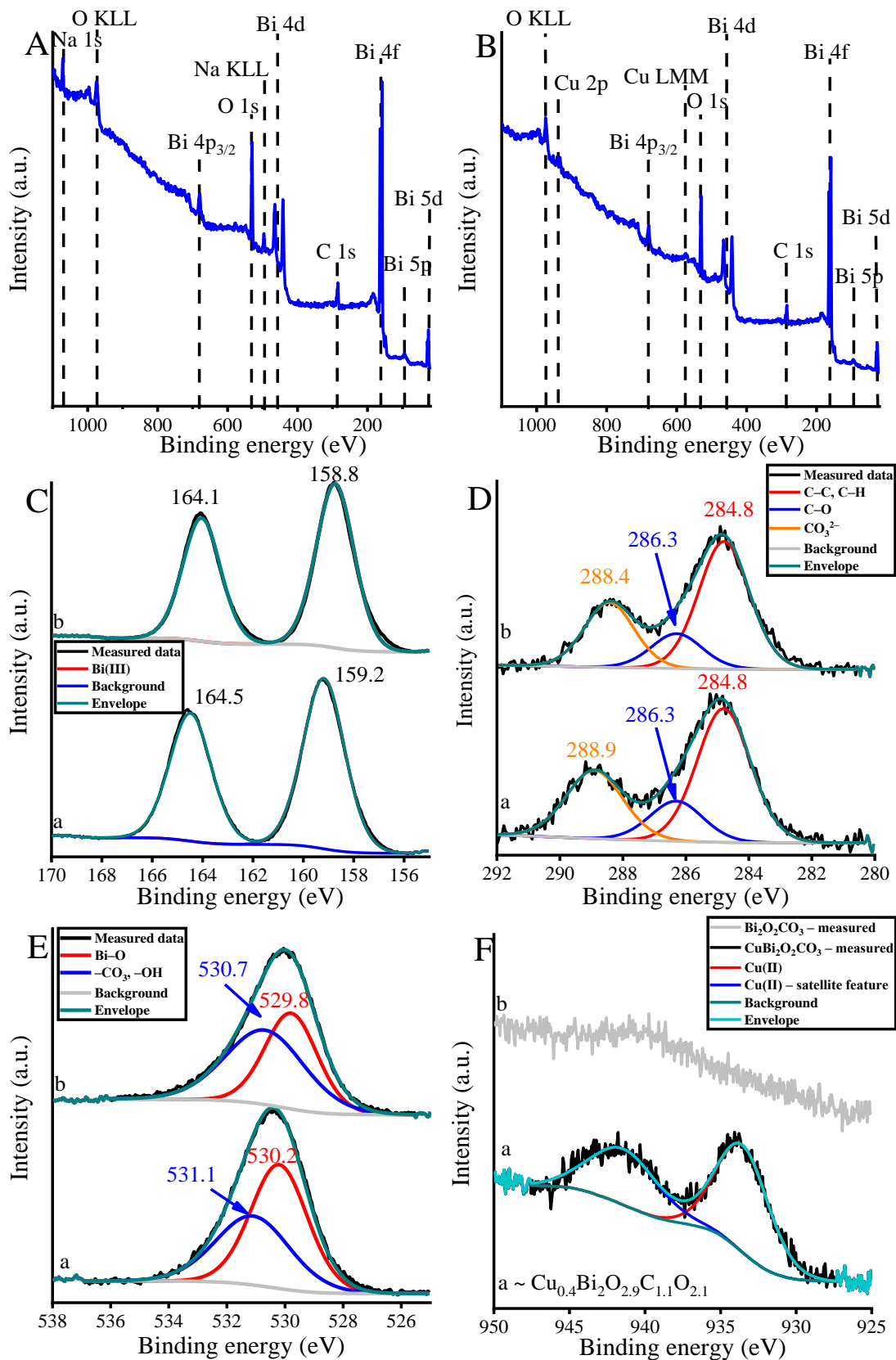


**Figure 9.** XPS survey scans of  $\text{Bi}_2\text{O}_2\text{CO}_3$  (A) and  $\text{CuBi}_2\text{O}_2\text{CO}_3$  (B) and Bi 4f (C), C 1s (D), O 1s (E) and Cu 2p<sub>3/2</sub> (F) XP spectra of  $\text{CuBi}_2\text{O}_2\text{CO}_3$  (a) and  $\text{Bi}_2\text{O}_2\text{CO}_3$  (b).<sup>176</sup>



Finally, **Table 10.** compares the most probable surface composition of the framework-modified copper-bismutite composite calculated from the XPS data with the bulk composition based on analytical measurements (ICP-MS, TG/DTG).

**Table 10.** The most probable compositions of copper-modified bismutite composite

Original formula	Surface composition*	Bulk composition**	Specific surface area (m <sup>2</sup> /g)***
CuBi <sub>2</sub> O <sub>2</sub> CO <sub>3</sub>	Cu <sub>0.4</sub> Bi <sub>2</sub> O <sub>2.9</sub> C <sub>1.1</sub> O <sub>2.1</sub>	Cu <sub>0.5</sub> Bi <sub>2</sub> O <sub>2.5</sub> C <sub>1.25</sub> O <sub>3.75</sub> H <sub>0.5</sub>	12

\* by XP spectroscopy

\*\* by ICP-MS, TG/DTG

\*\*\* by N<sub>2</sub> adsorption

From this it can be clearly deduced that the composition of the surface is almost identical to that determined for the bulk, so that copper-containing bismutite does not show any surface enrichment with copper.

#### 5.1.2. Structural and analytical analysis of Mn/Co/NiBi<sub>2</sub>O<sub>2</sub>CO<sub>3</sub>

Since the oxide phases belonging to the corresponding transition metals did not appear in the diffractograms of the co-precipitated samples, it can be assumed that the modifying elements were successfully incorporated into the bismutite framework, even if not by intercalation. However, since the spatial distribution of the manganese, cobalt and nickel ions was heterogeneous, it was necessary to investigate in which way and in which form the transition metal specimens are fixed on the surface of the support, and how this may affect the catalytic activity of the whole systems. Therefore, the samples produced by wet impregnation were used as references, where the TM oxides were most likely fixed to the surface of the host by weak intermolecular bonds. Let us remember, the formula MBi<sub>2</sub>O<sub>2</sub>CO<sub>3</sub> denotes the samples produced by co-precipitation, while the formula M–Bi<sub>2</sub>O<sub>2</sub>CO<sub>3</sub> marks the impregnated references.

The combination of ICP-MS and TG/DTG measurements (**Table 11).** and **Fig. 10.**), confirmed the anchoring of the TM specimens in/on the host bismutite, but also showed large differences in the composition of the samples. The actual molar ratio of transition metals and bismuth ions or the water/hydroxide content of the solid samples depended on the quality of the guest molecules and the synthesis method used. We should also bear in mind that pure bismutite synthesized at 100°C is different from that synthesized at 80°C presented in the previous section. This is closely related to the non-negligible changes in the water/carbonate content of these samples. This is in good agreement with the XRD results which showed that the extent of the interlamellar region of the pure samples depends on the synthesis parameters.

**Table 11.** Molar ratios of the metallic components in Mn/Co/Ni modified bismutites and thermogravimetric analysis of the as-prepared Mn/Co/Ni modified bismutite structures<sup>194</sup>

Composite	Initial Bi:M ratio	Actual Bi:M* ratio	Original formula	T(°C)	Leaving species	Mass loss (%)	Formula of the obtained solids
$Bi_2O_2CO_3$	—	—	$(BiO)_2(CO_3)_{0.8}$ $7(OH)_{0.4}$	25–300 300–400	$H_2O$ $CO_3^{2-}/OH^-$	4 10	$\alpha-Bi_2O_3$
$Mn-Bi_2O_2CO_3$		7.8	$Mn_{0.26}O_{0.35}/$ $(BiO)_2(CO_3)_{0.8}$ $5(OH)_{0.60}$	25–300 300–400	$H_2O$ $CO_3^{2-}/OH^-$	4 11	$MnO_2-$ $\alpha-Bi_2O_3$
$Ni-Bi_2O_2CO_3$	0.5	13.0	$Ni_{0.64}O_{0.64}/$ $(BiO)_2(CO_3)_{0.8}$ $9(OH)_{0.55}$	25–300 300–400	$H_2O$ $CO_3^{2-}/OH^-$	4 11	$NiO-$ $\alpha-Bi_2O_3$
$Co-Bi_2O_2CO_3$		3.1	$Co_{0.15}O_{0.20}/$ $(BiO)_2(CO_3)_{0.8}$ $3(OH)_{0.58}$	25–300 300–400	$H_2O$ $CO_3^{2-}/OH^-$	4 11	$Co_3O_4-$ $\alpha-Bi_2O_3$
$MnBi_2O_2CO_3$		8.3	$Mn_{0.24}(BiO)_2$ $(CO_3)_{1.05}(OH)_{0.35}$	25–400 400–500	$H_2O$ $CO_3^{2-}/OH^-$	4 13	$MnO_2-$ $\alpha-Bi_2O_3$
$NiBi_2O_2CO_3$	1.0	14.3	$Ni_{0.66}(BiO)_2$ $(CO_3)(OH)_{4.47}$	25–250 250–600	$H_2O/OH^-$ $CO_3^{2-}/OH^-$	6 7	$NiO-$ $\alpha-Bi_2O_3$
$CoBi_2O_2CO_3$		3.0	$Co_{0.14}(BiO)_2$ $(CO_3)_{1.08}(OH)_{0.98}$	25–150 150–270 270–370 370–600	$H_2O$ $H_2O/OH^-$ $CO_3^{2-}/OH^-$ $CO_3^{2-}$	6 5 7 2	$Co_3O_4-$ $\alpha-Bi_2O_3$

\*M: Mn, Co, Ni; determined by ICP-MS

In general, lower levels of transition metals were found in the co-precipitated samples than in the impregnated references, although the initial ratio of metal ions was exactly the same. On the other hand, the binding affinity was independent of the synthesis method: the content of metal ions to be fixed decreased in the order  $Ni \gg Mn > Co$ . (For comparability, the ratios that led to the formation of impregnated composites with almost the same metal ion molar ratio as in the co-precipitated counterparts were chosen for the syntheses of the references.)

**Fig. 10.** and **Table 11.** show the large variations in the water/hydroxide content of the solid samples compared to pure bismutite. While the water/hydroxide content of the co-precipitated Sillén structures increased when nickel- and cobalt were used, no significant changes were observed, when manganese was used as a dopant. In contrast, neither the amount of hydroxyl ions nor the carbonate content showed comparable changes in the three impregnated samples.

TG/DTG curves of the co-precipitated samples (**Fig. 10. B-D**) illustrate the variations in the number of endothermic peaks depending on the guest molecules.

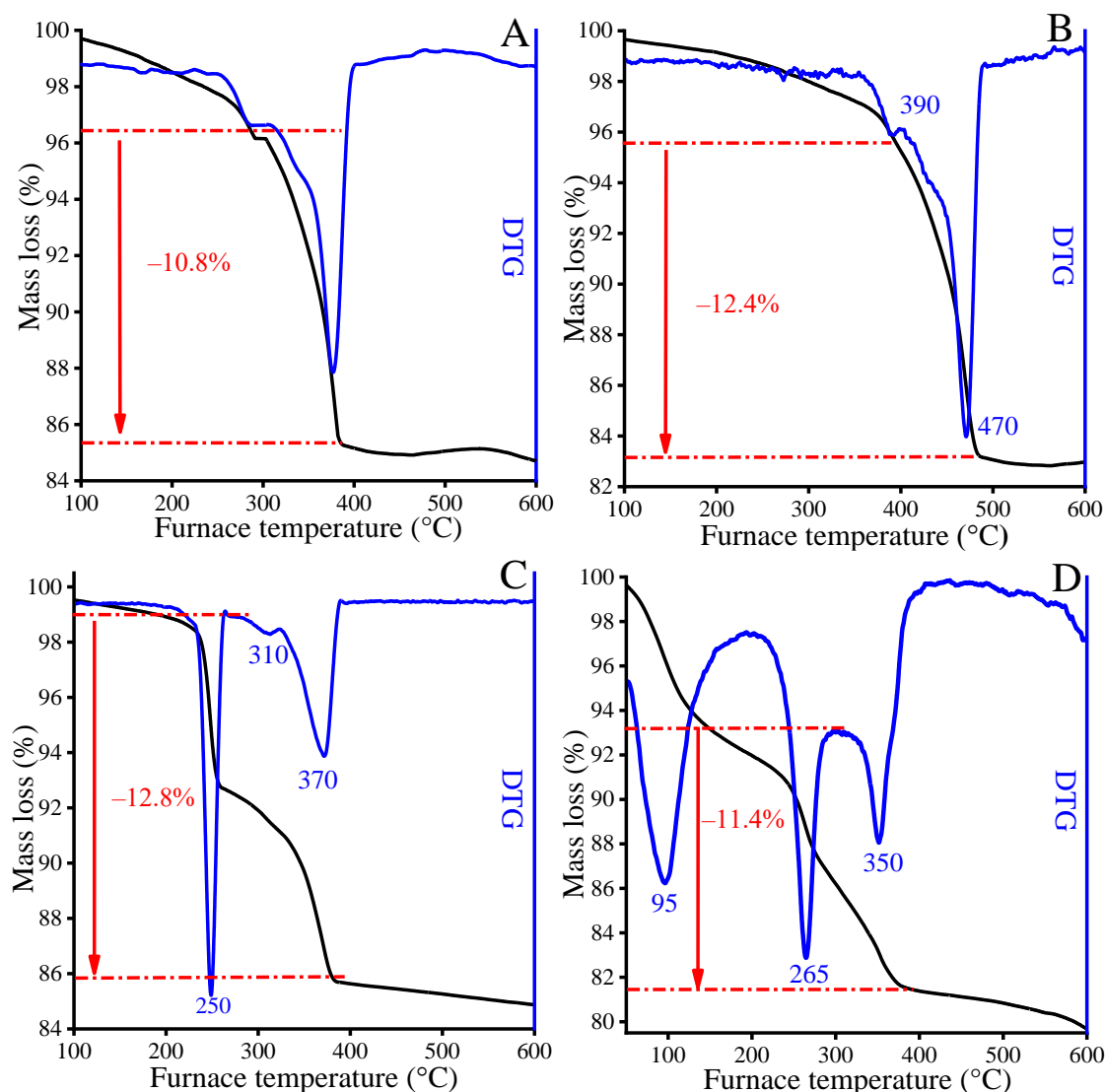


**Figure 10.** Thermogravimetric behavior of as-prepared  $\text{Mn-Bi}_2\text{O}_2\text{CO}_3$  (A),  $\text{CoBi}_2\text{O}_2\text{CO}_3$  (B),  $\text{NiBi}_2\text{O}_2\text{CO}_3$  (C) and  $\text{MnBi}_2\text{O}_2\text{CO}_3$  (D); (wet impregnation: A, co-precipitation: B-D).<sup>194</sup>

Similar to the pure bismutite and the impregnated references (**Fig. 10. A**), the DTG curve of the manganese-modified counterpart (**Fig. 10. B**) shows only one endothermic peak at 470 °C, which is due to the decarboxylation of the structure (verified by TG-MS measurements). Parallel to the collapse of the long-range ordered structure, the formation of  $\text{Bi}_2\text{O}_3$  (PDF#4-294)<sup>176</sup> (**Fig. 11. A**) and its doped analogue,  $\text{Bi}_2\text{Mn}_4\text{O}_{10}$  (PDF#74-1096)<sup>195</sup> can be detected in the *ex-situ* diffractogram (**Fig. 11. B**). For Ni- and Co-containing samples, the complete collapse of the layered structures occurs in a two-step process due to the strongly bound hydroxyl groups. In the first step (~250–265 °C), the layered structure remains untouched and a phase transition occurs, which is clearly confirmed by the *ex-situ* XRD (**Fig. 11. C,D**).

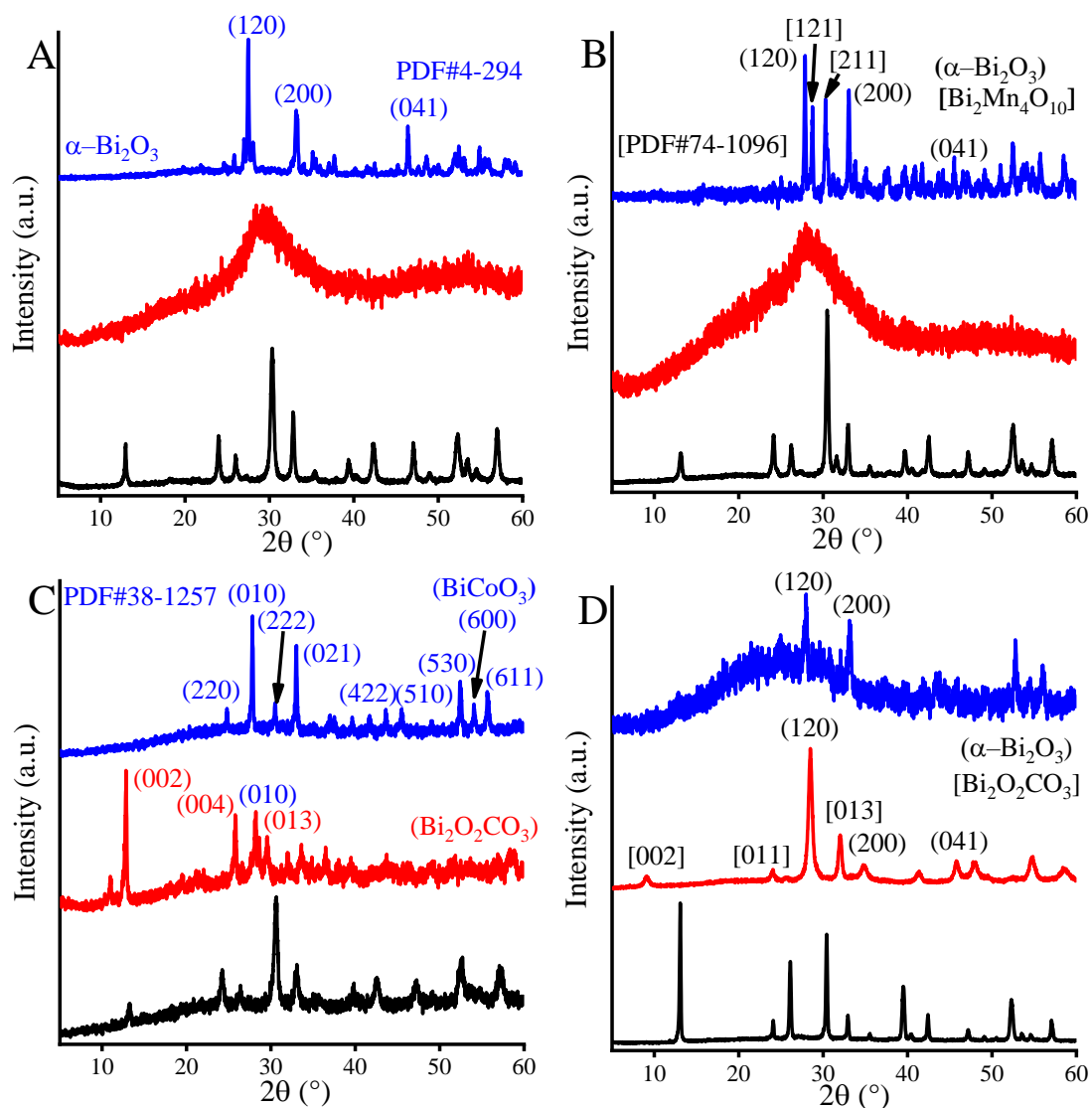


**Figure 11.** XRD patterns of as-prepared (black lines) and heat-treated (at 350 °C: red lines, at 600 °C: blue lines) of  $\text{Bi}_2\text{O}_2\text{CO}_3$  (A),  $\text{MnBi}_2\text{O}_2\text{CO}_3$  (B),  $\text{CoBi}_2\text{O}_2\text{CO}_3$  (C) and  $\text{NiBi}_2\text{O}_2\text{CO}_3$  (D).<sup>194</sup>

In order to resolve the contradiction between the XRD results (no phase other than bismutite) and SEM-EDX (TMs and bismuth ions are heterogeneously distributed), TEM/TEM-EDX measurements were also performed on the co-precipitated bismutites (**Fig. 12.**).

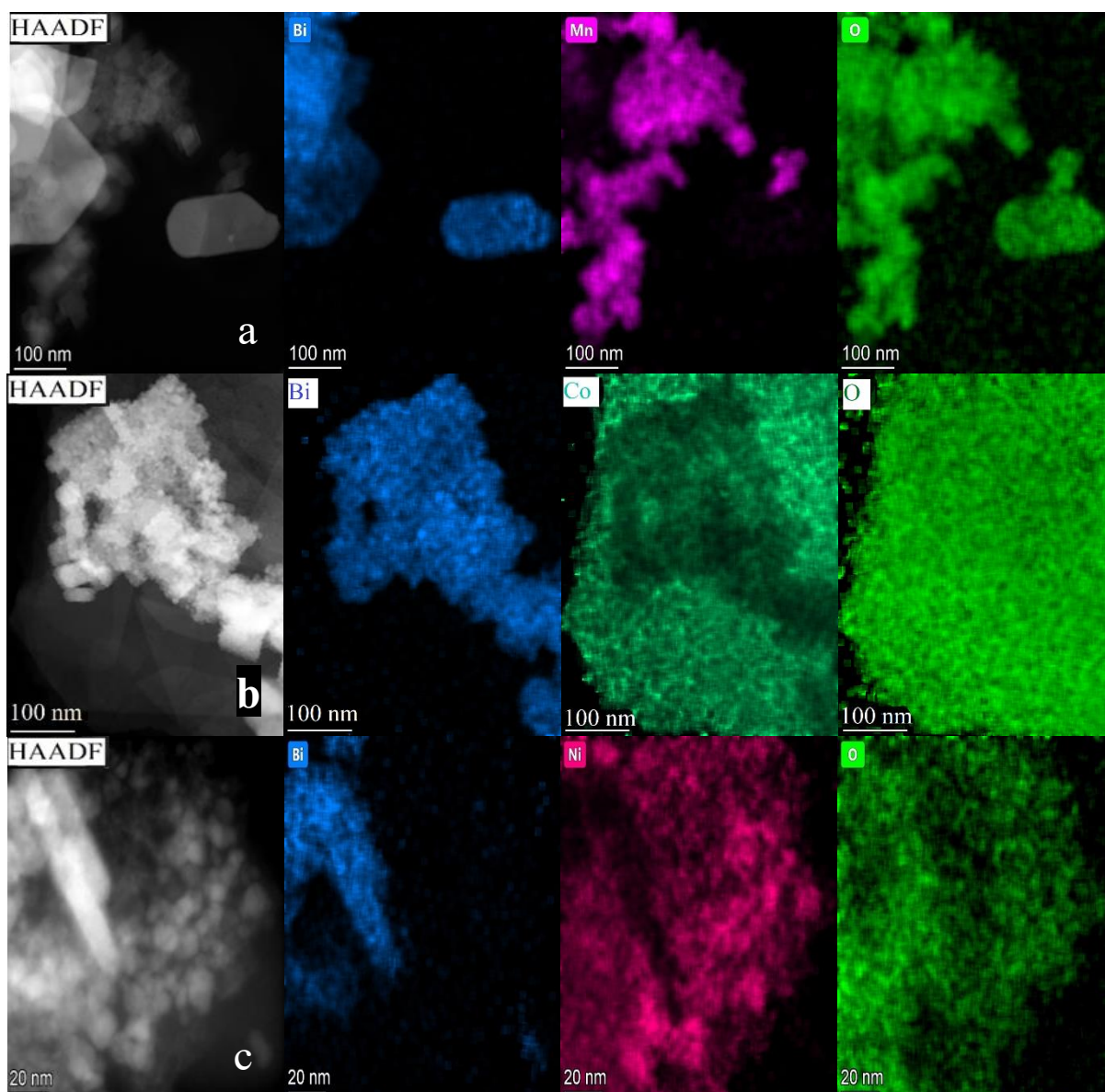


**Figure 12.** TEM images and TEM-EDX elemental maps of MnBi<sub>2</sub>O<sub>2</sub>CO (a), CoBi<sub>2</sub>O<sub>2</sub>CO<sub>3</sub> (b), NiBi<sub>2</sub>O<sub>2</sub>CO<sub>3</sub> (c).<sup>194</sup>

TEM images demonstrate that co-precipitated samples consist of nanoparticles with two morphologies and two dimensions, with the smaller, 5–20 nm spherical crystals sitting directly on top of the larger (~300–600 nm) cubic crystals. TEM-EDX images also show that the smaller, spherical crystals are rich in the corresponding transition metals and oxygen, while the larger ones are composed of bismuth and oxygen. From this information, it can be concluded that the formation of large aggregates can hinder the XRD pattern of smaller transition metal-rich particles and that the isolated "island" structures are due to the fact that the transition metal-rich particles have not completely covered the surface of the bismuth-rich particles.

Raman analysis allowed the TM specimens to be identified (**Fig. 13. A,C,E**). Using a near-infrared laser power in the far Raman shift region, bismutite host structure possess only three detectable Raman active modes at 358, 162 and 71 cm<sup>-1</sup>, corresponding to the external

vibrations of the  $[\text{Bi}_2\text{O}_2]^{2+}$  layer and the Bi–anion stretching mode vibration<sup>176</sup>. For impregnated samples, the characteristic Raman modes of  $\text{Mn}_3\text{O}_4$ ,<sup>196</sup> deformed (NiO or)  $\text{Ni}(\text{OH})_2$ <sup>197</sup> and  $\text{Co}_3\text{O}_4$ <sup>198</sup> specimens could be identified alongside the characteristic Raman peaks of the host, which can be assigned to the lattice mode vibrations of the oxides. This interpretation is in clear agreement with the XRD results shown in **Fig. 3. B**. Since neither  $\text{MnO}_2$ <sup>196</sup> nor  $\text{CoO}$ <sup>198</sup> have any Raman active vibration mode, detection of these oxides by Raman spectroscopy is not possible. The formation of these non-Raman active oxides during impregnation was excluded by XRD.

In contrast, several differences are observed in the Raman spectra of the co-precipitated samples. First, the intensity of the Raman peaks belonging to the host decreased significantly (Mn) or disappeared completely (Co). These observations are a consequence of the different Raman scattering coefficients of the building blocks. Second, the intense characteristic peaks that appear in the presence of the corresponding metal ions can be associated much more with the vibrations of Bi–O–M (M: Mn, Co) bond,<sup>199</sup> rather than with the Raman activity modes of some commercially available oxides or metal particles. These specimens most likely formed at the interfaces and clearly illustrate the direct interaction between the host and the manganese or cobalt ions. Due to the use of a near-IR laser source, Raman detection has bulk sensitivity, so no information is available on the quality of the transition metal species at greater distances from the interfaces.

The nickel-containing system differs from the Mn- or Co system. In the absence of other peaks, its Raman bands can be easily interpreted as bonds of deformed  $\text{Ni}(\text{OH})_2$  and bismutite components. It can therefore be assumed that no Ni-containing interfacial species have formed.

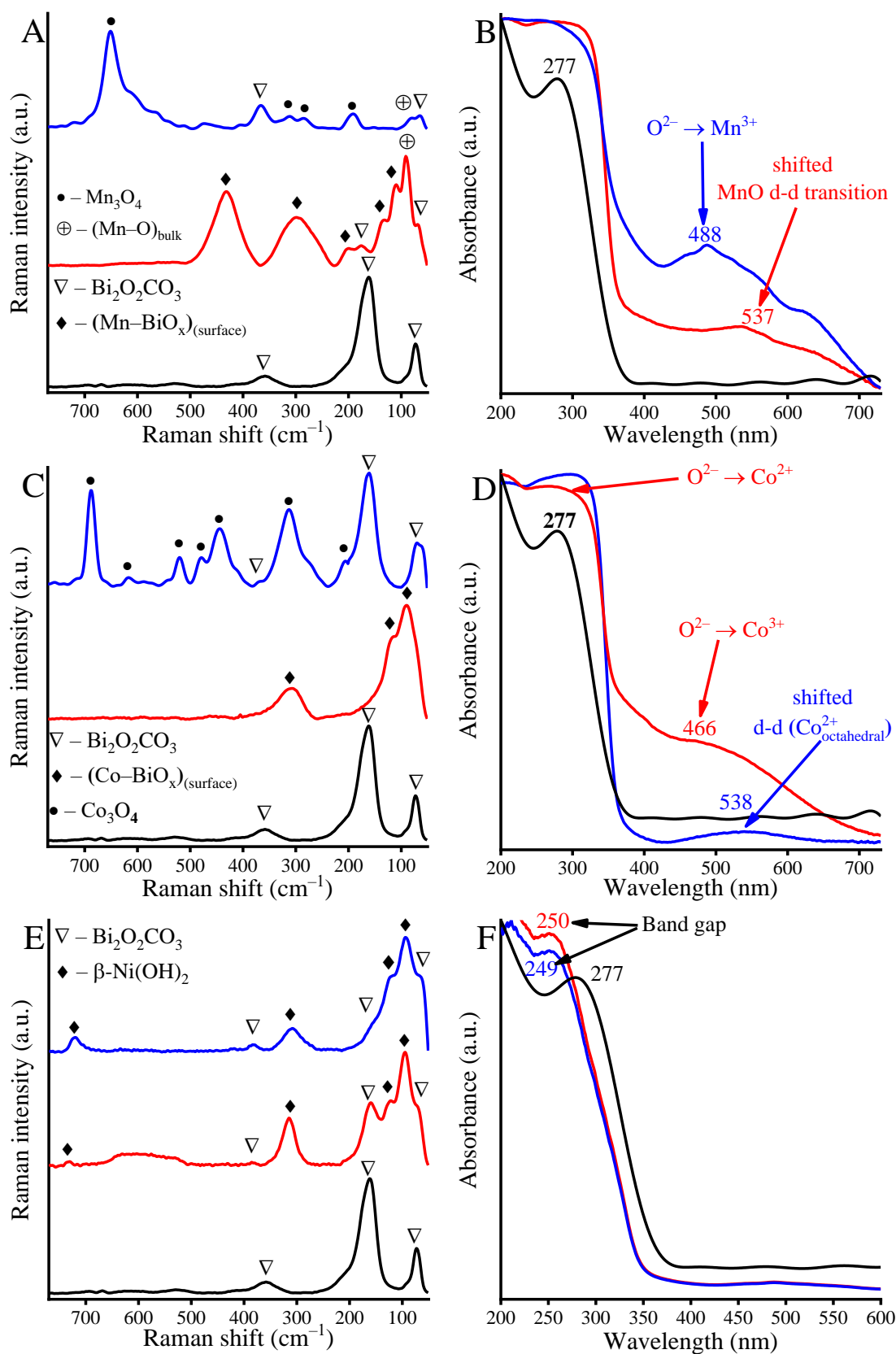


**Figure 13.** Raman- (A, C, E) and UV-DRS spectra (B, D, F) of as-prepared  $\text{Bi}_2\text{O}_2\text{CO}_3$  (black lines),  $\text{MnBi}_2\text{O}_2\text{CO}_3$ ,  $\text{CoBi}_2\text{O}_2\text{CO}_3$ ,  $\text{NiBi}_2\text{O}_2\text{CO}_3$  (red lines) and  $\text{Mn-Bi}_2\text{O}_2\text{CO}_3$ ,  $\text{Co-Bi}_2\text{O}_2\text{CO}_3$ ,  $\text{Ni-Bi}_2\text{O}_2\text{CO}_3$  (blue lines).<sup>194</sup>

The UV-Vis measurements on the right side of **Fig. 13. B,D,F**, also confirm the statement that interfacial sites are only formed in the Mn- and Co systems, but not in the nickel-containing sample. This can be seen from the fact that the bathochromic shifts of the characteristic transitions of the metal species related to charge transfer<sup>200,201</sup> can be unambiguously identified for the two systems mentioned, while the absorption spectra of the impregnated references and the nickel-containing co-precipitated sample are a linear combination of the transitions related to the bismutite and the corresponding transitions (mainly the charge transfer ones<sup>202–204</sup>) of the 3d metal species.

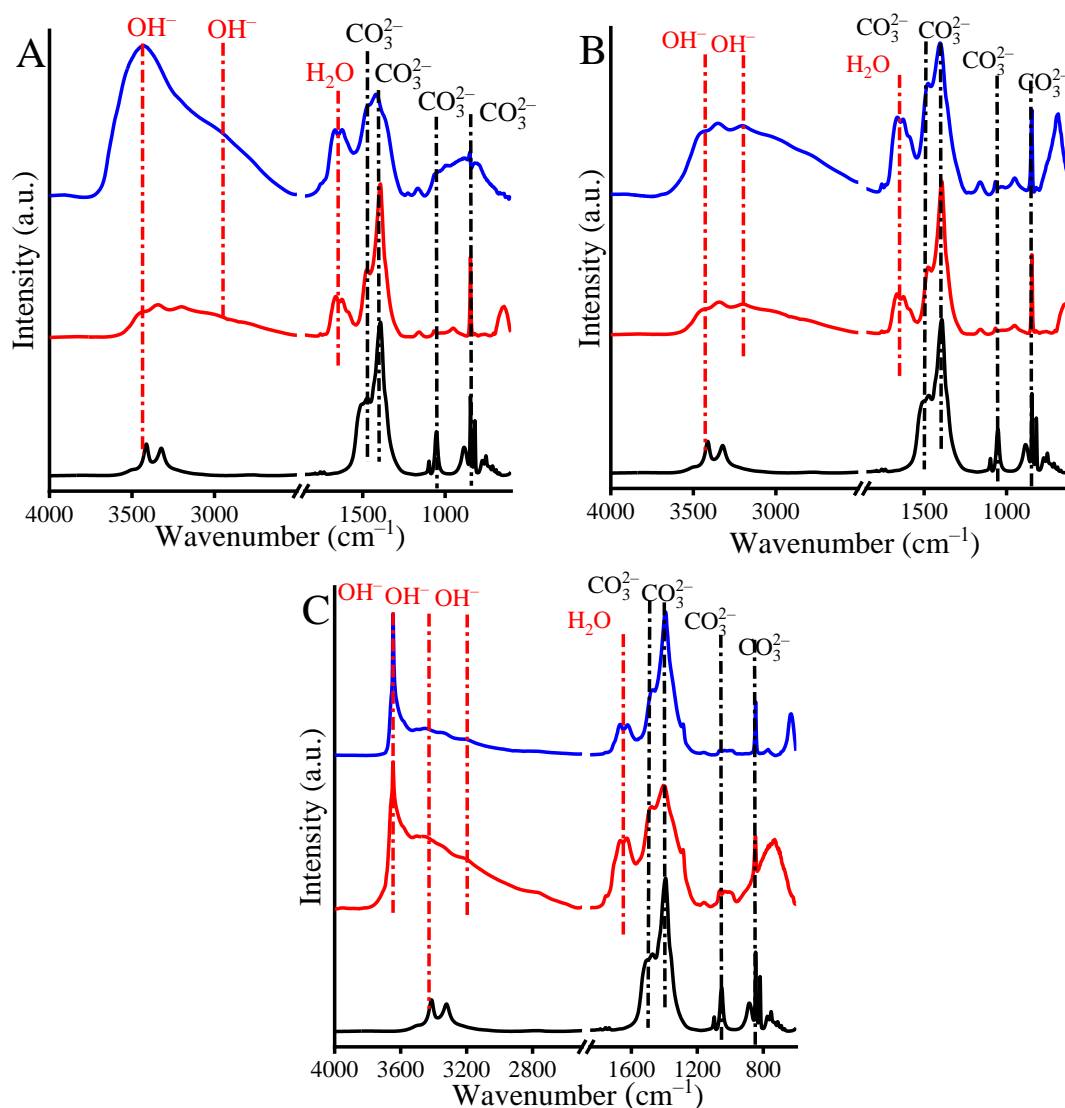


**Figure 14.** Infrared spectra of the as-prepared  $\text{Bi}_2\text{O}_2\text{CO}_3$  (black lines),  $\text{MnBi}_2\text{O}_2\text{CO}_3$ ,  $\text{CoBi}_2\text{O}_2\text{CO}_3$ ,  $\text{NiBi}_2\text{O}_2\text{CO}_3$  (red lines) and  $\text{Mn-Bi}_2\text{O}_2\text{CO}_3$ ,  $\text{Co-Bi}_2\text{O}_2\text{CO}_3$ ,  $\text{Ni-Bi}_2\text{O}_2\text{CO}_3$  (blue lines).<sup>194</sup>

To obtain information about the surface of the TM specimens, XPS measurements were taken (**Figs. 15-16.**). As can be seen on **Figure 15. A**, the exact position of the Bi 4f band and its separation of 5.3 eV, representing bismuth ions with oxidation state +3 on the surface. These



peaks can be fitted by considering only one component at 164.1 and 158.8 eV binding energies attributed to Bi(III) species incorporated into a Sill  n-type bismutite framework.<sup>178</sup> After modification of the bismutite framework with manganese and cobalt ions, these characteristic bands are shifted and broadened towards higher binding energies, which change does not occur in the spectrum of the nickel modified sample. The Bi 4f bands of the nickel-containing composite are almost identical to those of the pure bismutite. These observations confirm the hypothesis about the interfacial specimens and agree with the interpretation of the Raman and UV-Vis measurements.

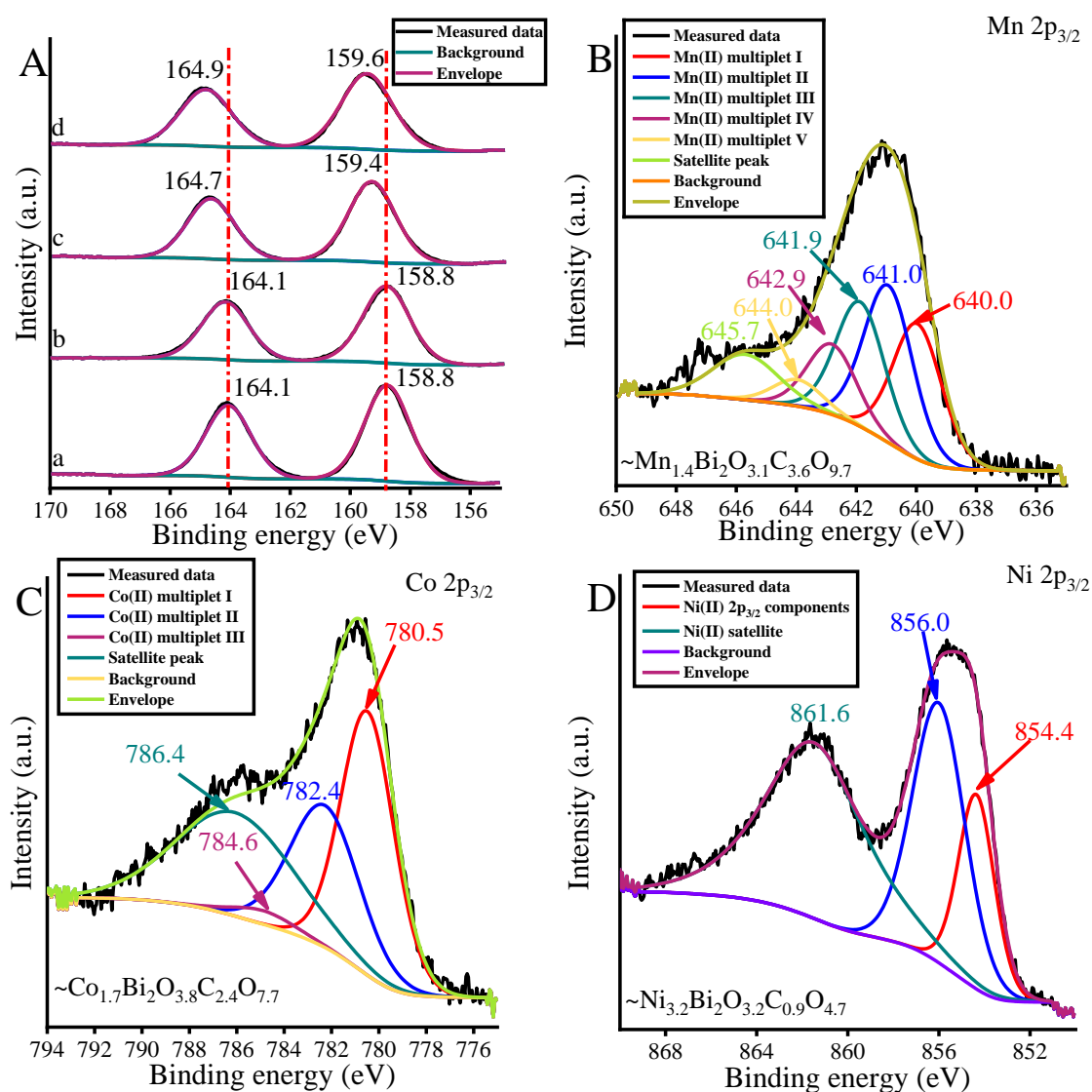


**Figure 15.** Bi 4f (A), Mn 2p<sub>3/2</sub> (B), Co 2p<sub>3/2</sub> (C) and Ni 2p<sub>3/2</sub> (D) XPS spectra of the as-prepared Bi<sub>2</sub>O<sub>2</sub>CO<sub>3</sub>, MnBi<sub>2</sub>O<sub>2</sub>CO<sub>3</sub>, CoBi<sub>2</sub>O<sub>2</sub>CO<sub>3</sub>, NiBi<sub>2</sub>O<sub>2</sub>CO<sub>3</sub>.<sup>194</sup>

The 2p bands of manganese and cobalt of the modified samples (**Fig. 15. B,C**) can be described with one component as MnO and Co(OH)<sub>2</sub>, respectively.<sup>205</sup>

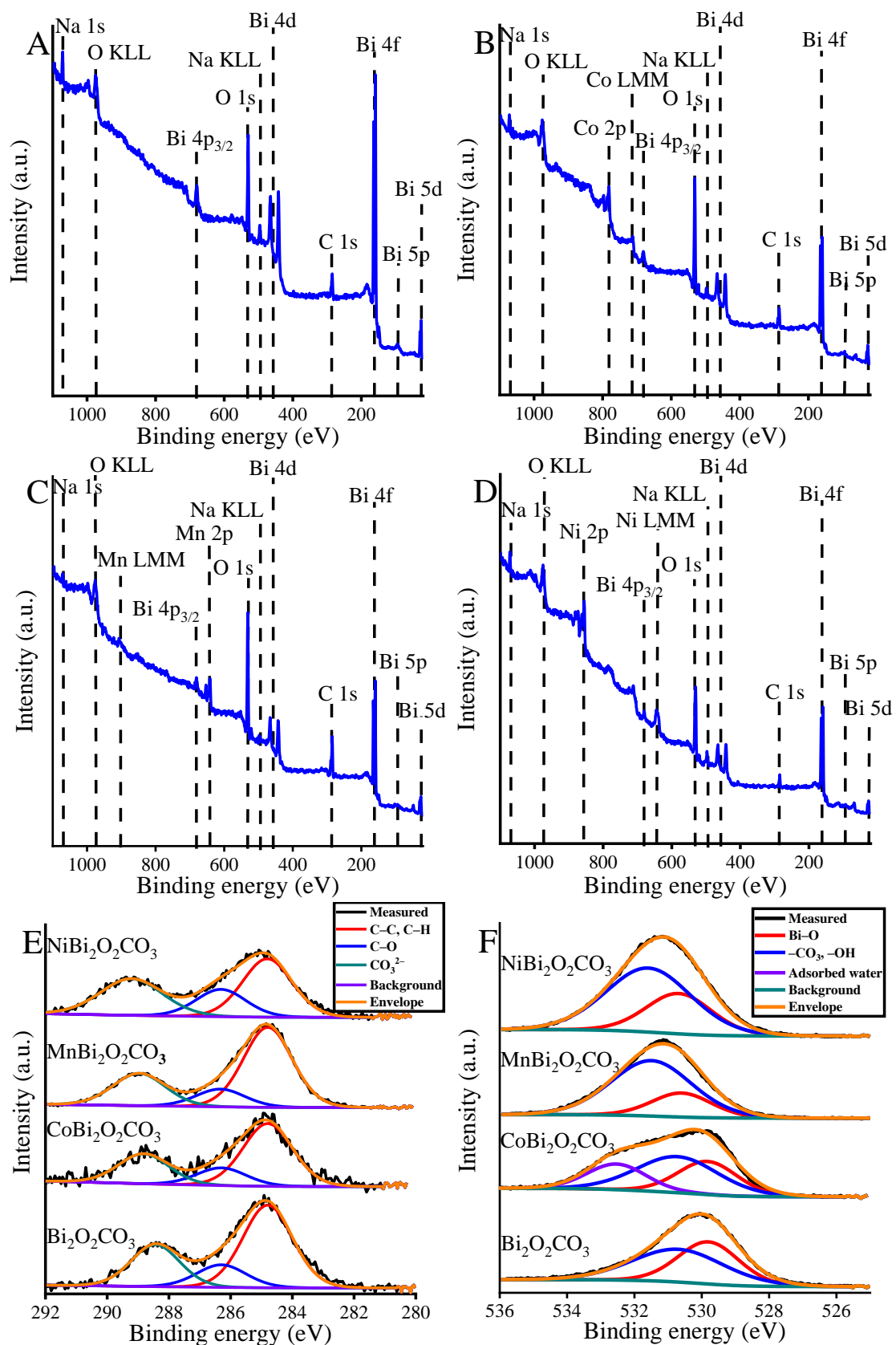


**Figure 16.** Individual survey scans of  $\text{Bi}_2\text{O}_2\text{CO}_3$  (A),  $\text{CoBi}_2\text{O}_2\text{CO}_3$  (B),  $\text{MnBi}_2\text{O}_2\text{CO}_3$  (C),  $\text{NiBi}_2\text{O}_2\text{CO}_3$  (D) and C 1s (E) as well as O 1s (F) XP spectra of the co-precipitated samples.<sup>194</sup>

Accordingly, Mn(II) and Co(II) ions can exclusively occupy the right positions on the surface of the composite. For the nickel-bismutite system, there are no identical chemical environments of nickel that can be directly identified, so some kind of unidentifiable linear combination of NiO, Ni(OH)<sub>2</sub>- and NiOOH species can describe the surface species in the sample.<sup>206</sup> Moreover, for the correct description of this curve, two different, independent components should be considered. The oxygen and carbon components of the spectra could be represented as almost identical surface species of the bismutite host (**Fig. 16.**)

In summary, **Table 12.** shows the most probable surface composition of the framework-modified manganese/cobalt and nickel-bismutite composites calculated from XP spectroscopy compared to the bulk composition based on analytical measurements (ICP-MS, TG/DTG). In addition, the last column shows the specific surface area of the composites, which was determined by N<sub>2</sub> adsorption measurements. From this, it can be deduced that the surface composition of the TM modified samples shows an enrichment of TM species compared to the bulk. From the comprehensive analytical and spectroscopic characterization, it can also be concluded that the solids obtained by the co-precipitation methods contain the guest specimens immobilized *via* stronger bonds than those immobilized by impregnation. In co-precipitated samples containing manganese and cobalt, well-detectable M-BiOX interfaces can be identified, indicating a strong interaction between the bismutite framework and the guest species TM.

**Table 12.** The most probable compositions and the specific surface areas of manganese, cobalt and nickel-modified bismutites

<b>Original formula</b>	<b>Surface composition*</b>	<b>Bulk composition**</b>	<b>Specific surface area (m<sup>2</sup>/g)***</b>
MnBi <sub>2</sub> O <sub>2</sub> CO <sub>3</sub>	Mn <sub>1.4</sub> Bi <sub>2</sub> O <sub>2.9</sub> C <sub>3.6</sub> O <sub>9.7</sub>	Mn <sub>0.24</sub> Bi <sub>2</sub> O <sub>2</sub> C <sub>1.05</sub> O <sub>3.5</sub> H <sub>0.35</sub>	32
CoBi <sub>2</sub> O <sub>2</sub> CO <sub>3</sub>	Co <sub>1.7</sub> Bi <sub>2</sub> O <sub>3.8</sub> C <sub>2.4</sub> O <sub>7.7</sub>	Co <sub>0.14</sub> Bi <sub>2</sub> O <sub>2</sub> C <sub>1.08</sub> O <sub>4.22</sub> H <sub>0.98</sub>	48
NiBi <sub>2</sub> O <sub>2</sub> CO <sub>3</sub>	Ni <sub>3.2</sub> Bi <sub>2</sub> O <sub>3.2</sub> C <sub>0.9</sub> O <sub>4.7</sub>	Ni <sub>0.66</sub> Bi <sub>2</sub> O <sub>2</sub> CO <sub>7.47</sub> H <sub>4.47</sub>	38

\* by XP spectroscopy

\*\* by ICP-MS, TG/DTG

\*\*\* by N<sub>2</sub> adsorption

## 5.2. Catalytic studies

### 5.2.1. Catalytic capability of $\text{CuBi}_2\text{O}_2\text{CO}_3$ as heterogeneous catalyst in the synthesis of phenothiazine and its derivatives

Since, the copper modified system proved to be the only new Sillén structural analogue, its catalytic ability was investigated independently of the other TM-modified bismutites. The synthesis of phenothiazine was selected as model reaction, described in detail in the Experimental Part (**Scheme 4.**). Yield and selectivity values were used to express the efficiency of the catalyst in forming new C-S and C-N bonds. The reaction conditions of the scouting experiments are listed in **Table 6.** and also in Chapter 4.

While the conversion of 2-iodoaniline was negligible in the absence of the catalyst and sulfur-containing by-products were produced in a competitive side reaction *via* a thermal pathway (**Fig. 17. A.**), the framework-modified  $\text{CuBi}_2\text{O}_2\text{CO}_3$  proved to be an efficient catalyst producing phenothiazine with high yield (90%) and high selectivity (90%). The side reaction of thermal homocoupling of 2-bromobenzenethiol gave 10 mol% of sulfur-containing by-products, mainly 1,3-bis(2-bromophenyl)disulfide. In comparison, pure  $\text{Bi}_2\text{O}_2\text{CO}_3$  gave moderate yields and lower selectivities.

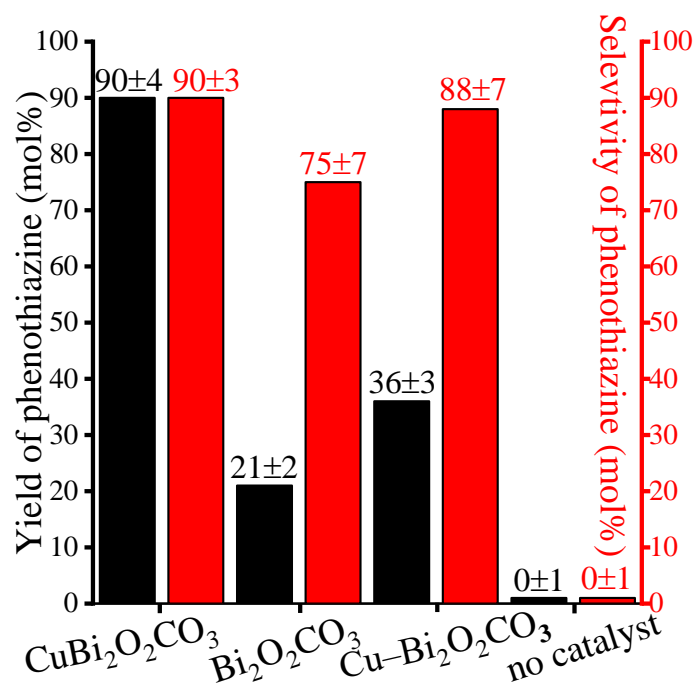


**Figure 17.** Cascade-like C-S and C-N heterocyclization reaction catalyzed by  $\text{CuBi}_2\text{O}_2\text{CO}_3$ ,  $\text{Bi}_2\text{O}_2\text{CO}_3$ ,  $\text{Cu-Bi}_2\text{O}_2\text{CO}_3$  and in the absence of catalyst. Reaction conditions: 1 equiv. (0.25 M) of 2-iodoaniline, 1.1 equiv. of 2-bromobenzenethiol, 5 equiv. of  $\text{K}_2\text{CO}_3$ , 10 mol% of catalyst, 90 °C for 24 h, 110 °C for further 48 h.<sup>176</sup>

It is worth noting that while the fact that Bi(III) can act as a Lewis acid catalyst in heterocyclization reactions is not unprecedented,<sup>207,208</sup> to the best of our knowledge, there is no relevant information on the use of heterogeneous bismuth catalysts to promote similar reactions. Furthermore, these catalysts could offer additional advantages over known catalysts. *E.g.* in contrast with the original conditions used by Dawei and co-workers,<sup>148</sup> the as-prepared catalyst promoted the formation of the desired product in DMSO instead of dimethoxyethane, in the absence of any co-catalytic additives or ligands, unavoidable presence of which was previously demonstrated in homogeneous catalytic processes.<sup>147,209</sup>

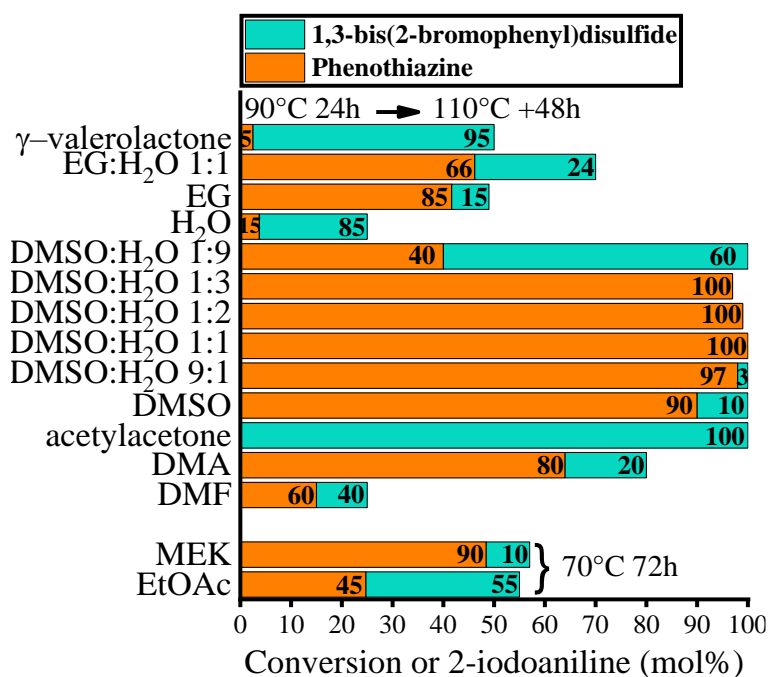


**Figure 18.** Solvent screening in cascade-like C–S and C–N heterocyclization reaction catalyzed by  $\text{CuBi}_2\text{O}_2\text{CO}_3$ . Reaction conditions: 1 equiv. (0.25 M) of 2-iodoaniline, 1.1 equiv. of 2-bromobenzenethiol, 5 equiv. of  $\text{K}_2\text{CO}_3$ , 10 mol% of catalyst, 90 °C for 24 h, 110 °C for further 48 h.<sup>176</sup>

A marked decrease in phenothiazine yield was observed in the solvent compatibility tests<sup>210</sup> except for the solvent mixtures DMSO:water (**Fig. 18.**). The 1:1 and 1:2 mixtures performed extremely well, achieving 100% selectivity with quantitative conversion. This finding is particularly promising as generally non-polar and aprotic solvents (THF, diethyl ether), which pose significant environmental issues, have so far proven to be efficient.

In further optimization, the excellent activity of the copper-containing bismutite led to a reduction in the reaction temperature and reaction time (**Fig. 19.**). The amount of base added, and the catalyst loading were also successfully reduced without deteriorating the catalytic indicator values (**Fig. 20.**). The mildest reaction conditions for heterocyclization were: DMSO:water 1:2 solvent at 90 °C for 72 h using 5 mol%  $\text{CuBi}_2\text{O}_2\text{CO}_3$  as catalyst and 2.5 equiv.

of base. There is no example in the literature of using a similarly low concentration of a base to yield phenothiazine exclusively.

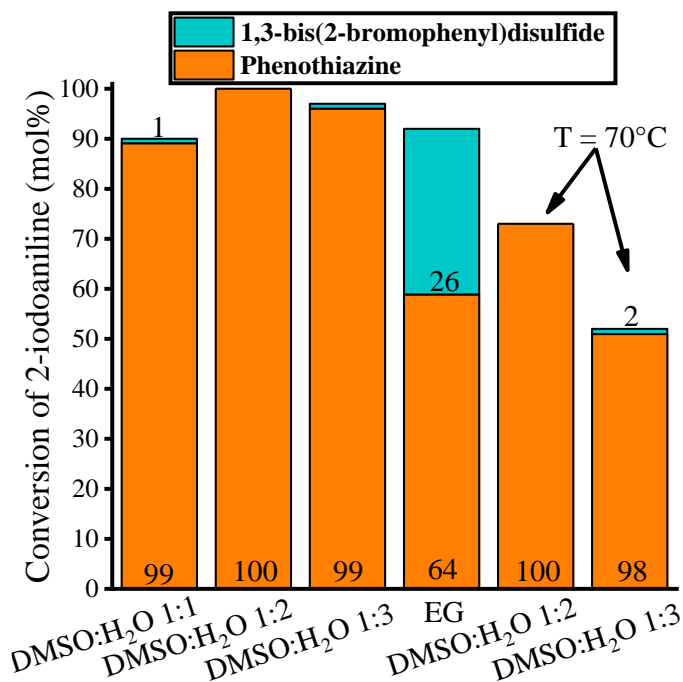


**Figure 19.** The effect of reaction temperature in cascade-like C–S and C–N heterocyclization reaction catalyzed by  $\text{CuBi}_2\text{O}_2\text{CO}_3$ . Reaction conditions: 1 equiv. (0.25 M) of 2-iodoaniline, 1.1 equiv. of 2-bromobenzenethiol, 5 equiv. of  $\text{K}_2\text{CO}_3$ , 10 mol% of catalyst, 90 °C for 24 h, 110 °C for further 48 h.<sup>176</sup>

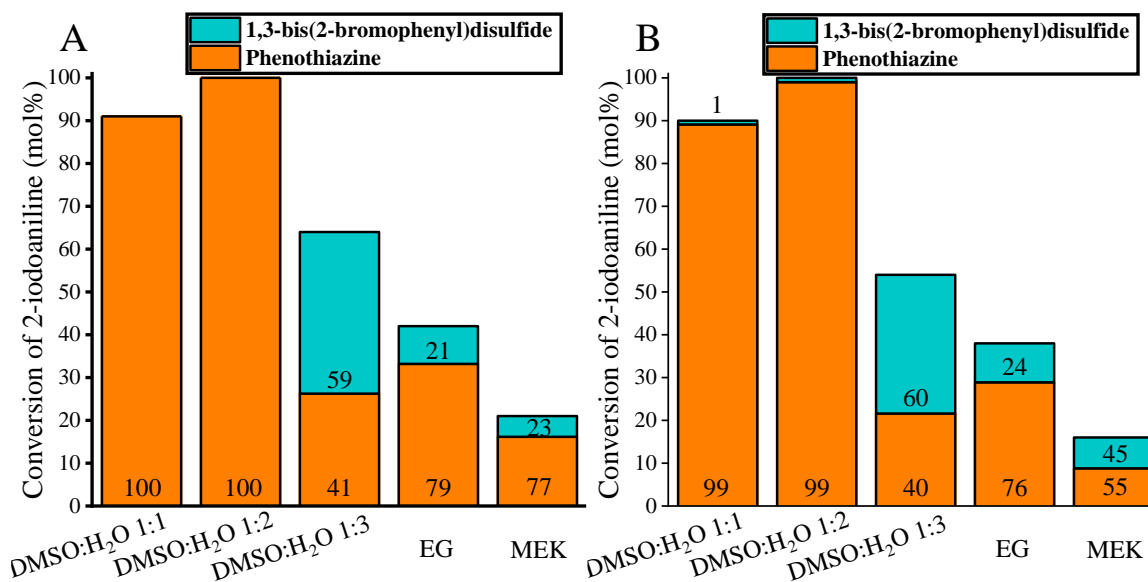


**Figure 20.** The effect of the quantity of added base and the catalyst load in cascade-like C–S and C–N heterocyclization reaction catalyzed by  $\text{CuBi}_2\text{O}_2\text{CO}_3$ . Reaction conditions: 1 equiv. (0.25 M) 2-iodoaniline, 1.1 equiv. 2-bromothiophenol, 2.5 equiv.  $\text{K}_2\text{CO}_3$  and 5 (A) or 2.5 (B) mol%  $\text{CuBi}_2\text{O}_2\text{CO}_3$ , 90 °C (70 °C for EG and MEK), 72h.<sup>176</sup>

In time-dependent experiments, it was found that due to the unique activity of  $\text{CuBi}_2\text{O}_2\text{CO}_3$ , the formation of C–S and C–N bonds was quantitatively available below 15h (**Fig. 21.**). In comparison, one of the most efficient homogeneous catalytic systems ( $\text{CuI-L-}$

proline system), which also provided the initial experimental conditions for our model reaction, gave a 77% yield of phenothiazine at 90 °C for 24 h (for C-S coupling) and subsequently at 110 °C for 48 hours (for C-N coupling) with 10 mol% catalyst and 5 equivalent base loadings.<sup>148</sup> Based on this experience, it can be concluded that  $\text{CuBi}_2\text{O}_2\text{CO}_3$  can catalyze the cyclization reaction in a concerted manner under mild conditions.<sup>211–217</sup>

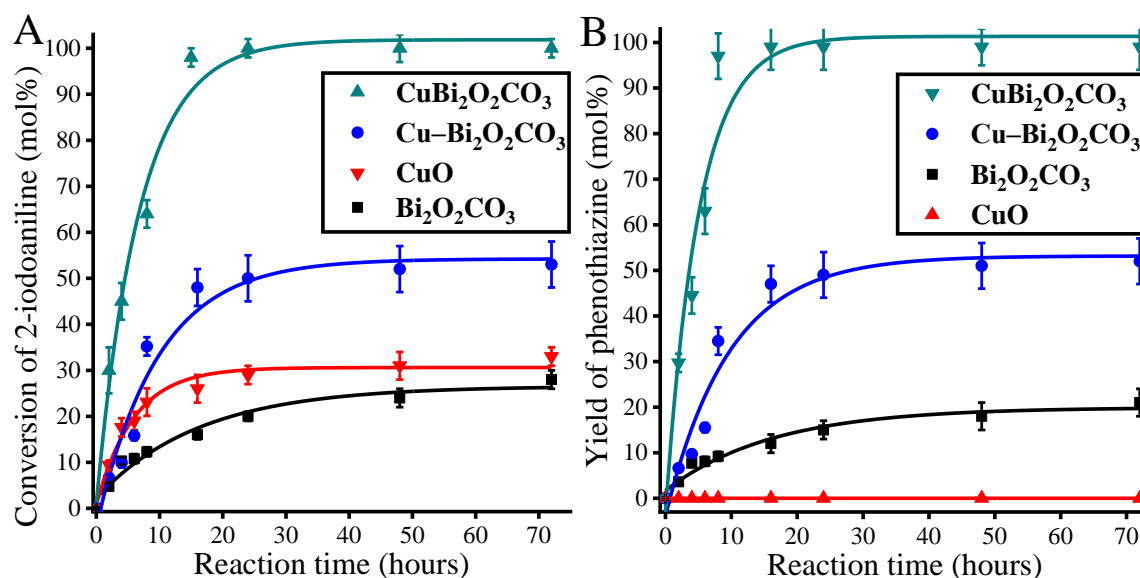


**Figure 21.** Conversions of 2-iodoaniline (A) and yields of phenothiazine (B) as the function of time in cascade-like C–S and C–N heterocyclization reaction catalyzed by  $\text{Bi}_2\text{O}_2\text{CO}_3$ ,  $\text{CuO}$ ,  $\text{Cu-Bi}_2\text{O}_2\text{CO}_3$  and  $\text{CuBi}_2\text{O}_2\text{CO}_3$ . Reaction conditions: 1 equiv. (0.25 M) of 2-iodoaniline, 1.1 equiv. of 2-bromobenzenethiol, solvent: DMSO:water 1:2, 2.5 equiv. of  $\text{K}_2\text{CO}_3$ , 2.5 mol% catalyst, 90 °C.<sup>176</sup>

**Table 13.** Catalytic activities and product yields over 5 mol% catalysts in cascade-like C–S and C–N heterocyclization reaction in a mixture of DMSO:water 1:2, using 2.5 equiv. of bases at 90 °C<sup>176</sup>

—	Initial TOF (1/h)	Phenothiazine yield (mol%) <sup>1</sup>	2-iodoaniline conversion (mol%) <sup>1</sup>	Phenothiazine sel. (%) <sup>1</sup>	1,3-bis(2-bromophenyl)disulfide sel. (%) <sup>1</sup>
$\text{Bi}_2\text{O}_2\text{CO}_3$	$1.3 \pm 0.1$	$12 \pm 1.1$	$16 \pm 1.3$	$75 \pm 1.5$	$25 \pm 0.8$
$\text{CuO}$	$2.6 \pm 0.3$	0	$24 \pm 2.0$	0 <sup>2</sup>	$2 \pm 0.5$
$\text{Cu-Bi}_2\text{O}_2\text{CO}_3$	$2.5 \pm 0.1$	$47 \pm 3.2$	$48 \pm 2.7$	$98 \pm 2.1$	$2 \pm 0.3$
$\text{CuBi}_2\text{O}_2\text{CO}_3$	$10.4 \pm 0.5$	$99 \pm 1.2$	$100 \pm 1.8$	$99 \pm 1.7$	$1 \pm 0.3$

<sup>1</sup>After 15h; <sup>2</sup>Only S-arylation occurred

The linear parts of the kinetic curves were also suitable for determining the initial TOF values.<sup>218</sup> Both the activities and the selectivities of the catalysts increased in the order of

$\text{Bi}_2\text{O}_2\text{CO}_3 < \text{CuO} < \text{Cu-Bi}_2\text{O}_2\text{CO}_3$  (impregnated reference)  $< \text{CuBi}_2\text{O}_2\text{CO}_3$ . The selectivity over the pure bismutite (75%) is far below the level (>95%) achieved with all other copper-containing materials. However, it was interesting to observe that pure CuO was not able to catalyze the final cyclization step but could only selectively promote S-arylation. This finding suggests that Bi(III) centers are necessary for the promotion of N-arylation. The highest yields achieved (**Table 13**, column 3) were also significantly different from each other, indicating that the local structure of the copper/bismuth ions is a crucial factor.

The bimetallic, bismuth-copper systems were found to be more efficient than the single metallic systems. However, framework-modified bismutites exhibited the best catalytic indicators, which can be attributed to the fixed Cu(II) ions inserted into the layered structure. For pure CuO and the impregnated system, the initial TOF values (**Table 13**, column 2) were almost identical, since in both cases the active sites are the Cu(II) ions and their dispersion is similarly low. In contrast, the much higher initial TOF value of  $\text{CuBi}_2\text{O}_2\text{CO}_3$  could be the direct consequence of the almost atomic dispersion and consequently the better accessibility of the Cu(II) sites. However, the variations in catalytic performance of the catalysts cannot be explained by the differences in specific surface areas, since the modified bismutite does not have a higher specific surface area ( $12 \text{ m}^2/\text{g}$ ) than that of the building blocks (bismutite:  $11 \text{ m}^2/\text{g}$ , CuO:  $18 \text{ m}^2/\text{g}$ ) or the impregnated reference ( $22 \text{ m}^2/\text{g}$ ). In fact, the excellent catalytic performance is due to the cooperation between the metallic component (CuO) and the framework ( $\text{Bi}_2\text{O}_2\text{CO}_3$ ), which originates from the ordered modification of the host structure with copper ions.

To verify the heterogeneity of the reaction, a hot filtration test<sup>219</sup> was performed under the optimized reaction condition and the catalytic indicators of the obtained solution were determined (**Fig. 22. A**). The solid catalyst was readily removed by simple filtration after 4 h, and in the absence of  $\text{CuBi}_2\text{O}_2\text{CO}_3$ , the conversion of 2-iodoaniline remained at the value before hot filtration. Since the filtrate proved to be catalytically inactive and there were no leached metal ions, which was verified by ICP-MS measurements, it can be explained that the metallic components were not washed out and the transformation was catalyzed heterogeneously.



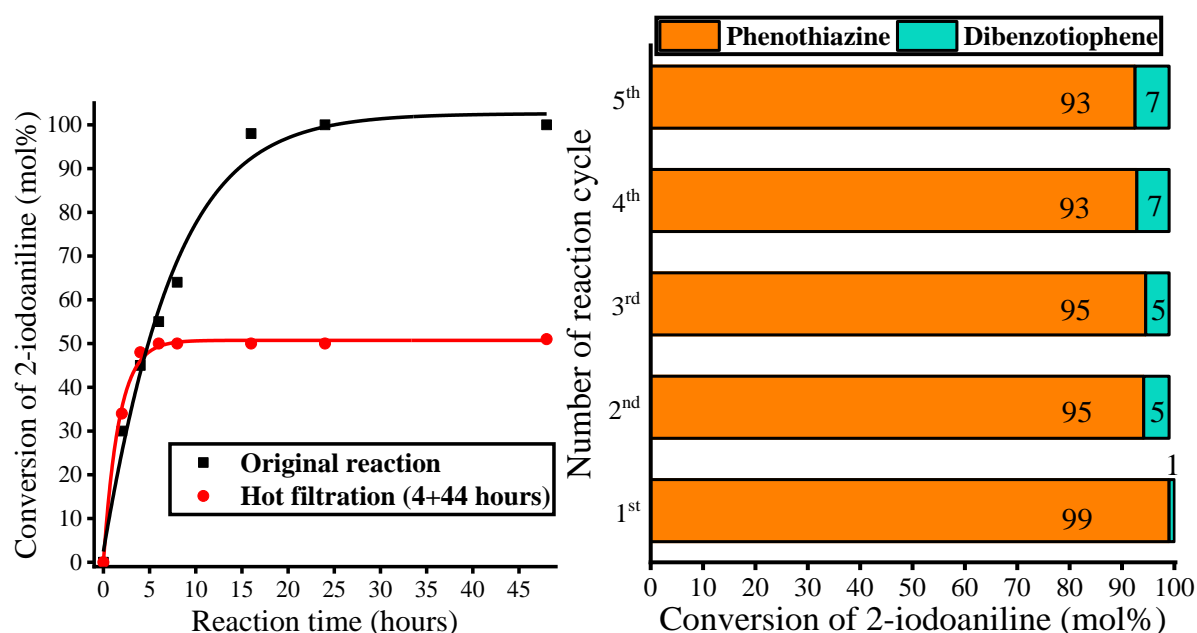


**Figure 22.** Hot filtration test (A) and investigation of the reusability of  $\text{CuBi}_2\text{O}_2\text{CO}_3$  (B) in in cascade-like C–S and C–N heterocyclization reaction catalyzed by  $\text{CuBi}_2\text{O}_2\text{CO}_3$ . Reaction conditions: 1 equiv. (0.25 M) of 2-iodoaniline, 1.1 equiv. of 2-bromobenzenethiol, solvent: DMSO:water 1:2, 2.5 equiv. of  $\text{K}_2\text{CO}_3$ , 5 mol% of  $\text{CuBi}_2\text{O}_2\text{CO}_3$  as catalyst, 90 °C, 72h (A) or 15h (B).<sup>176</sup>

Since this is a heterogeneous catalyst, it was necessary to investigate the reusability of the copper-containing bismutite. Therefore, the active catalyst was separated from the reaction mixture after the first reaction cycle and reused under identical conditions in another four cycles (**Fig. 22. B**). After the fifth run, no significant loss of phenothiazine yield was observed, and ICP-MS measurements confirmed that no leaching occurred during the five runs.

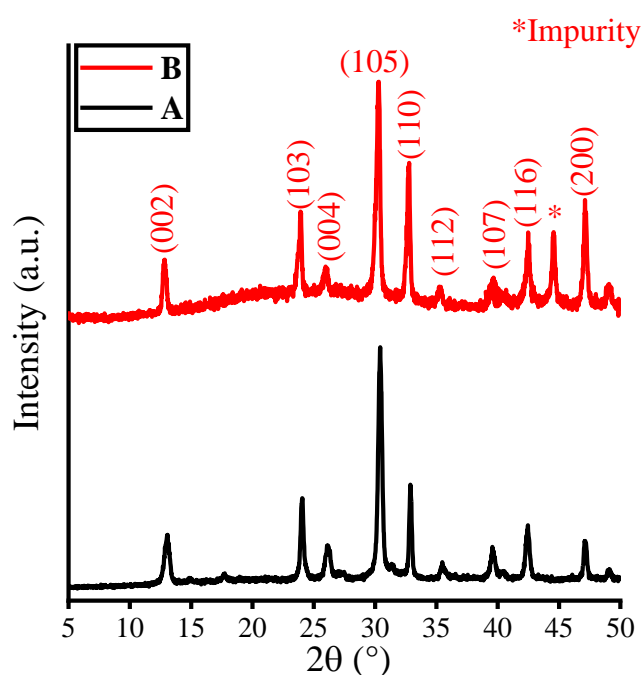


**Figure 23.** XRD patterns of (A) as-prepared and (B) reused (after fifth run)  $\text{CuBi}_2\text{O}_2\text{CO}_3$ .<sup>176</sup>



**Table 14.** Scope of phenothiazine formation *via* cascade-like C–S and C–N heterocyclization reaction catalyzed by  $\text{CuBi}_2\text{O}_2\text{CO}_3$ <sup>176</sup>

#	Substrate	Yield <sup>1</sup> (%)	Sel. <sup>1</sup> (%)	#	Substrate	Yield <sup>1</sup> (%)	Sel. <sup>1</sup> (%)
<b>1</b>		99	99	<b>7</b>		77	78
<b>2</b>		99	99	<b>8</b>		71	81
<b>3</b>		98	98	<b>9</b>		74	76
<b>4</b>		97	100	<b>10</b>		1	100
<b>5</b>		100	100	<b>11</b>		16	100
<b>6</b>		80	73				

<sup>1</sup>Determined by GC-MS analysis of the crude product; <sup>2</sup>T = 110 °C.

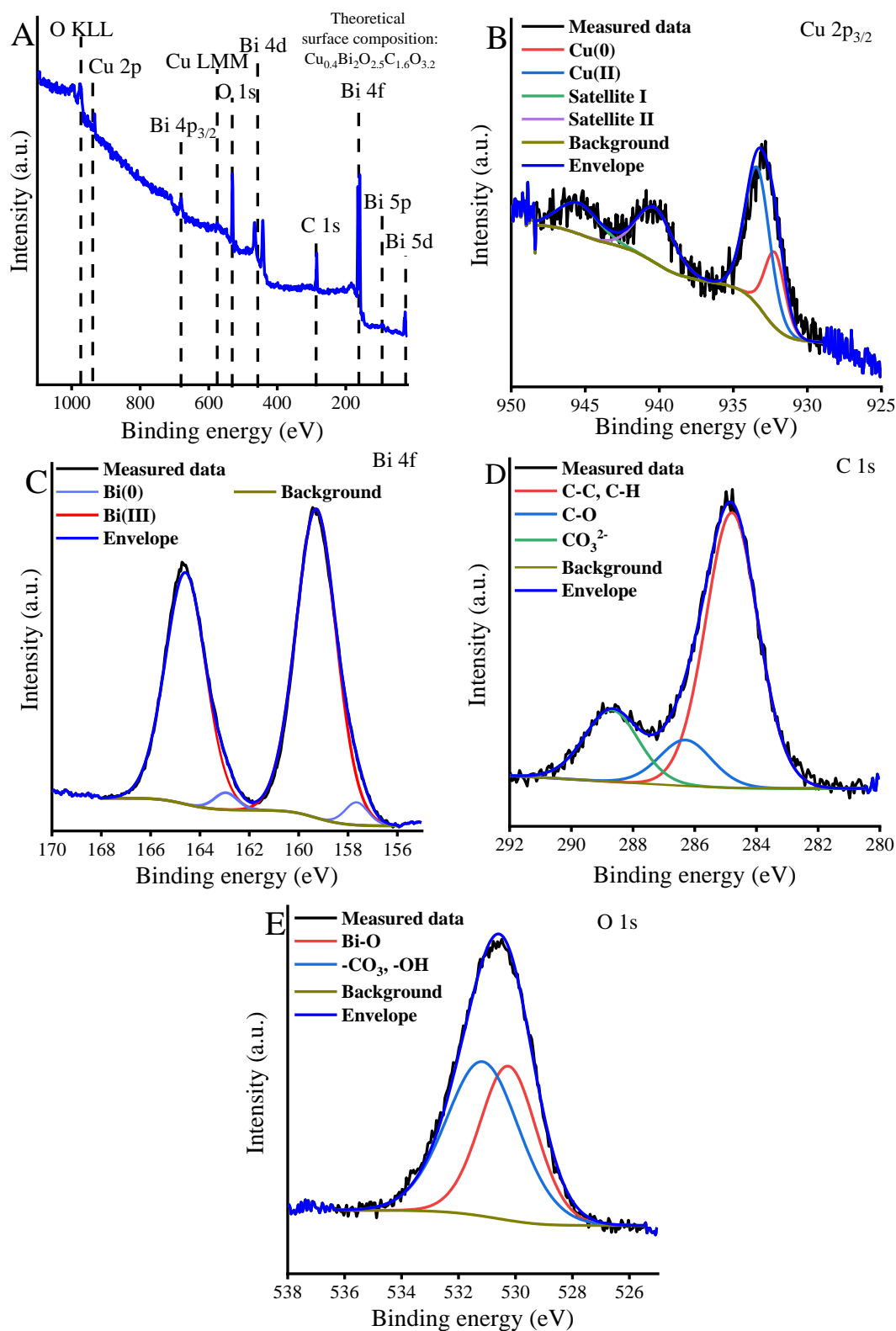


**Figure 25.** XPS survey scans (A) and Cu 2p<sub>3/2</sub> (B), Bi 4f (C), C 1s (D) as well as O 1s (E) XP spectra of recycled CuBi<sub>2</sub>O<sub>2</sub>CO<sub>3</sub> after the fifth run.<sup>176</sup>

To complete the study on the catalytic ability of CuBi<sub>2</sub>O<sub>2</sub>CO<sub>3</sub>, the range of viable derivatives of 2-iodo-aniline (**Table 16.**) was also examined. It can be concluded that high

yields and selectivities can be achieved under the optimized reaction conditions. In the presence of electron-donating groups, a proportional decrease in yield and selectivity was observed. Furthermore, the replacement of 2-iodoaniline as starting material with a bromo- or chloro-derivative does not allow efficient heterocyclization. However, the time-efficient catalyst ensured a high efficiency in the heterocyclization of all starting materials presented, which is higher than ever before.

### 5.2.2. Catalytic capabilities of $Mn/Co/NiBi_2O_2CO_3$ as heterogeneous catalysts in the synthesis of 2-phenylbenzimidazole, its isomers and derivatives

To investigate the catalytic performance of manganese-, cobalt- and nickel-modified bismutite structures, a multi-step reaction cascade was chosen as a model reaction. The reaction sequence and the initial reaction conditions are described in detail in Chapter 4., **Scheme 5.** and **Table 7.** In order to evaluate the effectiveness of the catalysts, yield and selectivity values were determined after each reaction.

Since limited and less relevant information is available on the catalytic use of commercial and self-prepared bismuth compounds in oxidative annulations, in our preliminary experiments we investigated some salts, bismuth oxide and bismuth oxide subcarbonate for the oxidative coupling of *o*-phenylenediamine (2-aminoaniline; **(2)**) and benzylamine (**(1)**). The reaction conditions used were similar to those of Gopalaiah and Chandrudu.<sup>155</sup>

**Table 15.** Oxidative coupling of benzylamine and 2-aminoaniline catalyzed by different bismuth compounds. Reaction conditions: 1 equiv. (0.25 M) of benzylamine, 1.2 equiv. of 2-aminoaniline, DMSO (2 mL), 10 mol% of catalyst, 110 °C for 24 h<sup>194</sup>

Bi-compounds	conversion of 1 (%)	selectivity of 3 (%)*	selectivity of 4 (%)**	selectivity of 5 (%)***
—	4±1	—	—	100
<b>BiCl<sub>3</sub></b>	3±2	—	—	100
<b>BiI<sub>3</sub></b>	4±1	—	—	100
<b>Bi(NO<sub>3</sub>)<sub>3</sub></b>	4±2	—	—	100
<b>BiOCl</b>	2±3	—	—	100
<b>NaBiO<sub>3</sub></b>	3±4	—	—	100
<b>Bi<sub>2</sub>O<sub>3</sub></b>	11±2	11	9	80
<b>Bi<sub>2</sub>O<sub>2</sub>CO<sub>3</sub></b>	19±3	18	5	77

\*2-(benzylideneamino)aniline, \*\*2-phenylbenzimidazole, \*\*\*benzylidenebenzylamine

As shown in **Table 15.** the commercial bismuth compounds showed very poor efficiency, similar to the non-catalyzed reaction (~4% conversion). On the other hand, **Bi<sub>2</sub>O<sub>3</sub>** and as-

prepared  $\text{Bi}_2\text{O}_2\text{CO}_3$  were found to be slightly active in the reaction with a conversion of 11 and 19% respectively. It is important to emphasize that without preliminary heat treatment at  $\sim 150^\circ\text{C}$ , even this low catalytic efficiency would not have been achieved due to the water adsorbed on the surface during the synthesis. The active promoters unfortunately, showed a high degree of selectivity toward the undesired self-coupling product of benzylamine (5).

In the following solvent compatibility tests were carried out with environmentally compatible solvents in the presence of  $\text{Bi}_2\text{O}_3$  and  $\text{Bi}_2\text{O}_2\text{CO}_3$ , based on the general experience that the selectivity and reaction rate of both oxidative transformations can be influenced by the solvent used. Accordingly, **Fig. 26.** shows that compared to the ineffectiveness of the catalysts in water, 2-methyl-tetrahydrofuran and under solvent-free conditions, an improved benzylamine conversion and a significant increase in product selectivity were observed in DMSO:water mixtures and in  $\gamma$ -valerolactone. The tendency for the amount of homo-coupled dimer (5) to gradually decrease with increasing water content in DMSO leads to the complete disappearance of the by-product in the 1:9 mixture. Like the increase in water content,  $\gamma$ -valerolactone as a solvent did not favor the side reaction. Together with the decrease in the self-coupling of benzylamine, a remarkable improvement in the selectivity of the products of oxidative coupling (3) and oxidative annulation (4) was observed. The best benzylamine conversion (69%) and the highest achievable 2-phenylbenzimidazole selectivity (73%) were obtained in the presence of  $\text{Bi}_2\text{O}_2\text{CO}_3$  in the solvent DMSO:H<sub>2</sub>O 1:9.

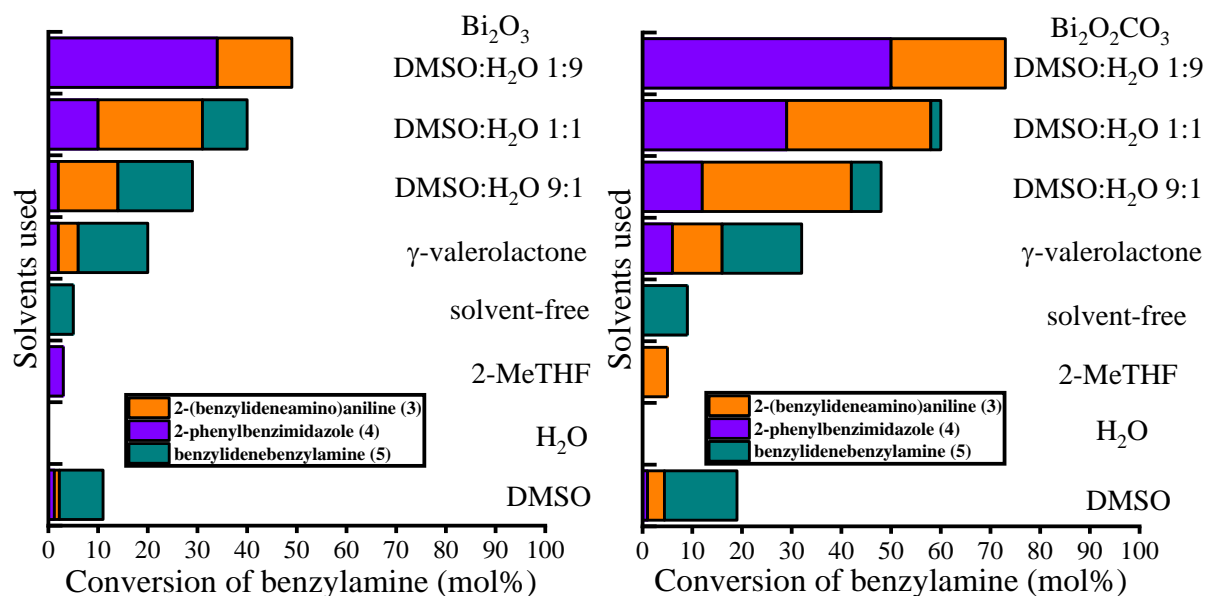


**Figure 26.** Solvent screen in the oxidative coupling of benzylamine and 2-aminoaniline catalyzed by  $\text{Bi}_2\text{O}_3$  and  $\text{Bi}_2\text{O}_2\text{CO}_3$ . Reaction conditions: 1 equiv. (0.25 M) of benzylamine, 1.2 equiv. of 2-aminoaniline, solvent (2 mL), 10 mol% of catalyst,  $110^\circ\text{C}$  (or reflux temperature) for 24 h.<sup>194</sup>

On the basis of these results, it can be concluded that bismuth compounds may represent undiscovered catalytic opportunities in such reactions, which are also comparable to the catalytic activity of the most commonly used homogeneous catalysts.

For reasons of comparability, it was also necessary to investigate the catalytic behavior of pure 3d TM oxides, as further building blocks of cooperative catalysts. Therefore, the catalytic properties of various manganese, cobalt and nickel oxides were tested under reaction conditions considered optimal for bismuth compounds (**Table 16.**). This study was also interesting because, to our knowledge, non-supported 3d transition metal oxides have not yet been studied in oxidative aniline coupling reactions.

**Table 16.** Oxidative coupling of benzylamine and 2-aminoaniline catalyzed by different transition metal compounds. Reaction conditions: 1 equiv. (0.25 M) of benzylamine, 1.2 equiv. of 2-aminoaniline, DMSO:H<sub>2</sub>O 1:9 (2 mL), 10 mol% of catalyst, 100 °C for 24 h<sup>194</sup>

Catalysts	conversion of 1 (%)	selectivity of 3 (%)*	selectivity of 4 (%)**	selectivity of 5 (%)***
—	5±1	—	—	100
MnO	2±2	—	—	100
Mn <sub>3</sub> O <sub>4</sub>	31±4	—	100	—
Mn <sub>2</sub> O <sub>3</sub>	—	—	—	—
MnO <sub>2</sub>	26±2	—	100	—
CoO	1±1	—	—	100
Co(OH) <sub>2</sub>	5±3	—	—	100
Co <sub>3</sub> O <sub>4</sub>	35±5	—	100	—
NiO	—	—	—	—
Ni(OH) <sub>2</sub>	—	—	—	—
NiOOH	—	—	—	—
Bi <sub>2</sub> O <sub>2</sub> CO <sub>3</sub>	69±4	27	73	—

\*2-(benzylideneamino)aniline, \*\*2-phenylbenzimidazole, \*\*\*benzylidenebenzylamine

Review of the results shows that only the compounds MnO<sub>2</sub>, Mn<sub>3</sub>O<sub>4</sub> and Co<sub>3</sub>O<sub>4</sub> showed appreciable catalytic activity (26–35% conversion) in the oxidative reaction, but they formed the annulation product (**4**) selectively. Moreover, the reactivity of the nickel catalysts was zero as they could not convert benzylamine into a product. Therefore, the nickel-modified bismuth was excluded from further optimization.

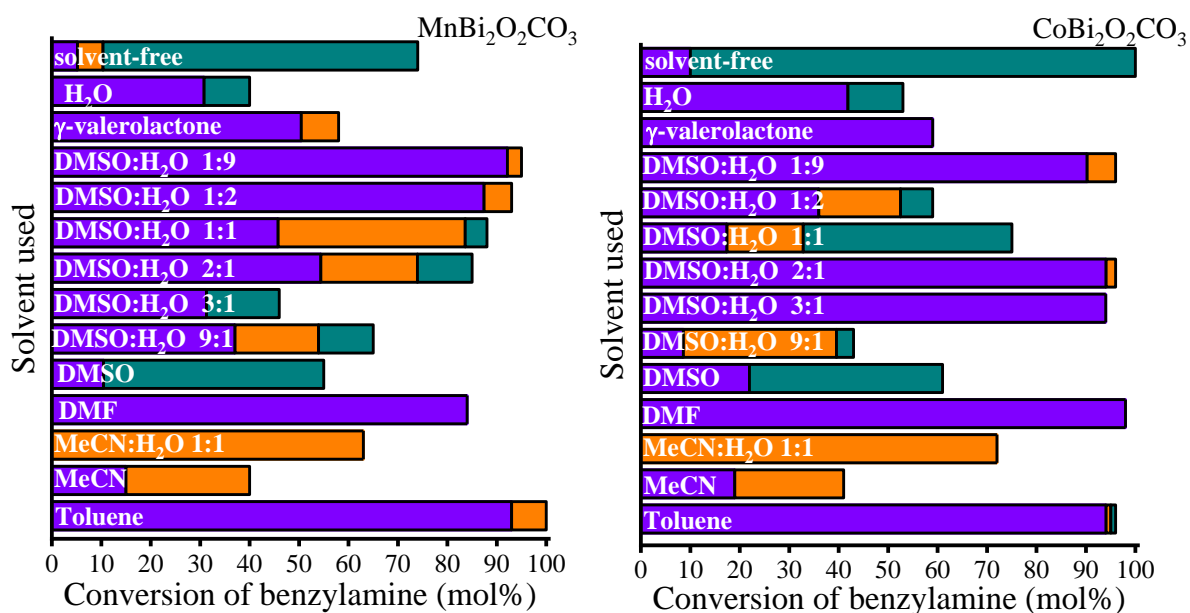


**Figure 27.** The effect of various solvents in the oxidative coupling of benzylamine and 2-aminoaniline. Reaction conditions: 1 equiv. (0.25 M) of benzylamine, 1.2 equiv. of 2-aminoaniline, 10 mol% of MnBi<sub>2</sub>O<sub>2</sub>CO<sub>3</sub> (**left side**) and CoBi<sub>2</sub>O<sub>2</sub>CO<sub>3</sub> (**right side**), 110 °C (100 °C: DMSO:water mixtures, water; reflux: MeCN-containing solvents) for 24 h. (Products: cyan: benzyldenebenzylamine; orange: 2-(Benzyldenebenzylamino)aniline; violine: 2-Phenylbenzimidazole).<sup>194</sup>

Once all the basic information about the possible contributions of the metallic components was available, the optimization process was continued with solvent experiments in the presence of manganese- and cobalt-modified bismutites. Both catalysts showed remarkable tolerance to a variety of organic solvents as well as to water (**Fig. 27.**), and the best performances were observed in DMSO:H<sub>2</sub>O 1:9 mixtures (MnBi<sub>2</sub>O<sub>2</sub>CO<sub>3</sub>: ~95% conv./~97% sel., CoBi<sub>2</sub>O<sub>2</sub>CO<sub>3</sub>: ~96% conv./~95% sel.) similar to the unmodified bismutite. Compared to the pristine host, modification of the framework with 3d metal species generally enhanced benzylamine conversion, regardless of the solvent used. Moreover, the chemoselectivities approached the excellent 2-phenylbenzimidazole (**4**) selectivities obtained for the pure metal oxides. The composition of the final product could be controlled by the choice of the appropriate solvent. While the annulation product was selectively obtained in γ-valerolactone by the cobalt-containing bismutite, the solvent acetonitrile:water 1:1 exclusively promoted the formation of 2-(benzyldeneamino)aniline (**3**).



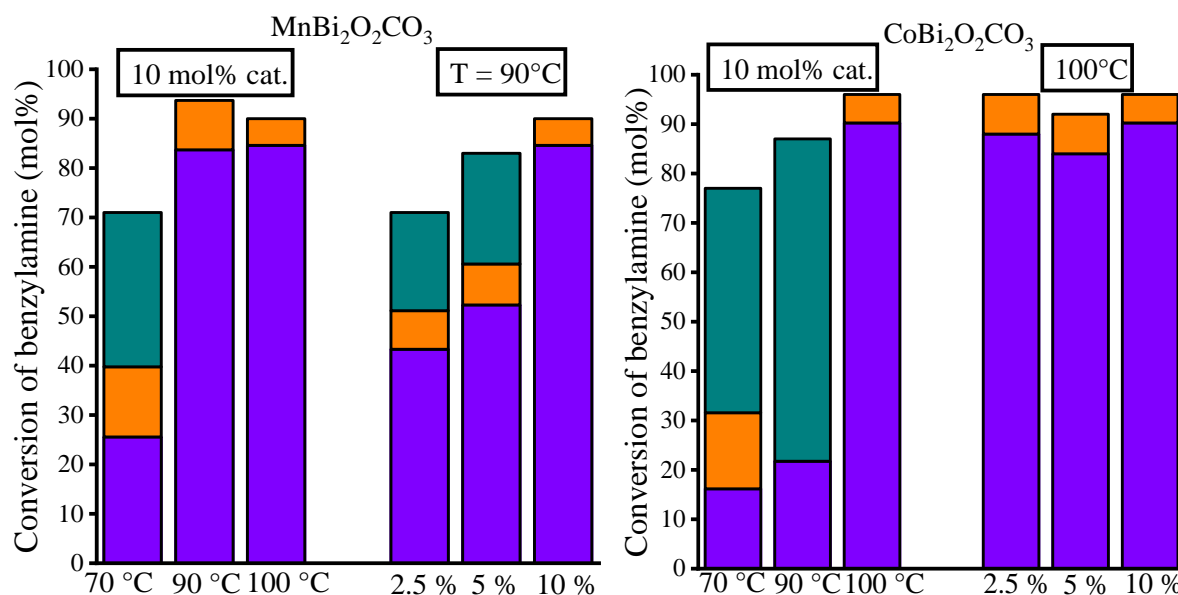


**Figure 28.** The effect of various reaction temperature and catalyst loading in the oxidative coupling of benzylamine and 2-aminoaniline. Reaction conditions: 1 equiv. (0.25 M) of benzylamine, 1.2 equiv. of 2-aminoaniline, DMSO:H<sub>2</sub>O 1:9 (2 mL), 10 mol% of  $\text{MnBi}_2\text{O}_2\text{CO}_3$  (**left side**) and  $\text{CoBi}_2\text{O}_2\text{CO}_3$  (**right side**), 100 °C/ marked temperature for 24 h. (Products: cyan: benzyldenebenzylamine; orange: 2-(Benzyldenebenzylamino)aniline; violine: 2-Phenylbenzimidazole).<sup>194</sup>

**Figure 28.** shows the effect of the quality of the modifying 3d metal ions. The effect becomes clear when examining the catalyst loading and the temperature dependence. While the presence of 2.5 mol% cobalt-containing bismutite was sufficient to sustain the large-scale formation of the annulation product (4), 10 mol% manganese-containing catalyst was required to achieve the same productivity. The optimum temperature for both catalysts was 90 °C or higher.

After instrumental characterization revealed the heterogeneous spatial distribution of manganese and cobalt ions in the co-precipitated samples, the comparative role of the impregnated samples came to the fore. To prove the cooperative catalytic behavior of the interfacial centers in the composites, comparative tests were performed in the presence of the modified bismutites, the impregnated references and the building blocks under the optimized reaction conditions (**Fig. 29.**). Based on the results, the following conclusions can be drawn: First, all systems in which the transition metal centers are connected to the bismutite support in some way proved to be much more efficient than those in which no support was present. Second, it is clear from the conversion and selectivity values that the common system of Bi(III) centers and the transition metal ions effectively promotes oxidative transformation. Third, although the impregnated samples exhibited lower catalytic activity (lower benzylamine conversion) than their co-precipitated counterparts, the product composition (selectivity toward 2-phenylbenzimidazole) was the same for both catalysts. It can be concluded that there is a clear

relationship between the co-presence of metal species on the bismutite surface forming a real cooperative active site for annulation.

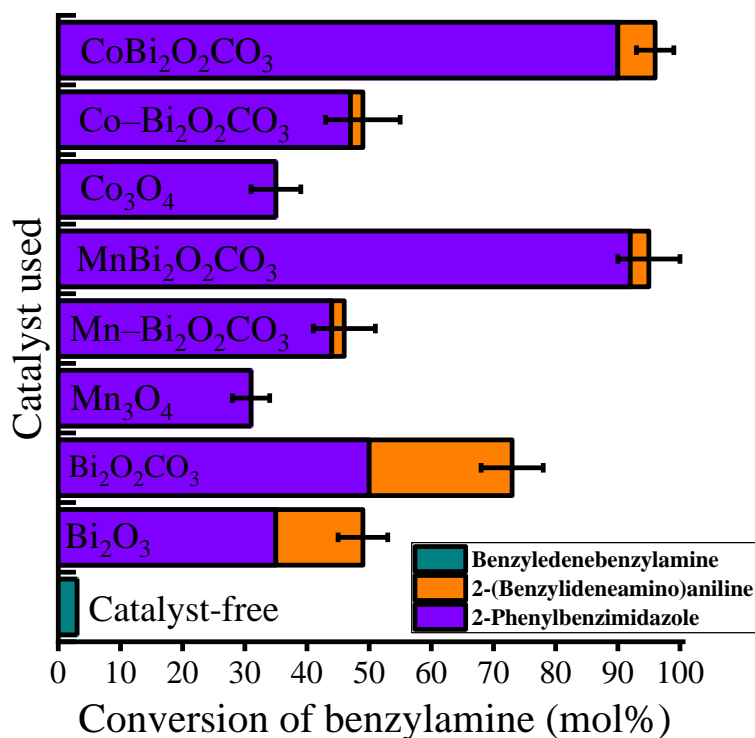


**Figure 29.** The effect of the quality of the catalysts in the oxidative coupling of benzylamine and 2-aminoaniline. Reaction conditions: 1 equiv. (0.25 M) of benzylamine, 1.2 equiv. of 2-aminoaniline, DMSO:H<sub>2</sub>O 1:9 (2 mL), 10 mol% of catalyst, 100 °C for 24 h. (MBi<sub>2</sub>O<sub>2</sub>CO<sub>3</sub>: co-precipitated samples; M-Bi<sub>2</sub>O<sub>2</sub>CO<sub>3</sub>: impregnated samples).<sup>194</sup>

Time-dependent experiments were carried out to determine the kinetic profile of the reaction and to attempt to quantify the contribution of the active sites. The number of molecules transformed per hour and per metal ion (turnover frequency, TOF) was calculated from the initial reaction rates of the kinetic curves shown in **Figure 30**. The highest achievable yield of 2-phenylbenzimidazole was obtained with all catalysts in 24 hours, with CoBi<sub>2</sub>O<sub>2</sub>CO<sub>3</sub> proving to be the most efficient. 88% of the desired product was produced within 8h. The TOF value calculated for the cobalt-containing system was much higher than that of the manganese containing counterpart. In general, it can also be observed that the TOF values of the co-precipitated samples were almost 4 times higher than those of the impregnated references, which clearly confirms the generation of the interface effect in the modified co-precipitation methods. Since large differences are observed when comparing the initial activities of the supported catalysts, it can be concluded that Bi(III) and transition metal ions are jointly responsible for the manifested catalytic activity. This finding is consistent with the observation from the basic experiments (**Table 17.** and **18.**), according to which both bismuth and TM ions can catalyze the oxidative coupling of benzylamine and 2-aminoaniline.

In addition, time-dependent reactions were also carried out with  $\gamma$ -valerolactone as a solvent (**Fig. 31**).

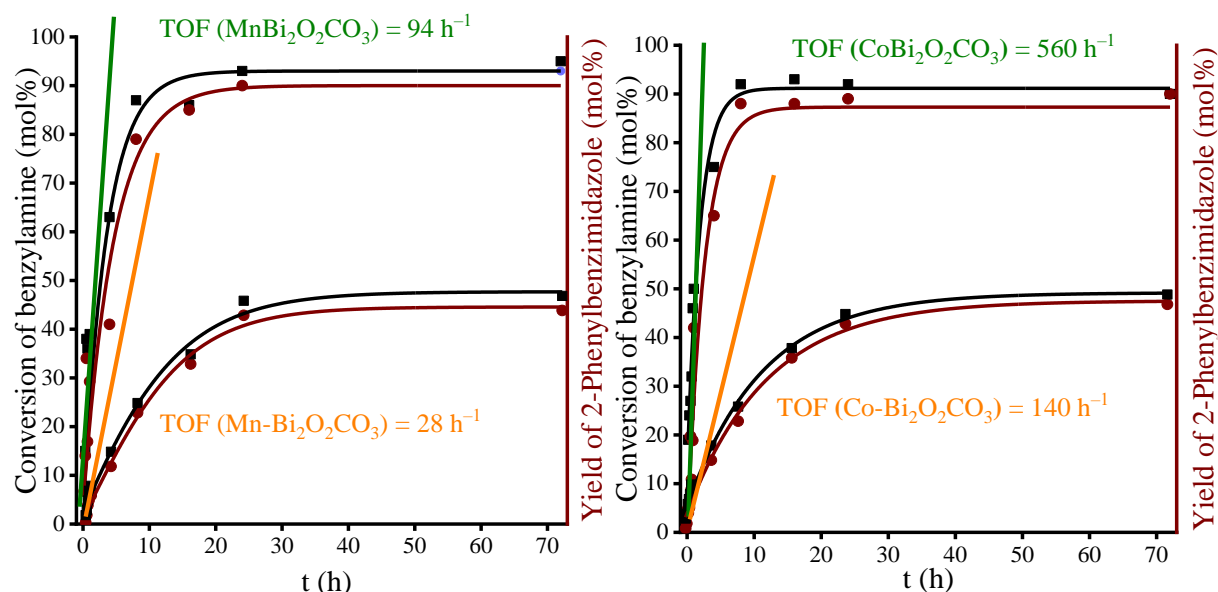


**Figure 30.** Conversions of benzylamine and yields of 2-phenylbenzimidazole as a function of time in the oxidative coupling of benzylamine and 2-aminoaniline catalyzed by  $\text{MnBi}_2\text{O}_2\text{CO}_3$  (**left side**) and  $\text{CoBi}_2\text{O}_2\text{CO}_3$  (**right side**) catalysts. Reaction conditions: 1 equiv. (0.25 M) of benzylamine, 1.2 equiv. of 2-aminoaniline,  $\text{DMSO}:\text{H}_2\text{O}$  1:9 (2 mL), 10 mol% of  $\text{MnBi}_2\text{O}_2\text{CO}_3$  or 2.5 mol%  $\text{CoBi}_2\text{O}_2\text{CO}_3$ , 90 °C (**left side**)/100 °C (**right side**).<sup>194</sup>

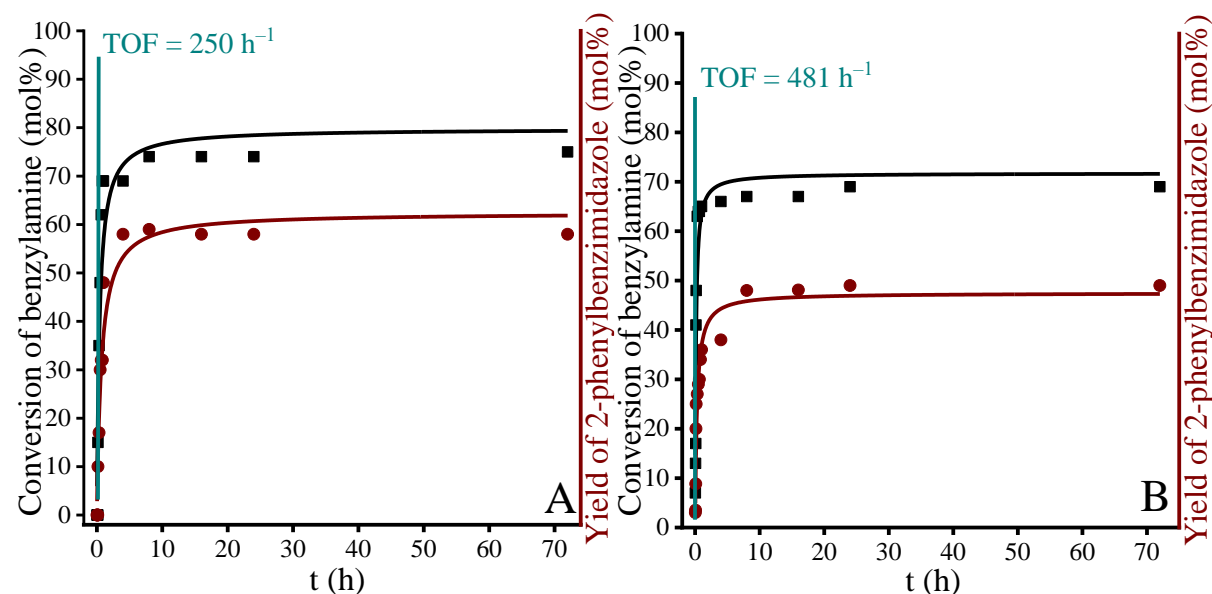


**Figure 31.** Conversions of benzylamine and yields of 2-Phenylbenzimidazole as a function of time in the oxidative coupling of benzylamine and 2-aminoaniline catalyzed by  $\text{MnBi}_2\text{O}_2\text{CO}_3$  (**A**) and  $\text{CoBi}_2\text{O}_2\text{CO}_3$  (**B**) catalysts. Reaction conditions: 1 equiv. (0.25 M) of benzylamine, 1.2 equiv. of 2-aminoaniline,  $\gamma$ -valerolactone (2 mL), 10 mol% of  $\text{MnBi}_2\text{O}_2\text{CO}_3$  or 2.5 mol%  $\text{CoBi}_2\text{O}_2\text{CO}_3$ , 80 °C.<sup>194</sup>

The TOF values calculated for the co-precipitated bismutites proved to be very high, for the manganese-containing sample even higher than in the solvent  $\text{DMSO}:\text{H}_2\text{O}$  1:9, but the

selectivity and yield values obtained for the final heterocycle were lower than those obtained so far.

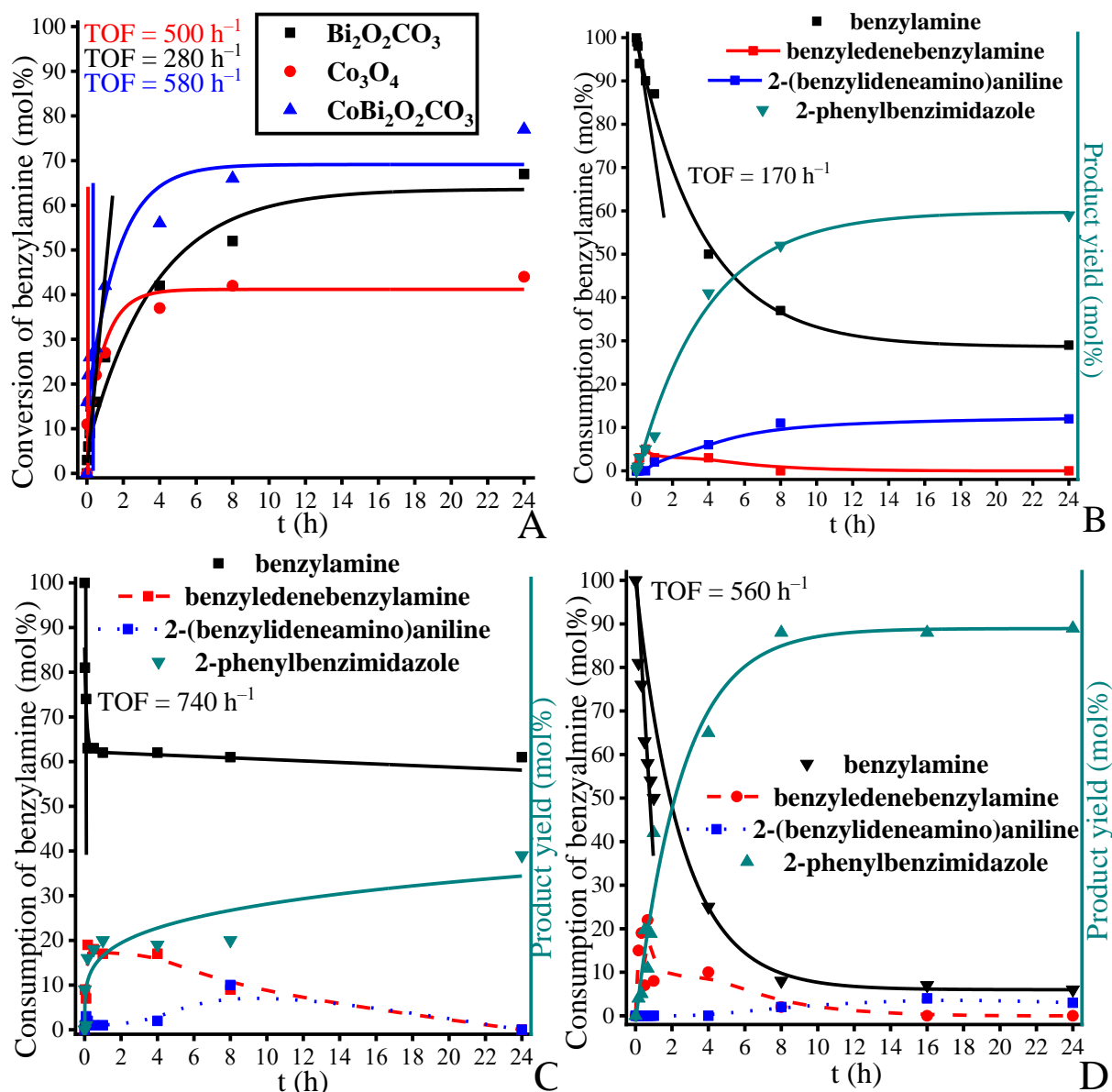


**Figure 32.** Benzylamine conversion as a function of time in the oxidation reaction of benzylamine catalyzed by  $\text{CoBi}_2\text{O}_2\text{CO}_3$ ,  $\text{Bi}_2\text{O}_2\text{CO}_3$  and  $\text{Co}_3\text{O}_4$  catalysts (A). Reaction conditions: 1 equiv. (0.25 M) of benzylamine, DMSO:H<sub>2</sub>O 1:9 (2 mL), 2.5 (D)/10 mol% (B, C) of catalyst, 100 °C. Consumption of benzylamine and product distribution as a function of time in the oxidative coupling/annulation of benzylamine and 2-aminoaniline catalyzed by  $\text{Bi}_2\text{O}_2\text{CO}_3$  (B),  $\text{Co}_3\text{O}_4$  (C) and  $\text{CoBi}_2\text{O}_2\text{CO}_3$  (D) catalysts. Reaction conditions: 1 equiv. (0.25 M) of benzylamine, 1.2 equiv. of 2-aminoaniline, DMSO:H<sub>2</sub>O 1:9 (2 mL), 2.5 (D)/10 mol% (B, C) of catalyst, 100 °C.<sup>194</sup>

Further experiments were conducted in an attempt to determine the exact contribution of each component in the cooperative  $\text{CoBi}_2\text{O}_2\text{CO}_3$  system. For this purpose, the catalytic ability of cobaltite ( $\text{Co}_3\text{O}_4$ ), bismutite and the co-precipitated sample were compared in the oxidation

reaction of benzylamine and in the oxidative coupling of benzylamine and 2-aminoaniline. The results are shown in **Fig. 32**.

In the oxidation of benzylamine, all catalysts showed moderate activity with complete selectivity towards benzyldenebenzylamine (5). The direct oxidation product (benzylimine) could not be detected in any of the reaction mixtures due to its high reactivity.<sup>220</sup> The TOF value of cobaltite was higher than that of pure bismutite, and the highest activity was achieved by the cooperative catalyst. In contrast, the chemoselectivity was the same regardless of the catalysts used. In the presence of 2-aminoaniline, the only product observed was 2-phenylbenzimidazole when bismutite was used as catalyst. When cobaltite was used, the product composition was more complex, as all possible products were formed, but their distribution changed as a function of time. This observation probably indicates that the conversion of benzylimine to 2-(benzyldeneamino)aniline is faster in the presence of bismutite than when the reaction is catalyzed by cobaltite. In parallel, the consumption of the starting material (benzylamine) was higher with  $\text{Co}_2\text{O}_3$  than with  $\text{Bi}_2\text{O}_2\text{CO}_3$ . In the reaction promoted by the cooperative catalyst, a similar product distribution was observed as in bismutite catalysis, on the other hand, the consumption of benzylamine was similar to that in the cobalt-catalyzed reaction. In view of the above results, it is assumed that the rate-controlling step of the reaction sequence is the oxidation of benzylamine, which takes place at cobalt oxide centers on the surface of the cooperative catalyst, while the active site of the coupling/annulation step(s) is the bismuth species.

To investigate the recyclability of the supported catalysts, the impregnated and co-precipitated bismutite powders were separated (by centrifugation), washed (with ethanol, water and DMSO) and reused in a five-cycle reaction series. All reactions were carried out under the conditions given in the optimization. Using the co-precipitated samples, no significant decrease in benzylamine conversion was observed until the fifth run (**Fig. 33**), but the distribution between the oxidative coupling (3) and oxidative annulation (4) products changed significantly. From the second cycle onwards, the selectivity of the final heterocycle (4) slowly started to decrease and then stabilized at about 65%. The leaching of the metal components could not be measured during the ICP-MS measurements. On the other hand, the *ex-situ* XRD results showed a slight decrease in the crystallinity of the host, which could consequently hinder the accessibility of some active sites at the end of the third catalytic run.

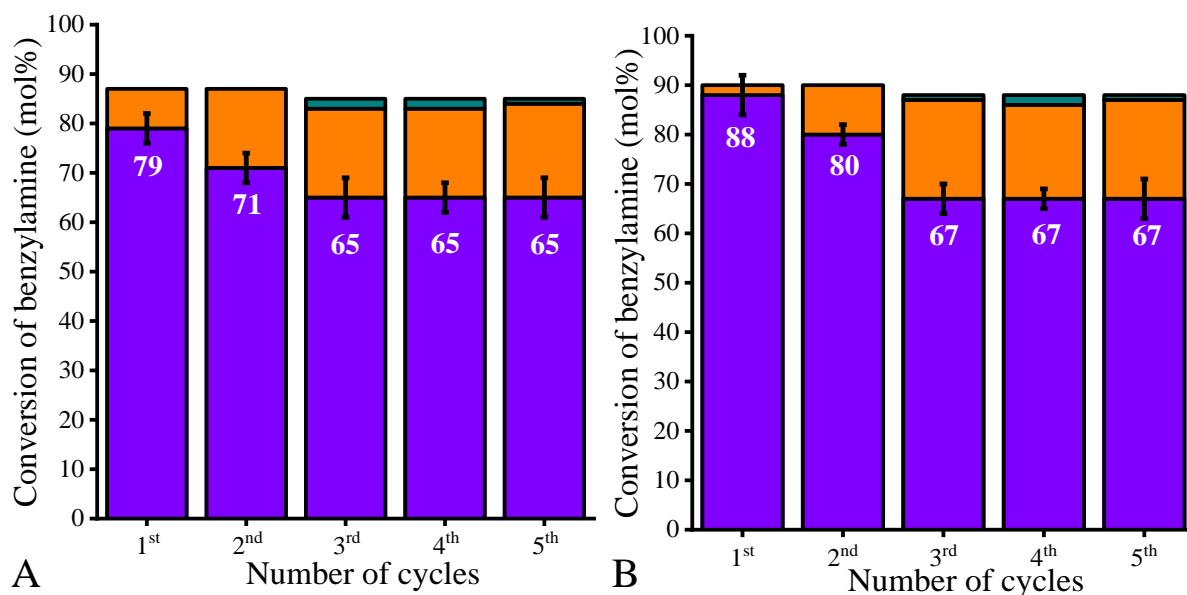


**Figure 33.** Reusability of MnBi<sub>2</sub>O<sub>2</sub>CO<sub>3</sub> (A) and CoBi<sub>2</sub>O<sub>2</sub>CO<sub>3</sub> (B) in the oxidative coupling of benzylamine and 2-aminoaniline. Reaction conditions: 1 equiv. (0.25 M) of benzylamine, 1.2 equiv. of 2-aminoaniline, DMSO:H<sub>2</sub>O 1:9 (2 ml), 10 mol% of MnBi<sub>2</sub>O<sub>2</sub>CO<sub>3</sub> or 2.5 mol% of CoBi<sub>2</sub>O<sub>2</sub>CO<sub>3</sub>, 90 °C (A) or 100 °C (B) for 8 h. (Products: cyan: benzyldenebenzylamine; orange: 2-(Benzyldenebenzylamino)aniline; violine: 2-Phenylbenzimidazole).<sup>194</sup>

When the impregnated samples were used, the catalytic activity of the composites decreased sharply, and after three consecutive cycles the original productivity fell to one fifth (Fig. 34.).

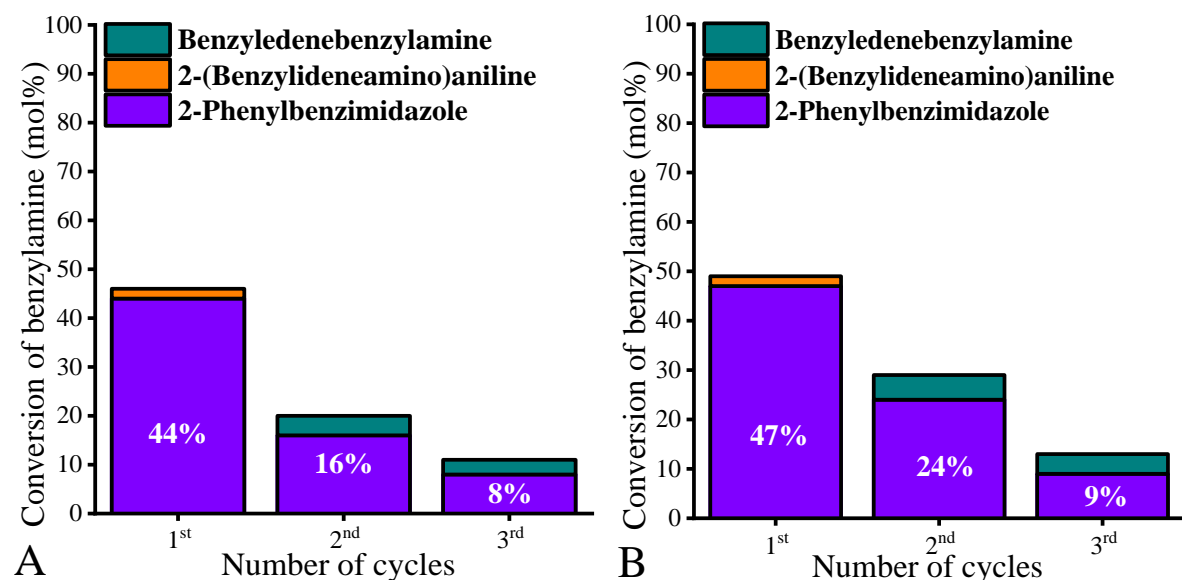


**Figure 34.** Reusability of Mn-Bi<sub>2</sub>O<sub>2</sub>CO<sub>3</sub> (A) and Co-Bi<sub>2</sub>O<sub>2</sub>CO<sub>3</sub> (B) in the oxidative coupling of benzylamine and 2-aminoaniline. Reaction conditions: 1 equiv. (0.25 M) of benzylamine, 1.2 equiv. of 2-aminoaniline, DMSO:H<sub>2</sub>O 1:9 (2 mL), 10 mol% of MnBi<sub>2</sub>O<sub>2</sub>CO<sub>3</sub> or 10 mol% of CoBi<sub>2</sub>O<sub>2</sub>CO<sub>3</sub>, 100 °C for 24 h.<sup>194</sup>

At the same time, a larger amount of the non-ring-closed intermediate (3) remained in the product mixture. Significant leaching of 3d metals confirmed by ICP-MS, eventually led to

complete wash out of the active components at the end of the third cycle. Due to the impregnation technique, the 3d transition metal samples are only weakly bound to the bismutite surfaces and leaching of the TM content can occur without degradation of the bismutite host, as clearly shown in **Figure 35**.

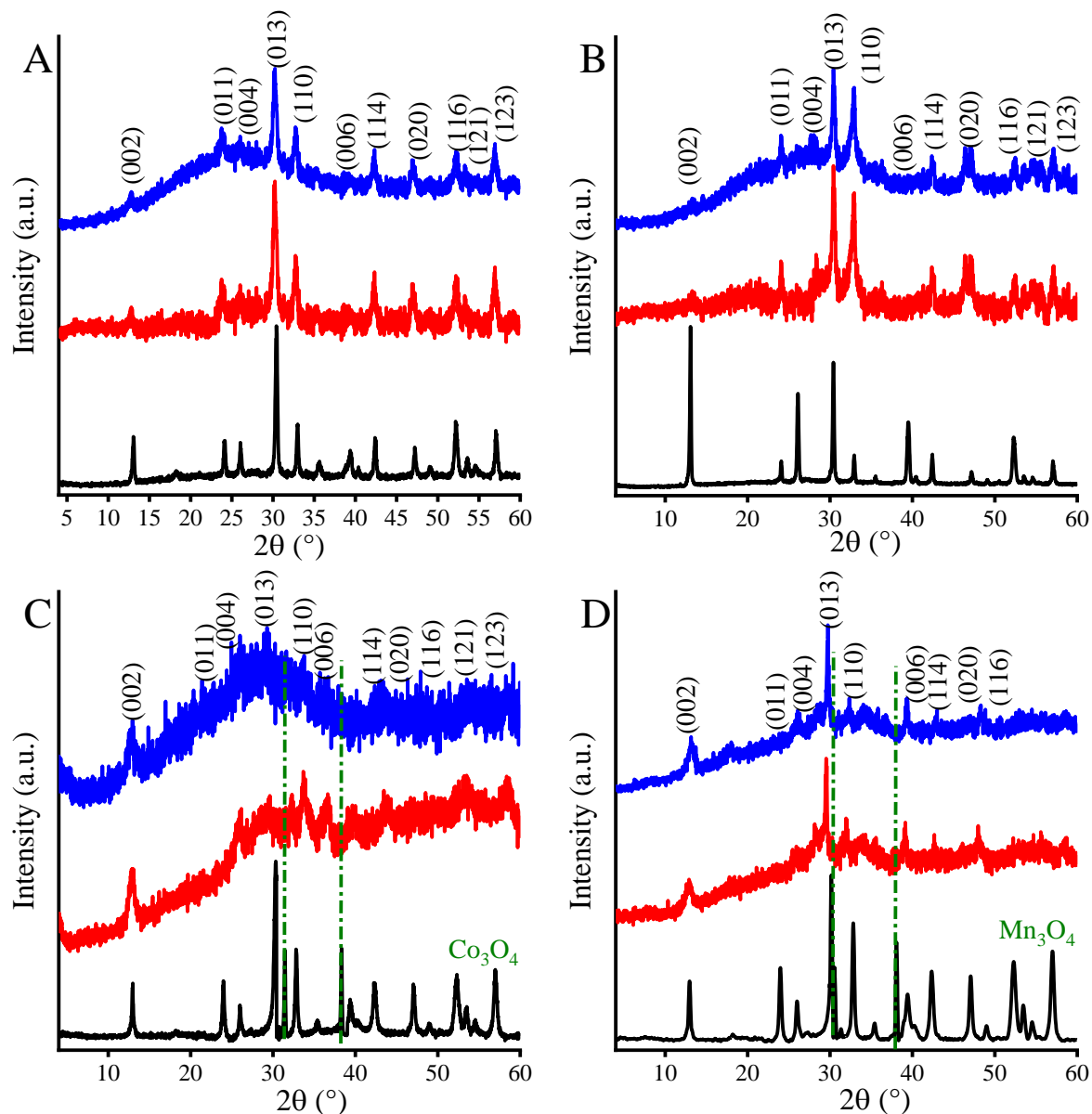


**Figure 35.** XRD patterns of the as-prepared (black lines), used after third run (red lines) and used after fifth run (blue lines) of  $\text{CoBi}_2\text{O}_2\text{CO}_3$  (A),  $\text{MnBi}_2\text{O}_2\text{CO}_3$  (B),  $\text{Co-Bi}_2\text{O}_2\text{CO}_3$  (C) and  $\text{Mn-Bi}_2\text{O}_2\text{CO}_3$  (D).<sup>194</sup>

**Figure 36.** shows the same phenomenon in the hot filtration tests carried out in the presence of the structurally modified and the impregnated bismutites. While all transformations were quenched by removing the co-precipitated bismutites, oxidative coupling and annulation continued after filtering the impregnated catalysts. These results are thus evidence of the heterogeneous nature of the  $\text{CoBi}_2\text{O}_2\text{CO}_3$ - and  $\text{MnBi}_2\text{O}_2\text{CO}_3$ -catalyzed reactions.

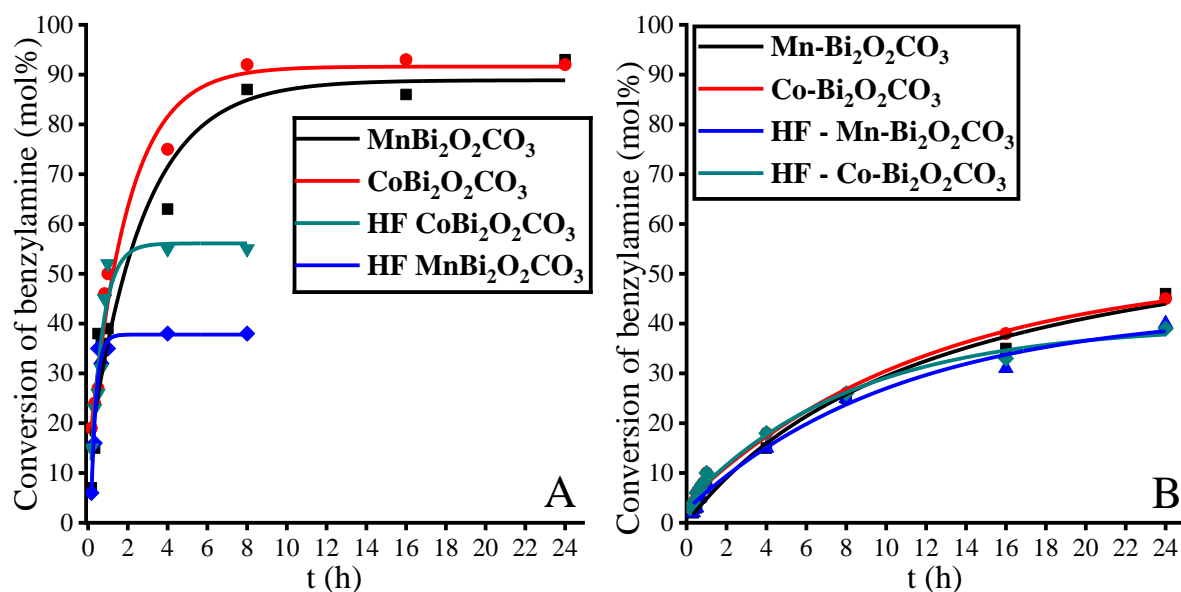


**Figure 36.** Hot filtration test of MnBi<sub>2</sub>O<sub>2</sub>CO<sub>3</sub>/CoBi<sub>2</sub>O<sub>2</sub>CO<sub>3</sub> and Mn-Bi<sub>2</sub>O<sub>2</sub>CO<sub>3</sub>/Co-Bi<sub>2</sub>O<sub>2</sub>CO<sub>3</sub> in the oxidative coupling of benzylamine and 2-aminoaniline producing 2-phenylbenzimidazole (see Scheme 5.): Conversions of benzylamine. Reaction conditions: 1 equiv. (0.25 M) benzylamine, 1.2 equiv. 2-aminoaniline, solvent: DMSO:water 1:9, 10 mol% of MnBi<sub>2</sub>O<sub>2</sub>CO<sub>3</sub>, at 90 °C, or 2.5 mol% of CoBi<sub>2</sub>O<sub>2</sub>CO<sub>3</sub>, at 100 °C and 10 mol% of Mn-Bi<sub>2</sub>O<sub>2</sub>CO<sub>3</sub>/Co-Bi<sub>2</sub>O<sub>2</sub>CO<sub>3</sub>, at 100 °C. (Hot filtration of used catalyst occurred after 1 hour for MBi<sub>2</sub>O<sub>2</sub>CO<sub>3</sub> and after 8 hours for M-Bi<sub>2</sub>O<sub>2</sub>CO<sub>3</sub> (M: Mn, Co)).<sup>194</sup>

Summarizing the results presented so far, one can conclude that manganese- and cobalt-containing materials can be competitive and attractive alternatives in oxidative coupling/annulation.

As a final step of the catalytic study, the extensibility of the reaction with different substituted benzylamines was investigated (Table 17.). For most starting materials, high selectivity (64-88%) and good conversion (37-100% after 8h) were achieved, successfully avoiding the formation of the undesirable dimeric by-products. For *ortho*-methoxy and *meta*-nitro substituents, only the formation of the corresponding annulation products was observed.

In the following, the cooperative catalysts were not limited to the couplings of 2-aminoaniline. In the catalytic transformations of 2-amino-phenols and 2-amino-benzenethiols the corresponding benzoxazoles and benzothiazoles were also successfully synthesized. Nevertheless, the selectivity results often show the presence of large amounts of non-ring-closed intermediates for the isosteres. Therefore, it could be assumed that the efficiency of the catalytic ring-closing is influenced by the reaction temperature.



**Table 17.** Scope of N-, O- and S-containing heterocycles production *via* oxidative coupling of benzylamine-derivatives and 2-amino /hydroxy /mercapto anilines over MnBi<sub>2</sub>O<sub>2</sub>CO<sub>3</sub> and CoBi<sub>2</sub>O<sub>2</sub>CO<sub>3</sub> catalysts<sup>194</sup>

$$\text{R-CH}_2\text{NH}_2 + \text{C}_6\text{H}_4\text{X} \xrightarrow[\text{DMSO:H}_2\text{O} = 1:9, 90 \text{ or } 100^\circ\text{C}, 8 \text{ h}]{\text{MnBi}_2\text{O}_2\text{CO}_3}$$

$$\text{R-CH=N-C}_6\text{H}_4\text{X} + \text{Benzimidazole derivative}$$

**(1)**                      **(2)**                      **(3)**                      **(4)**

$c = 0.25\text{M}$                        $1.2 \text{ eqv.}$

		MnBi <sub>2</sub> O <sub>2</sub> CO <sub>3</sub> (90 °C)			CoBi <sub>2</sub> O <sub>2</sub> CO <sub>3</sub> (100 °C)		
#	X= NH	conversion of 1 (%)	selectivity of 3 (%) <sup>1</sup>	selectivity of 4 (%) <sup>2</sup>	conversion of 1 (%)	selectivity of 3 (%) <sup>1</sup>	selectivity of 4 (%) <sup>2</sup>
1	R= <i>p</i> -OMe	57 93*	88 33*	12 67*	57 97*	48 20*	52 80*
2	R= <i>o</i> -OMe	72 99* 76**	64 17* 59**	36 83* 39**	43 79* 48**	— —* —**	100 100* 92**
3	R= <i>p</i> -Cl	73 100*	84 23*	16 77*	68 91*	74 19*	26 81*
4	R= <i>o</i> -Cl	80 100*	73 15*	23 85*	68 95*	82 23*	18 77*
5	R= <i>m</i> -nitro	71 100*	— —*	100 100*	76 100*	— —*	100 100*
#	X= O	conversion of 1 (%)	selectivity of 3 (%) <sup>1</sup>	selectivity of 4 (%) <sup>2</sup>	conversion of 1 (%)	selectivity of 3 (%) <sup>1</sup>	selectivity of 4 (%) <sup>2</sup>
1	R= H	100	70	30	23	—	100
2	R= <i>p</i> -OMe	59 100*	46 19*	54 81*	69 100*	19 6*	81 94*
3	R= <i>o</i> -OMe	75	80	20	47	—	100
4	R= <i>p</i> -Cl	37	73	27	19	37	63
5	R= <i>o</i> -Cl	57	49	51	95	63	37
6	R= <i>m</i> -nitro	91	94	6	100	86	14
#	X= S	conversion of 1 (%)	selectivity of 3 (%) <sup>1</sup>	selectivity of 4 (%) <sup>2</sup>	conversion of 1 (%)	selectivity of 3 (%) <sup>1</sup>	selectivity of 4 (%) <sup>2</sup>
1	R= H	37	68	32	88	43	57
2	R= <i>p</i> -OMe	52 99*	46 22*	54 78*	17 45*	53 33*	47 67*
3	R= <i>o</i> -OMe	79	80	20	50	—	100
4	R= <i>p</i> -Cl	31	77	23	68	50	50
5	R= <i>o</i> -Cl	74	99	1	62	—	100
6	R= <i>m</i> -nitro	39	100	—	83	99	1

<sup>1</sup>cross-coupled imines and their isosteres

<sup>2</sup>benzimidazoles and their isosteres

\*subsequent reactions: Mn: 90 °C for 8h + 110 °C for 4h and Co: 100 °C for 8h + 110 °C for 4h

\*\*subsequent reactions without catalysts

To verify this, a temperature-programmed reaction sequence was introduced in which the chosen reactions were repeated by following the 8-hour step at 90 (Mn-based catalysts)/100 °C (Co-based catalysts) by a 4-hour step at 110 °C. In this way, the rings were closed and the annulation products formed. (Note: at the end of the reaction, practically pure DMSO remained as solvent.) Indeed, for several benzylamine analogues, the selectivity of both the oxidative coupling product and the oxidative annulation product could be controlled by the temperature program. To eliminate the possibility of terminal ring closure, the elevated temperature step was repeated for some reactions after the catalyst had been removed from the reaction mixtures. The result was that neither the conversion nor the selectivity changed significantly compared to the original, confirming the catalytic nature of the second step.

### 5.2.3. *Catalytic capabilities of Mn/Co/NiBi<sub>2</sub>O<sub>2</sub>CO<sub>3</sub> as heterogeneous catalysts in oxidative dehydrogenative couplings of anilines*

To further investigate the utility of TM modified bismutites in oxidative dehydrogenative reactions, homo- and hetero-couplings of anilines with a well-known mechanism<sup>221</sup> were investigated as a scouting experiment. The results presented in **Table 18**. shows that although moderate yields were achieved in the presence of all catalysts without the formation of significant by-products, the detailed optimization procedure did not significantly improve the available product yield. The initial reaction conditions were as follows: DMSO as solvent, 150 °C for 72 h in the presence of 10 mol% catalyst. The only but very promising exception was the manganese-containing catalyst which gave a 71% yield of the azobenzene product under solvent-free conditions. Without a catalyst and under argon atmosphere, no reaction took place and the use of an external oxidizer or oxygen atmosphere was not necessary.

**Table 18.** Optimization procedure of the TM modified bismutites promoted oxidative dehydrogenative homocoupling of aniline. Reaction conditions: 0.5 ml solvent, T = 64–175 °C for 12–72h and 10 mol% catalyst; c (aniline) = 0.6 M (when using other solvents than aniline)<sup>222</sup>

#	Composites	Solvent	T (°C)	Catalyst loading (mol%)	Reaction time (h)	Aniline conv. (mol%)	Azobenzene selectivity (mol%)
1	—	DMSO	150	—	72	3	—
2	Bi <sub>2</sub> O <sub>2</sub> CO <sub>3</sub>	DMSO	150	10	72	7	90
3	MnBi <sub>2</sub> O <sub>2</sub> CO <sub>3</sub>	DMSO	150	10	72	29	100
4	CoBi <sub>2</sub> O <sub>2</sub> CO <sub>3</sub>	DMSO	150	10	72	19	100
5	NiBi <sub>2</sub> O <sub>2</sub> CO <sub>3</sub>	DMSO	150	10	72	14	100
6	MnBi <sub>2</sub> O <sub>2</sub> CO <sub>3</sub> *	DMSO	150	10	72	2	100
7	MnBi <sub>2</sub> O <sub>2</sub> CO <sub>3</sub>	DMSO	110	10	72	9	100
8	MnBi <sub>2</sub> O <sub>2</sub> CO <sub>3</sub>	DMSO	175	10	72	30	100
9	MnBi <sub>2</sub> O <sub>2</sub> CO <sub>3</sub>	methanol	reflux	10	72	5	100
10	MnBi <sub>2</sub> O <sub>2</sub> CO <sub>3</sub>	toluene	reflux	10	72	20	75
11	MnBi <sub>2</sub> O <sub>2</sub> CO <sub>3</sub>	acetonitrile	reflux	10	72	—	—
12	MnBi <sub>2</sub> O <sub>2</sub> CO <sub>3</sub>	γ-valerolactone	reflux	10	72	15	100
13	MnBi <sub>2</sub> O <sub>2</sub> CO <sub>3</sub>	—	150	10	72	71	100
14	MnBi <sub>2</sub> O <sub>2</sub> CO <sub>3</sub>	—	reflux	10	72	73	96
15	MnBi <sub>2</sub> O <sub>2</sub> CO <sub>3</sub>	—	110	10	72	35	80
16	MnBi <sub>2</sub> O <sub>2</sub> CO <sub>3</sub>	—	150	5	72	49	90
17	MnBi <sub>2</sub> O <sub>2</sub> CO <sub>3</sub>	—	150	20	72	79	97
18	MnBi <sub>2</sub> O <sub>2</sub> CO <sub>3</sub>	—	150	10	48	34	100
19	MnBi <sub>2</sub> O <sub>2</sub> CO <sub>3</sub>	—	150	10	24	16	100
20	CoBi <sub>2</sub> O <sub>2</sub> CO <sub>3</sub>	—	150	10	48	75	100
21	CoBi <sub>2</sub> O <sub>2</sub> CO <sub>3</sub>	—	150	10	24	51	100
22	CoBi <sub>2</sub> O <sub>2</sub> CO <sub>3</sub>	—	150	10	12	23	100
23	CoBi <sub>2</sub> O <sub>2</sub> CO <sub>3</sub>	—	150	5	72	48	100
24	CoBi <sub>2</sub> O <sub>2</sub> CO <sub>3</sub>	—	150	2.5	72	12	100

If one compares the catalytic abilities of the modified bismutites with each other, significant differences can be observed (**Table 19.**), which become even more obvious with the heterocouplings. While an almost quantitative reaction (95% yield) took place with the cobalt-containing analog, the nickel-modified catalyst could only promote the formation of **3** to a small extent (23%).

**Table 19.** Oxidative dehydrogenative heterocoupling of anilines catalysed by TM modified bismutites (M-Bi<sub>2</sub>O<sub>2</sub>CO<sub>3</sub>). Reaction conditions: 0.5 ml aniline, T = 150 °C for 72h and 10 mol% catalyst; c (substituted aniline) = 0.5 M<sup>222</sup>

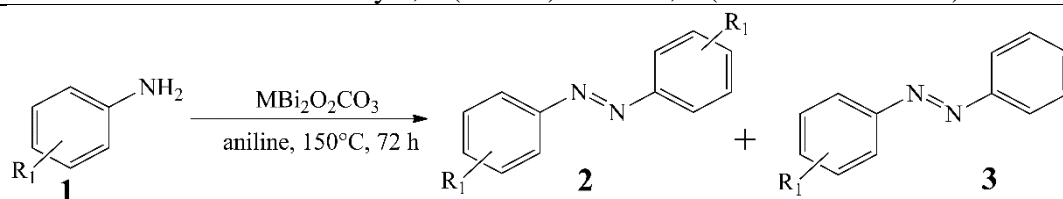
	MnBi <sub>2</sub> O <sub>2</sub> CO <sub>3</sub>		CoBi <sub>2</sub> O <sub>2</sub> CO <sub>3</sub>		NiBi <sub>2</sub> O <sub>2</sub> CO <sub>3</sub>	
	Conv. of <b>1</b> (mol%)	Yield of <b>3</b> (mol%)	Conv. of <b>1</b> (mol%)	Yield of <b>3</b> (mol%)	Conv. of <b>1</b> (mol%)	Yield of <b>3</b> (mol%)
R= H	71	71	95/51	95/51	23	23
R= <i>o</i> -OMe	78	44	100/93	88/80	14	13
R= <i>p</i> -OMe	100	52	100/100	60/56	100	72
R= <i>m</i> -nitro	43	4	100/56	75/34	3	2
R= <i>p</i> -Br	52	52	100/66	99/65	21	21
R= <i>p</i> -Cl	24	21	51/10	48/10	4	4
R= <i>o</i> -Me	29	22	100/75	84/57	22	17
R= <i>p</i> -Me	51	47	100/98	94/81	84	2
R= <i>p</i> -CN	12	9	35/5	34/4	5	1

2.5 mol% CoBi<sub>2</sub>O<sub>2</sub>CO<sub>3</sub>; t = 24h

Furthermore, the cobalt-containing compound proved to be the most active (34-88% yield) and the most selective for unsymmetric azo compounds. This feature allowed the catalyst loading to be reduced to 2.5 mol% with moderate to excellent yields (56-80%). (The significant excess of aniline probably also contributed to the unique selectivity for the asymmetric product in the presence of all catalysts.)

Therefore, an attempt was made below to isolate the effect of aniline excess and to re-examine the selectivity results by repeating three different asymmetric heterocoupling reactions (Table 20. A). DMSO and toluene were used as solvents. In all reactions, almost the same selectivities were obtained with reduced conversion, despite the lower aniline excess. This can be interpreted as direct evidence for the selectivity of the CoBi<sub>2</sub>O<sub>2</sub>CO<sub>3</sub> catalyst towards unsymmetric products. It is also important to note that the homocoupling of aniline in all cases can be explained by the presence of an aniline excess.

**Table 20.** Selectivity test of the as-prepared  $\text{CoBi}_2\text{O}_2\text{CO}_3$  catalyst in heterocoupling of aniline derivatives *via* oxidative dehydrogenative pathway. Reaction conditions: 0.5 ml solvent,  $T = 150^\circ\text{C}$  for 72h and 10 mol% catalyst;  $c$  (aniline) = 0.6 M,  $c$  (substituted aniline) = 0.5 M<sup>222</sup>



**A**

Starting material	Solvent	T (°C)	Catalyst loading (mol%)	Reaction time (h)	Conversion of 1 (mol%)	Selectivity of 3 (mol%)	Yield of 3 (mol%)
R= <i>o</i> -OMe	DMSO	150	10	72	17	88	15
R= <i>p</i> -Br	DMSO	150	10	72	28	96	27
R= <i>p</i> -Me	DMSO	150	10	72	25	95	24
R= <i>o</i> -OMe	toluene	reflux	10	72	51	90	46
R= <i>p</i> -Br	toluene	reflux	10	72	54	96	52
R= <i>p</i> -Me	toluene	reflux	10	72	54	92	50

**B**

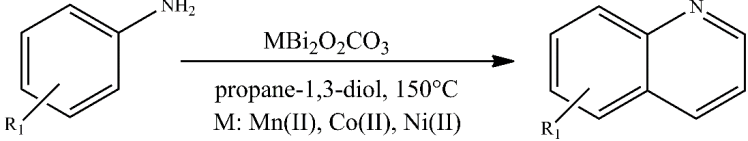
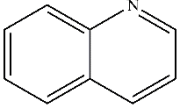
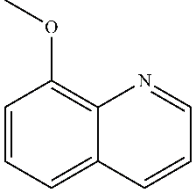
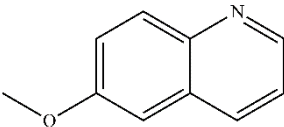
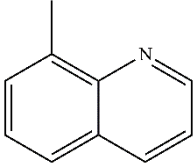
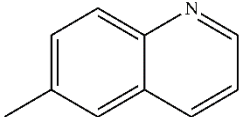
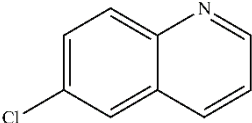
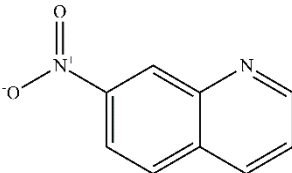
Catalyst	Solvent	T (°C)	Catalyst loading (mol%)	Reaction time (h)	Conversion of 1 (mol%)	Selectivity of 3 (mol%)	Yield of 3 (mol%)
$\text{CuBr}_2$ <sup>223</sup>	toluene	60	20	24	60–100*	50–100*	42–69*
meso- $\text{Mn}_2\text{O}_3$ <sup>294</sup>	toluene	110	32	12	80–100**	28–92**	28–87**

\* 1 bar  $\text{O}_2$ , 60 mol% pyridine

\*\* air atmosphere

Based on the above results, the hypothesis that TM modified bismutite analogues can have a significant influence to homo- and heterogeneous oxidative dehydrogenative couplings proved to be right. This is especially true for the cobalt-containing counterpart. In addition, compared to the benchmark catalysts known from the literature (**Table 20./B**<sup>221,223</sup>), there are some advantageous properties that should be highlighted. First, while  $\text{CuBr}_2$  and meso- $\text{Mn}_2\text{O}_3$  catalysts offer excellent azobenzene yields in non-green solvents, especially toluene, bismutites can work in pure aniline using ambient air as oxidant. Second, bismutites can selectively lead to unsymmetric azo derivatives, which is much more selective than reactions carried out in the presence of reference catalysts. Third, the required catalyst loading of bismutites (10 and 2.5 mol%), are much lower than that of the benchmark catalysts (32 mol%). Finally, unlike  $\text{CuBr}_2$ , no additional bases or additives are required to achieve the observed catalytic activity.

**Table 21.** Oxidative dehydrogenative heterocoupling of anilines and propane-1,3-diol producing quinolines. Reaction conditions: 1 equiv. (0.25 M) aniline or its derivatives, 2 mL propane-1,3-diol, 150 °C for 72 h (48 h upon using  $\text{CoBi}_2\text{O}_2\text{CO}_3$ ) and 10 mol% catalyst.<sup>222</sup>

			
Quinoline derivative	Aniline conversion (mol%)	Quinoline selectivity (%)	Quinoline yield (%)
	Mn: 100	Mn: 94	Mn: 94
	Co: 100	Co: 92	Co: 92
	Co: 100	Co: 100	Co: 100
	Ni: 82	Ni: 93	Ni: 76
	Mn: 67	Mn: 100	Mn: 67
	Co: 95	Co: 81	Co: 77
	Co: 100	Co: 91	Co: 91
	Ni: 85	Ni: 83	Ni: 71
	Mn: 66	Mn: 76	Mn: 50
	Co: 68	Co: 63	Co: 43
	Co: 95	Co: 96	Co: 91
	Ni: 79	Ni: 46	Ni: 36
	Mn: 98	Mn: 96	Mn: 94
	Co: 51	Co: 92	Co: 47
	Co: 93	Co: 100	Co: 93
	Ni: 52	Ni: 100	Ni: 52
	Mn: 89	Mn: 82	Mn: 73
	Co: 85	Co: 82	Co: 70
	Co: 100	Co: 100	Co: 100
	Ni: 84	Ni: 87	Ni: 73
	Mn: 52	Mn: 58	Mn: 30
	Co: 61	Co: 41	Co: 25
	Co: 100	Co: 65	Co: 65
	Ni: 33	Ni: 100	Ni: 33
	Mn: 0	Mn: 0	Mn: 0
	Co: 6	Co: 100	Co: 6
	Co: 11	Co: 88	Co: 10
	Ni: 4	Ni: 100	Ni: 4

2.5 mol%  $\text{CoBi}_2\text{O}_2\text{CO}_3$

To extend the applicability of bismutites as effective catalysts in oxidative dehydrogenative couplings, various syntheses of N-heterocycles were investigated. First, aniline derivatives were combined with propane-1,3-diol to produce the corresponding quinolines. The reaction conditions were the very same as those optimized for homo- and

heterocouplings of anilines. As a result, good to excellent quinoline yields were obtained for the most reactions shown in **Table 21**.

The remarkable nature of these results stems from the fact that the synthesis of quinolines from vicinal diols *via* an oxidative dehydrogenative pathway had not previously been described. (The synthesis of quinolines from vicinal diols has only been successful with double acceptorless dehydrogenative couplings combined with a Michael addition step of aniline derivatives with unsymmetrical vicinal diols. The disadvantages of this method are low to moderate yields, ruthenium- or platinum-based catalysts, and the use of various additives.<sup>224</sup>) The experienced success of the as-prepared bismutite catalysts is probably related to the soft Lewis acidic property<sup>225</sup> allowing the adaptation of another mechanism with an N-alkylation-cyclization tandem sequence.<sup>226,227</sup> This N-heterocyclisation mechanism is also known in quinoline synthesis, but has only been described in the presence of hydrogen acceptors.<sup>228,229</sup> The electronic character or steric effect of the substituent of the aniline derivative did not show any significant influence on the dehydrogenative coupling, the only exception being the nitro group in the *meta* position. In this case, however, the appearance of 3-hydroxypropanal as a by-product may also indicate oxidative dehydrogenation of the diol in this reaction.

In conclusion, despite the fact that homo-linked azo compounds of aniline derivatives can also be detected in small amounts, bismuth-based catalysts are highly selective for quinoline. The most active catalyst was also the cobalt-containing composite, which successfully reduced the reaction time to 48 hours and the catalyst loading to 2.5 mol%. Its catalytic ability is shown to be comparable to transition metal- or noble metal-catalyzed acceptorless dehydrogenative strategies<sup>224,230,231</sup>, but does not have many of the drawbacks of these methodologies. The reactions catalyzed by  $\text{CoBi}_2\text{O}_2\text{CO}_3$  were carried out in propane-1,3-diol (one of the reaction partners), without any other additives, and without the use of Ar or  $\text{N}_2$  atmosphere, providing a more applicable and environmentally friendly process than before.

To extend the study of the catalytic ability of bismutites, experiments were carried out on the synthesis of quinoxaline using the appropriate aniline and diol reactant on the model of quinoline synthesis. In the cross-coupling reactions of 2-aminoanilines and ethylene glycol, 34–100% yields of the desired quinoxaline derivatives were achieved with either Ni- or Co-based bismutites (**Fig. 37**). Compared to quinoline synthesis, a shorter reaction time (8–24 h) and lower reaction temperatures (90–110 °C) were sufficient. Based on this finding, it can be said, that the use of unsymmetrical diols containing secondary alcohol groups, which are essential for acceptorless dehydrogenative reactions, is not essential to ensure a high yield.

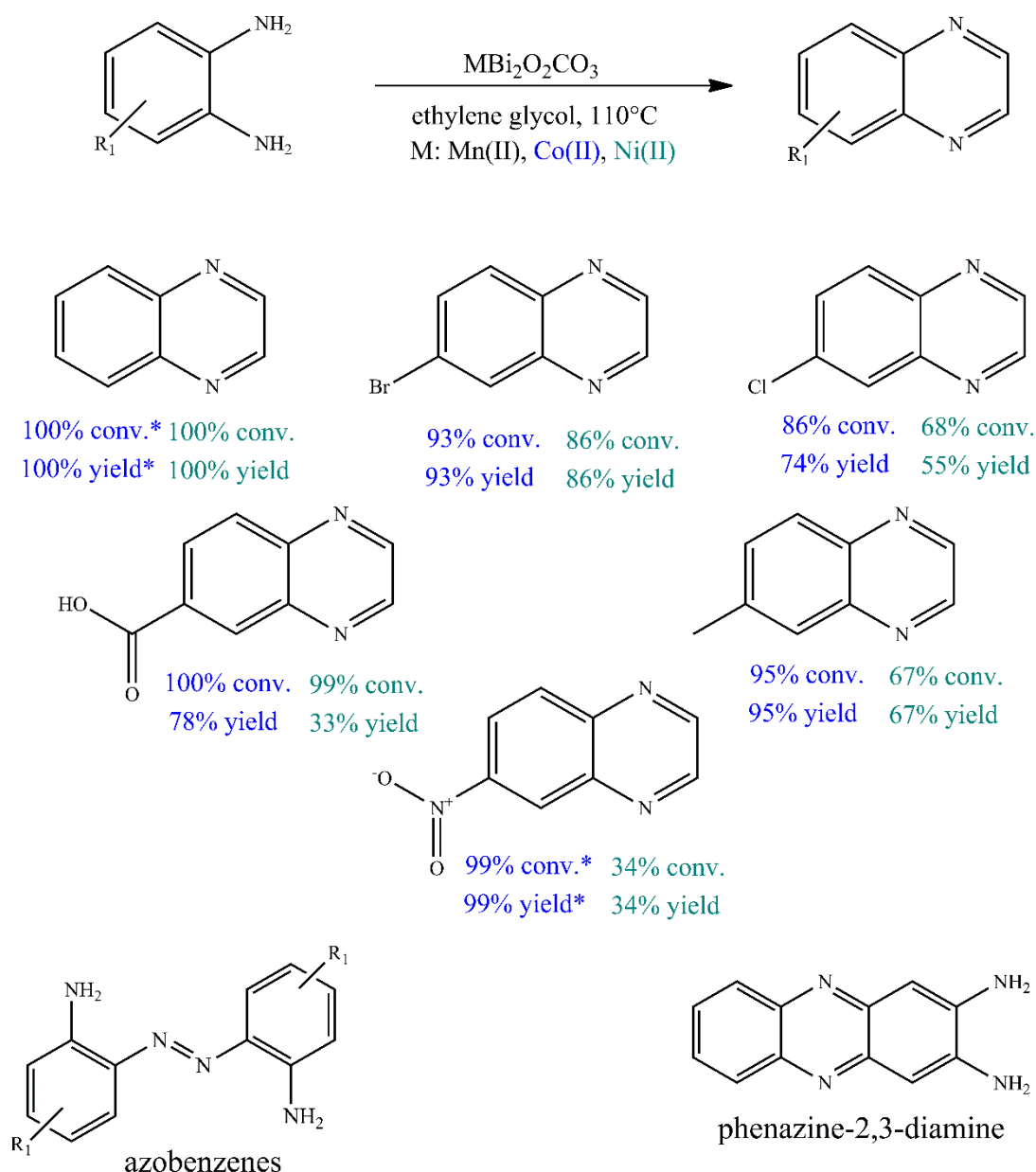
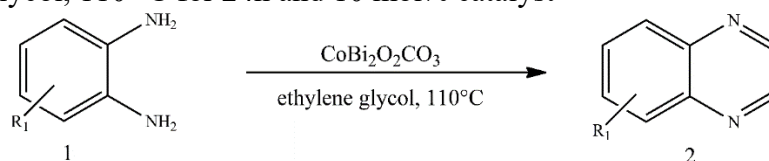


**Figure 37.** Oxidative dehydrogenative heterocoupling of o-phenylenediamines and ethylene glycol producing quinoxaline. Reaction conditions: 1 equiv. (0.25 M) o-phenylenediamine or its substituted derivative, 2 mL ethylene glycol, 110 °C for 24h and 10 mol% catalyst. (\*2.5 mol%  $\text{CoBi}_2\text{O}_2\text{CO}_3$ ).<sup>222</sup>

Surprisingly,  $\text{MnBi}_2\text{O}_2\text{CO}_3$  was less selective toward the coupling product than other bismutite analogs. When using Ni- or Co-based catalysts, the by-product was azobenzene, whereas in the presence of  $\text{MnBi}_2\text{O}_2\text{CO}_3$ , phenazine-2,3-diamine, the self-coupling product of 2-aminoaniline was detected. Furthermore, the native catalytic activity of  $\text{CoBi}_2\text{O}_2\text{CO}_3$  was superior compared to other homogeneous, heterogeneous or even benchmark catalysts.<sup>232,233</sup>



**Table 22.** Oxidative dehydrogenative heterocoupling of o-phenylenediamines and ethylene glycol. Reaction conditions: 1 equiv. (0.25 M) o-phenylenediamine or its substituted derivative, 2 mL ethylene glycol, 110 °C for 24h and 10 mol% catalyst<sup>222</sup>



Substituent	Yield of 2 (mol%)	Isolated yield (%)
R <sub>1</sub> = H	100*	85
R <sub>1</sub> = 4-Br	93	80
R <sub>1</sub> = 4-Cl	74	63
R <sub>1</sub> = 4-COOH	78	64
R <sub>1</sub> = 4-Me	95	84
R <sub>1</sub> = 4-nitro	99*	85

\* 2.5 mol% catalyst

Based on the determined yields of quinoxaline derivatives (63–85%), shown in Fig. 37. and in **Table 22.**, the cobalt containing catalytic system proved to be applicable for producing quinoxalines *via* base-free oxidative hydrogenative cross-coupling of 2-aminoaniline derivatives and ethylene glycol. Moreover, the reactions took place under ambient conditions, also using ethylene glycol as solvent which result the developed process to be considered as a green chemical process compared to the best available technologies in fine chemical industry.

After the catalytic capabilities of the self-supported catalysts were studied, it became necessary to investigate their physical and chemical stability. Thus, five recycling runs were performed in the presence of CoBi<sub>2</sub>O<sub>2</sub>CO<sub>3</sub> (**Fig. 38. B**) and both the used catalyst both the catalytic indicators were monitored. The conversion and selectivity values remained almost the same after even the fifth run, no leaching of the metallic component was shown by ICP-MS measurement, and the *post*-XRD (**Fig. 38. A**) also confirmed the unchanged structural integrity of the reused catalyst. Besides, to confirm the heterogeneous catalytic nature of the Co-based bismutite-promoted reaction, the catalyst powder was filtered out from the reaction slurry by centrifugation at low 2-aminoaniline conversion, and the remaining solution was further stirred under unchanged reaction conditions. **Figure 38. C** shows the results that active components did not dissolve in the reaction mixture as the conversion and product yield remained constant, indicating that the cross-coupling is catalyzed heterogeneously.

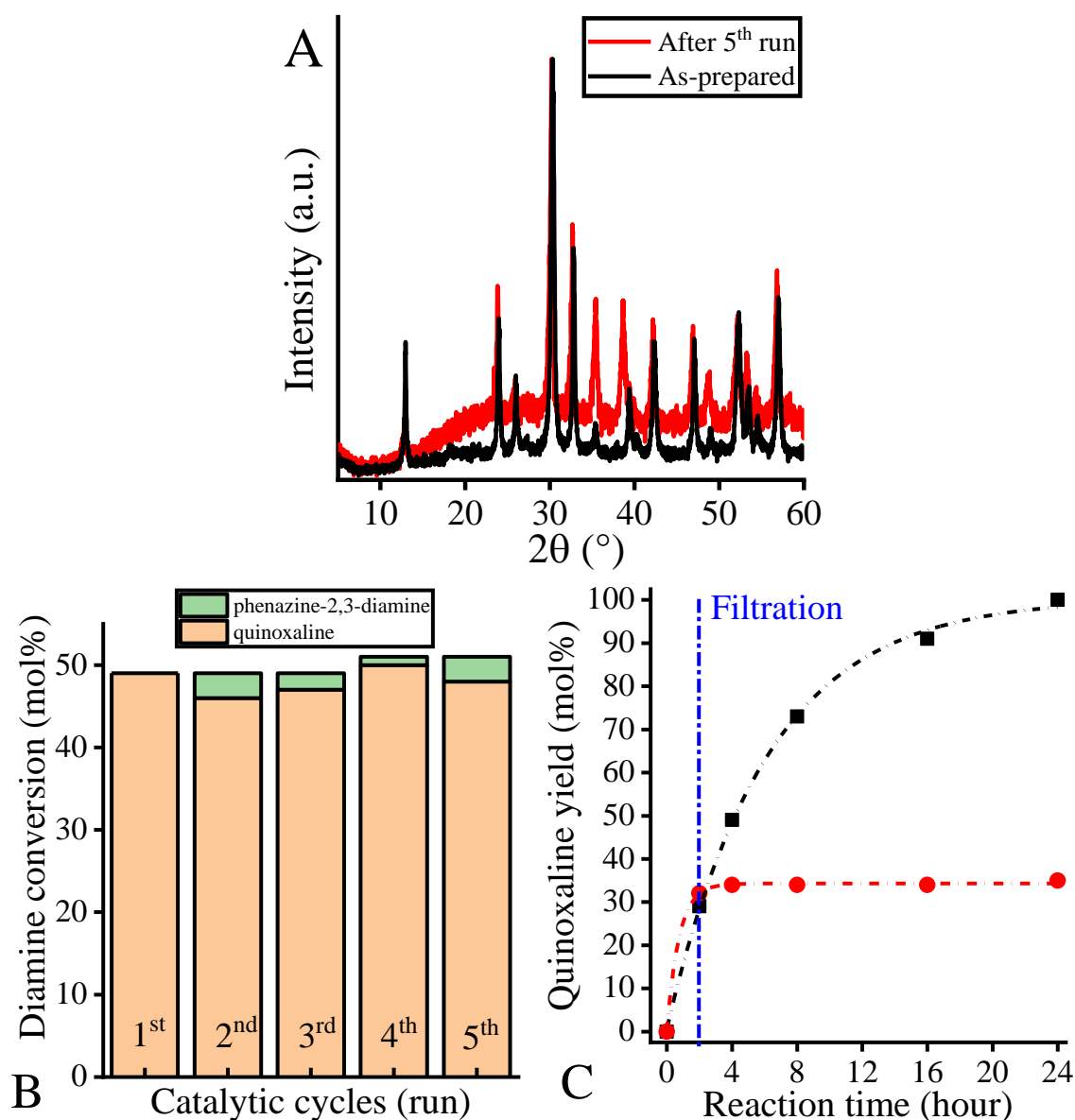


**Figure 38.** XRD patterns of  $\text{CoBi}_2\text{O}_2\text{CO}_3$  composite before and after a five run recycling test (A); catalytic indicators in the five run recycling test (B) and the hot filtration test (C) in the presence of  $\text{CoBi}_2\text{O}_2\text{CO}_3$  catalyst. Reaction conditions: 1 equiv. (0.25 M) o-phenylenediamine, 2 mL ethylene glycol,  $110^\circ\text{C}$  for 24h (4 h in the case of recycling) and 2.5 mol% catalyst.<sup>222</sup>

To explain the excellent performance of Co-containing bismutite, experiments were carried out to characterize the surface even more precisely. Both the interfacial effect between the components of the modified bismutites, presented in the previous work on the synthesis of 2-phenyl benzimidazoles, and the effect of the surface dimension, which proved to be very similar for all the as-prepared catalysts (Table 12.), can be excluded. Furthermore, no significant differences were detected in the acidity of the catalysts as determined by temperature-programmed desorption measurements with  $\text{NH}_3$  (Fig. 39. A). On the other hand,  $\text{CO}_2$ -TPD (Fig. 39. B) measurements indicated significant differences in the basicity of the catalysts. The basicity decreases in the order  $\text{CoBi}_2\text{O}_2\text{CO}_3 > \text{NiBi}_2\text{O}_2\text{CO}_3 > \text{MnBi}_2\text{O}_2\text{CO}_3 >$

$\text{Bi}_2\text{O}_2\text{CO}_3$ . This finding is essential, as the increasing basicity could facilitate the dehydrogenation of vicinal diols or the adsorption of alcohol on the active sites, which increases the final catalytic activity.<sup>234</sup>

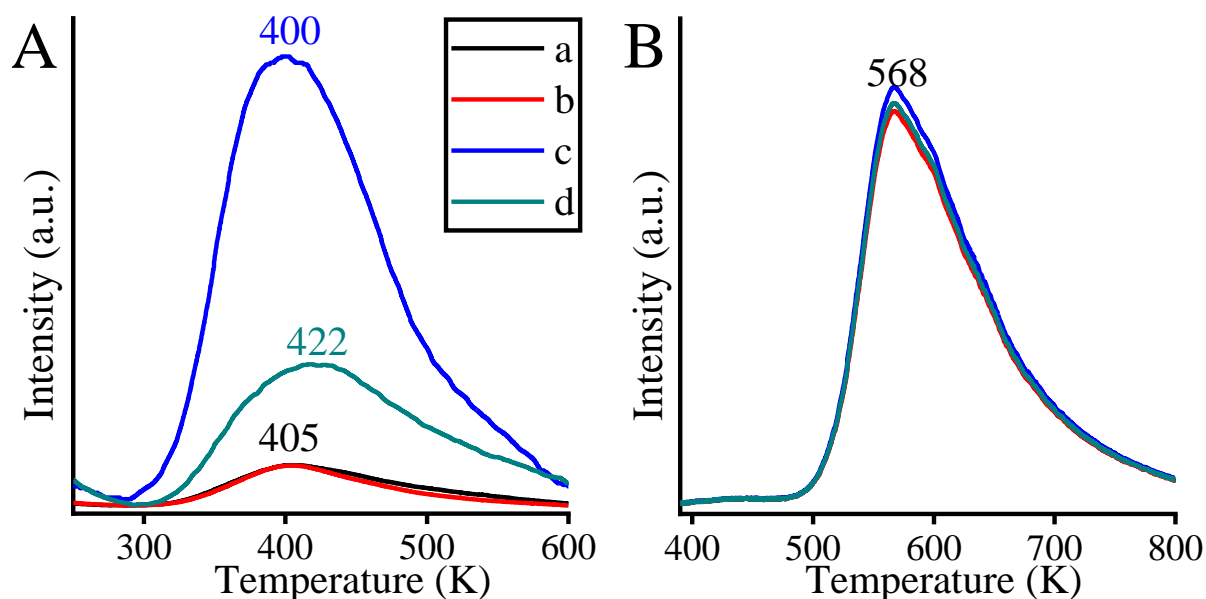
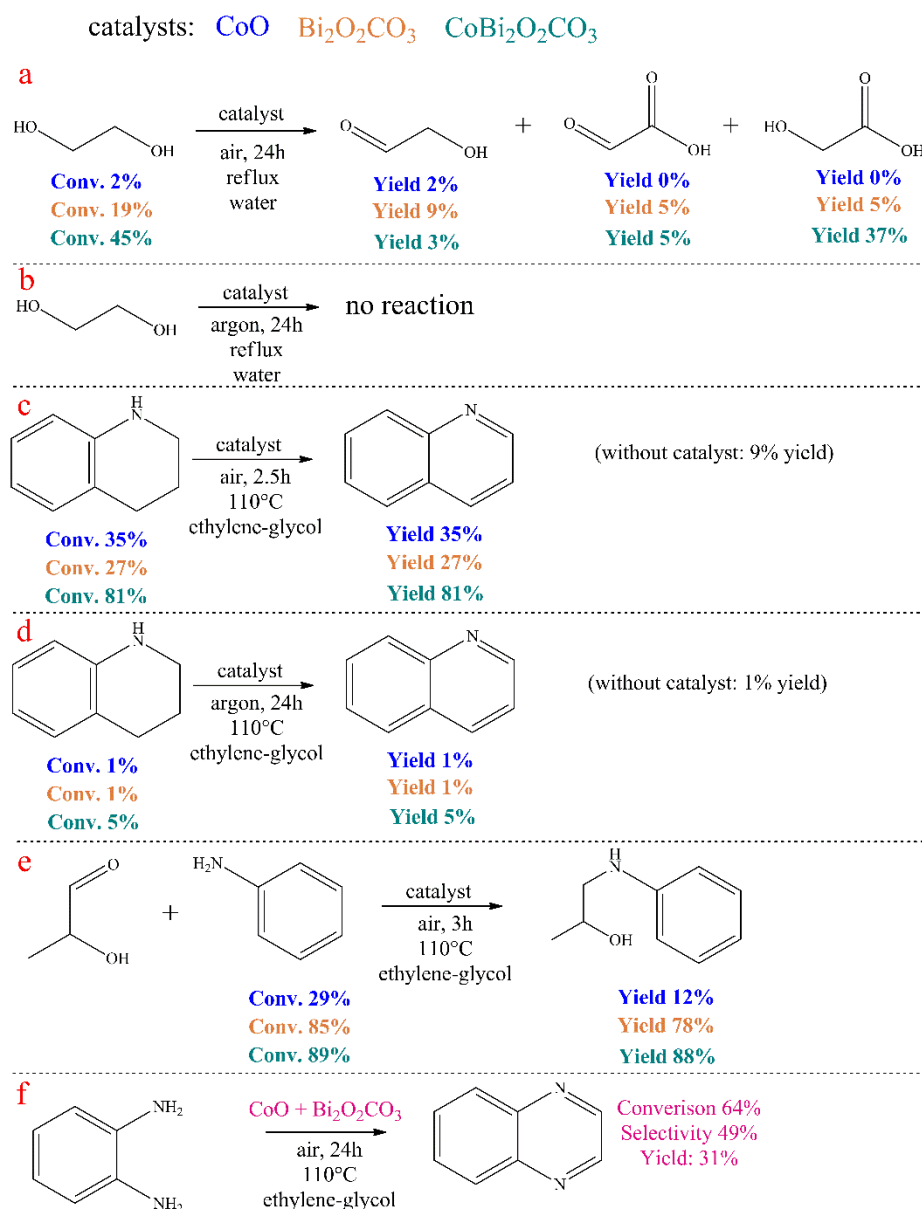


**Figure 39.** CO<sub>2</sub>-TPD curves (A) and NH<sub>3</sub>-TPD curves (B) of the bismutite-based composites:  $\text{Bi}_2\text{O}_2\text{CO}_3$  (a),  $\text{MnBi}_2\text{O}_2\text{CO}_3$  (b),  $\text{CoBi}_2\text{O}_2\text{CO}_3$  (c) and  $\text{NiBi}_2\text{O}_2\text{CO}_3$  (d).<sup>222</sup>

To propose a reaction mechanism for the  $\text{CoBi}_2\text{O}_2\text{CO}_3$  catalyzed synthesis of quinoxaline, control experiments were carried out in the presence of Co-modified bismutite, CoO and unmodified  $\text{Bi}_2\text{O}_2\text{CO}_3$  in the role of catalyst. Interestingly, no dicarbonyl product was formed in water at reflux temperature for 24h under ambient air (**Scheme 7**). This argues against the catalytic cycle being similar to the oxidative dehydrogenative coupling of quinoxaline with  $\text{Au/CeO}_2$ .<sup>166</sup> Beside, both pure CoO and bismutite showed poor activity compared to the modified catalyst, which achieved a large ethylene glycol conversion. Glycolic acid was formed as the main product, but glycolic acid and glycolaldehyde were also detected, which is already in good agreement with the well-accepted mechanism of ethylene glycol oxidation in water.<sup>235</sup> It is worth highlighting that the conversion of ethylene glycol is far from the stoichiometric value, which may indicate that the dehydrogenation equilibrium of vicinal diols may be shifted in the presence of anilines during the couplings. Furthermore, no reaction was detected when the experiments were repeated under an argon atmosphere (**Scheme 7. b**). The latter confirms that  $\text{CoBi}_2\text{O}_2\text{CO}_3$  can be an efficient promoter for the oxidative dehydrogenation of diols with molecular oxygen as the oxidant; however, this catalyst is not able to catalyze acceptorless dehydrogenation.



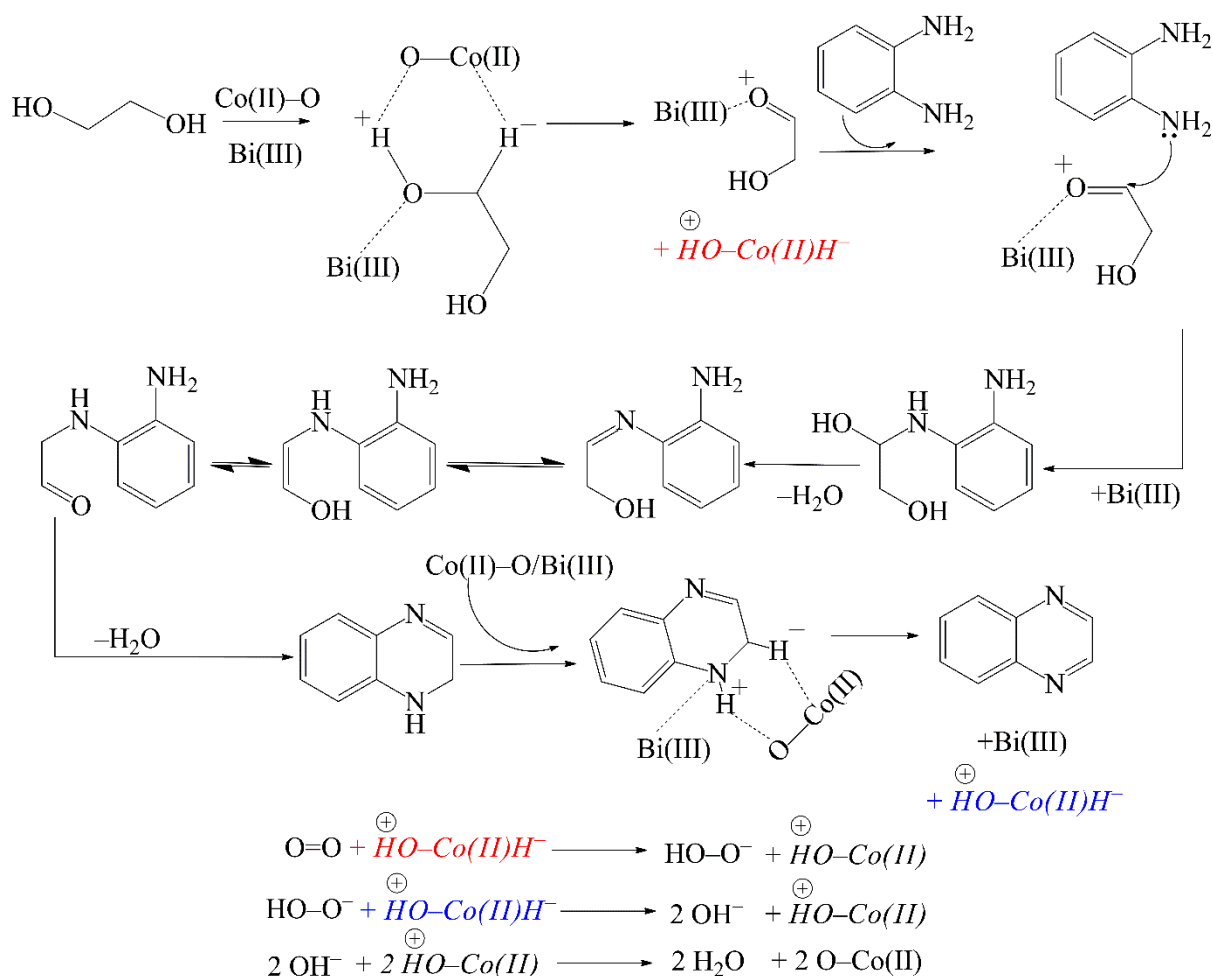
**Scheme 7.** Control experiments in the presence of CoBi<sub>2</sub>O<sub>2</sub>CO<sub>3</sub>, CoO and Bi<sub>2</sub>O<sub>2</sub>CO<sub>3</sub> as catalyst to explore the reaction mechanism of quinoxaline formation catalyzed by CoBi<sub>2</sub>O<sub>2</sub>CO<sub>3</sub>.<sup>222</sup>

Under the optimized reaction conditions, the aerobic oxidative dehydrogenation of 1,2,3,4-tetrahydroquinoline was only possible in the presence of CoBi<sub>2</sub>O<sub>2</sub>CO<sub>3</sub> (**Scheme 7. c, d**), the catalytic building blocks CoO and Bi<sub>2</sub>O<sub>2</sub>CO<sub>3</sub> alone could not effectively promote this reaction which strengthen the assumption that the cobalt ions and the bismutite framework operate cooperatively. In another control experiment, the coupling of 2-hydroxypropanal to aniline (**Scheme 7. e**), performed under the same conditions, suggests that the condensation step probably involved bismuth centers as active catalytic sites. Finally, the oxidative coupling of ethylene glycol and o-phenylenediamine was repeated catalyzed by a physical mixture of CoO and Bi<sub>2</sub>O<sub>2</sub>CO<sub>3</sub> (**Scheme 7. f**). It was found that the reaction can still be carried out in this

way, but with significantly reduced selectivity and conversion values. This also proves that randomly distributed active sites are less efficient than those with an ordered structure.

Based on the control results, it can be assumed that the oxidative dehydrogenation is catalyzed cooperatively by the CoO and bismutite components. In addition, the role of bismutite can also be to promote C–N coupling, which can also be realized in  $\text{Bi}^{3+}$  Lewis acid centers, as reported by Yadav et al.<sup>236</sup>

Taking into account our own observations and the previous suggestions of Milstein,<sup>237</sup> Corma,<sup>166</sup> Yadav<sup>236</sup> and Riisager<sup>234</sup>, Scheme 8. shows our proposed mechanism for the Co–bismutite -catalyzed cross-coupling reaction of o-phenylenediamine and ethylene glycol.



**Scheme 8.** Proposed mechanism of the oxidative dehydrogenative coupling reaction of o-phenylenediamine and ethylene glycol catalysed by  $\text{CoBi}_2\text{O}_2\text{CO}_3$ , providing quinoxaline.<sup>222</sup>

In the first step, adsorption of ethylene glycol takes place on the basic/Lewis acid surface of the catalyst, probably in the  $\text{Bi(III)}$  centers,<sup>238</sup> generating a metal alkoxide intermediate. Subsequently, the alcoholic hydroxy proton is abstracted by a surface oxygen – which is basically a surface oxygen of the CoO specimen – followed by a  $\beta$ -H elimination catalyzed by  $\text{Co(II)}$  centers. As a result, a  $\text{Co(II)}$ -hydride coupled with a protonated surface oxygen and a

Bi(III)-coordinated  $\alpha$ -hydroxycarbonyl compound is formed. Subsequently, Bi(III)-mediated condensation of the amino group of the o-phenylenediamine with the carbonyl sample – in parallel with Bi(III) decomplexation – results in an intermediate. This, in two rapid steps, undergoes a sequential proton shift and an enol-oxo tautomerization. The following condensation of the second amino group generates a 1,2-dihydroxyquinoxaline intermediate, which rapidly dehydrogenates similarly to the first step. This leads to the formation of the final product quinoxaline - which subsequently desorbs - as well as another Co(II)-hydride coupled with a protonated surface oxygen. In the final step, molecular oxygen reacts with the Co(II)-hydride to form a peroxide anion, which immediately reacts with a second Co(II)-hydride to generate two molecules of hydroxides. These hydroxides then undergo a rapid acid-base reaction with the protonated surface oxygen, which regenerates the original catalyst surface and also produces two molecules of water as the only by-product.

## 6. CONCLUSIONS

Based on a general search of Scifinder (<https://scifinder.cas.org>) on 2<sup>nd</sup> January, 2023, in the last 10 years *ca.* a quarter of the 260000 publication related to catalysis focused on the production and/or transformation of heterocycles.\* Most of them describe some kind of catalytic system (transition metal catalysis, Lewis acid catalysis, organocatalysis, biocatalysis, phase transfer catalysis, electrocatalysis), since the alternative route or mechanism they provide is much more economical and competitive than non-catalyzed processes.

Although the field of synthetic organic chemistry is dominated by homogeneous noble metal catalysis, heterogenized catalysts containing non-noble metal centers can also have many advantages. Not only can they offer the advantages of recyclability and robustness, which in itself can represent an economical and environmentally friendly alternative in catalyst selection, but they can even be more effective candidates compared to their monometallic counterparts (enhanced selectivity and/or yield, milder reaction conditions, greener solvents), if the different metal centers are able to cooperate with each other.

Targeting this possibility, our primary hypothesis was that by modifying the Lewis acidic bismutite ( $\text{Bi}_2\text{O}_2\text{CO}_3$ ) framework with copper, cobalt, manganese or nickel cations or oxide specimens, efficient multifunctional catalysts capable of promoting multi-step cyclization reactions in a heterogeneous manner can be produced. In addition, we hypothesized that their efficiency can be further enhanced by determining the structural factors that can most decisively affect the catalytic performance. Thus, the modified structures were thoroughly studied both structurally (XRD, Raman, XPS, *etc.*) and catalytically, in a series of catalytic tests, especially in cyclization reactions.

Initially, the modification of the bismutite framework with transition metal ions was carried out by the urea hydrolysis method, in which the amount of hydroxide and carbonate anions required for precipitation is provided by the controlled hydrolysis of urea. After the successful preliminary experiments, however, the bismutite structures could be synthesized by a modified co-precipitation method, in which ammonia and sodium-carbonate solutions of a certain concentration (0.6 M) were added directly to bismuth- and transition metal nitrate-containing solutions of a certain concentration (3.75 mmol). Then stirring was continuous for 24 hours at 80 °C for  $\text{CuBi}_2\text{O}_2\text{CO}_3$  and 100 °C for Co-, Mn-,  $\text{NiBi}_2\text{O}_2\text{CO}_3$ . The obtained,

---

\* A general search of Scifinder (<https://scifinder.cas.org>) on the 2<sup>nd</sup> of January, 2023, found 265,839 "catalysis"-related English-language journals published between 2012 and January 2023, of which 71,525 were for production and/or transformation of heterocycles.

colored products were then filtered, washed (distilled water) and dried (60 °C, overnight). With the exception of copper-bismutite, the fine powder solids were heat-treated at 290°C for 3 hours to remove any remaining traces of water before catalytic use.

Based on X-ray diffraction measurements, all modified bismutite systems could be identified as structural analogues of Sillén-type bismutite, where the cation insertion was isomorphous. After recording the SEM-EDX elemental maps, this assertion needed to be partially revised, since the copper-containing system showed a homogeneous cation distribution, but the distribution in the Mn-, Co- and Ni-containing bismutites proved to be heterogeneous. When determining the compositions (ICP-MS, TG and XPS), there was no difference in the bulk and surface composition of the copper-modified bismutite, while in the other TM-based systems an incisive surface enrichment of the transition metal specimens was observed. Based on the high-resolution transmission electron microscopy images, morphological differences also emerged: While the copper-bismutite was characterized by a Sillén-type plate-like morphology, the other transition metal-containing bismutites consisted of particles with two different morphologies. TEM-EDS the measurements revealed that these specimens differed not only in their morphology but also in their composition. On this basis, the existence of surface-adsorbed transition metal oxide specimens could be assumed.

Material science characterization revealed other important differences between the catalyst candidates. While the infrared, Raman, UV-DR and XP spectroscopies confirmed the intercalation of an azurite-type complex into the interlamellar gallery of bismutite after the modification with copper ions, the analyses of Co- and  $\text{MnBi}_2\text{O}_2\text{CO}_3$ , showed the formation of interfaces between the surface of the bismutite host and the transition metal oxides. The nickel-containing counterpart was not intercalated, and contained no interfacial sites. Based on this finding, differences in catalytic capabilities were also expected.

The catalytic capabilities of the copper-containing system were investigated in the coupling reaction of 2-iodoaniline and 2-bromothiophenol. This reaction is also interesting because  $\text{Bi}^{3+}$ , although is known as a Lewis acid catalyst, to the best of our knowledge, it has never been used in a similar reaction. The modified system not only proved to be active in the synthesis of phenothiazines, but it was also able to operate with excellent selectivity and quantitative conversion under much more environmentally friendly and simple conditions compared to the best available technology. Moreover, there is no example in the literature of using a similarly low concentration of a base to yield phenothiazine exclusively. The time-dependent experiments proved that  $\text{CuBi}_2\text{O}_2\text{CO}_3$  can catalyze the synthesis of phenothiazine as a cooperative catalyst and in a concerted manner. Moreover, the hot filtration and reusability



tests established that the catalyst is able to function heterogeneously and that its activity and selectivity do not decrease even after 5 consecutive cycles. Considering the extensibility of the reaction, it can be concluded that high yields and selectivities can be achieved for many derivatives under the optimized reaction conditions and the catalyst shows considerable robustness to structural degradation by the reactions (*ex situ* XRD, TEM and XPS).

To investigate the catalytic performance of manganese-, cobalt- and nickel-modified bismutite structures, several model reactions were introduced. First, the multi-step reaction cascade of 2-phenylbenzimidazole synthesis was investigated. Preliminary experiments were started with bismuth compounds in DMSO. Only  $\text{Bi}_2\text{O}_3$  and  $\text{Bi}_2\text{O}_3\text{CO}_3$  were found to be slightly active in the oxidative coupling leading to the imine intermediates and/or in the annulation step. Despite the initial modest performance, the fact that it was possible to improve the conversion and selectivity only by increasing the water content of the reaction media gave reason for confidence. To ensure comparability, the reaction was also carried out in the presence of pure transition metal oxides, and, with one exception, similar results were obtained. When the nickel-modified system was used as a catalyst, no activity was observed, so this catalyst candidate was excluded from further optimization process. During the optimization, it was possible to determine the most suitable experimental conditions for cobalt- and manganese-containing bismutite, and it was also found that the correctly chosen solvent/solvent mixture was suitable to control the composition of the product mixture. The possible contributions of the individual components were investigated under the optimum reaction conditions. It has been shown that even the performance of transition metal oxides fixed on a support by impregnation exceeded the performance of the individual components, but the samples synthesized by co-precipitation showed the highest catalytic performance. This can be interpreted as indirect evidence for the presence of interfacial sites.

The turnover frequency (TOF) calculated from time-dependent experiments also underpins this statement. In addition, the cobalt-containing system proved to be much more active than the manganese-containing counterpart. For the cobalt-containing system, the contribution of the individual components to each reaction in the reaction sequence was also determined. The heterogeneity and reusability studies showed that the catalysts operate heterogeneously and their catalytic performance does not decrease significantly after 5 consecutive cycles. Considering the extensibility of the reaction, it can be concluded that under optimized reaction conditions both catalysts are capable not only of direct derivative formation, but also of isosteres formation. Finally, *ex situ* XRD, TEM and XPS measurements exhibited that the structural integrity is unchanged after the reaction cycles.

In a final catalytic test, the catalytic abilities of Mn-, Co-, Ni-containing bismutites in oxidative dehydrogenative coupling reactions were investigated. Following the encouraging results experienced in the homo- and hetero-azo couplings of aniline and its derivatives, the syntheses of quinoline and quinoxaline were optimized. The reaction of various aniline and o-phenylenediamine derivatives with 1,3-propane diol and ethylene glycol, respectively, was investigated producing the corresponding quinolines or quinoxalines. In both reactions, the diol served simultaneously as reaction partner and solvent, and only ambient air was required as oxidant, resulting in very simple methods. In general, the catalysts were found to be highly selective for quinolines and quinoxalines with moderate to good conversion. Based on the hot filtration test and the reusability reaction series, we successfully demonstrated the heterogeneous nature of quinoxaline synthesis in the presence of  $\text{CoBi}_2\text{O}_2\text{CO}_3$ . Furthermore, a mechanism for the oxidative dehydrogenative coupling of o-phenylenediamine and ethylene glycol catalyzed by  $\text{CoBi}_2\text{O}_2\text{CO}_3$  was demonstrated in several control experiments.

In summary, the results of the structural characterization and catalytic studies showed that the TM modified bismutites synthesized *via* modified co-precipitation have proven to be robust heterogeneous catalysts in several syntheses, producing various heterocycles with high activity and selectivity. The copper-containing system could be considered as a new structural analogue of Sillén-type beyerite. Manganese- and cobalt-containing systems have been shown to have interfacial sites between the framework and the TM specimens, while the nickel-modified system does not contain any special sites other than the  $\text{Bi}^{3+}$  and  $\text{Ni}^{2+/3+}$  active centers. Accordingly, the systems containing copper, manganese and cobalt ions showed excellent catalytic performance, exceeding the catalytic performance of the single TM oxides or  $\text{Bi}_2\text{O}_2\text{CO}_3$ . Since clear correlations between the structure of the composites and the achieved activity and selectivity values were established, it can be concluded that our starting point that efficient heterogeneous cooperative catalysts can be prepared with a catalytically active support ( $\text{Bi}_2\text{O}_2\text{CO}_3$ ) and transition metal ions/oxides (Cu, Mn, Co) has been proven correct.

## ACKNOWLEDGEMENT

I am primarily grateful to my supervisors, Professor Dr. István Pálinkó<sup>†</sup> and Professor Dr. Pál Sipos, for their many advices, criticisms, financial help and morning banter.

I would like to express my special thanks to Dr. Gábor Varga, whose work proved to be indispensable in practice, writing and publishing. Also, let me thank Dr. Sándor B. Ötvös for his efforts, practical advice and detailed reviews.

Many thanks to Dr. Márton Szabados for the first SEM images and the thermogravimetric measurements, to Dr. Gergely F. Samu for the XPS analysis, and to Dr. Zsolt Fogarassy for the TEM records. Thanks to all my co-authors.

I would like to thank all the members of the Material and Solution Structure Research Group, as well as all the staff of the former Department of Organic Chemistry for their help. I wish to express my sincere thanks to Ferenc Kovács for his patient teaching of MestReNova and ChemDraw.

Finally, I owe a lot of thanks to my parents and my love for the enormous support they have given me. All this help made it possible to write my doctoral dissertation.

## REFERENCES

- 1 P. Arora, V. Arora, H. S. Lamba and D. Wandhwa, *Pharm Res Sci*, 2012, **3**, 2947–2955.
- 2 E. Campaigne, *J. Chem. Educ.*, 1986, **63**, 860–863.
- 3 J. N. Armor, *Catal. Today*, 2011, **163**, 3–9.
- 4 I. Nakamura and Y. Yamamoto, *Chem. Rev.*, 2004, **104**, 2127–2198.
- 5 S. Warnel and V. Siekermann, *Makromol. Chem. Rapid Commun.*, 1983, **4**, 423–427.
- 6 I. Leymet and A. Siove, *Makromol. Chem.*, 1989, **190**, 2397–2405.
- 7 R. H. Grubbs and S. Chang, *Tetrahedron*, 1998, **54**, 4413–4450.
- 8 V. Dragutan, I. Dragutan and A. Demonceau, *Platin. Met. Rev.*, 2005, **49**, 183–188.
- 9 P. Cao and X. Zhang, *Angew. Chemie Int. Ed.*, 2000, **39**, 4104–4106.
- 10 M. Hatano, M. Terada and K. Mikami, *Angew. Chemie Int. Ed.*, 2001, **41**, 249–253.
- 11 S. Ma and J. Zhang, *Chem. Commun.*, 2000, 117–118.
- 12 R. Zimmer, C. U. Dinesh, E. Nandan and F. A. Khan, *Chem. Rev.*, 2000, **100**, 3067–3125.
- 13 R. W. Bates and V. Satcharoen, *Chem. Soc. Rev.*, 2002, **31**, 12–21.
- 14 L. Ackermann and R. G. Bergman, *Org. Lett.*, 2002, **4**, 1475–1478.
- 15 V. M. Arredondo, F. E. McDonald and T. J. Marks, *J. Am. Chem. Soc.*, 1998, **120**, 4871–4872.
- 16 V. M. Arredondo, F. E. McDonald and T. J. Marks, *Organometallics*, 1999, **18**, 1949–1960.
- 17 I. U. Khand, G. R. Knox, P. L. Pauson, W. E. Watts and M. I. Foreman, *J. Chem. Soc. Perkin Trans.*, 1973, 977–981.
- 18 H. A. Reichard, 2010.
- 19 R. L. Halterman, T. M. Ramsey, N. A. Pailles and M. A. Khan, *J. Organomet. Chem.*, 1995, **497**, 43–53.
- 20 J. Louie, J. E. Gibby, M. V. Farnworth and T. N. Tekavec, *J. Am. Chem. Soc.*, 2002, **124**, 15188–15189.
- 21 V. Gandon, C. Aubert and M. Malacria, *Chem. Commun.*, 2006, 2209–2217.
- 22 L. V. R. Bonaga, H.-C. Zhang, A. F. Moretto, H. Ye, D. A. Gauthier, J. Li, G. C. Leo and B. E. Maryanoff, *J. Am. Chem. Soc.*, 2005, **127**, 3473–3485.
- 23 T. Takahashi, Y. Li, T. Ito, F. Xu, K. Nakajima and Y. Liu, *J. Am. Chem. Soc.*, 2002, **124**, 1144–1145.
- 24 F. Sato, H. Urabe and S. Okamoto, *Chem. Rev.*, 2000, **100**, 2835–2886.
- 25 M. Zhou, M. Lankelma, J. Ivar van der Vlugt and B. De Bruin, *Angew. Chemie Int. Ed.*, 2020, **59**, 11073–11079.
- 26 K. Sonogashira, Y. Tohda and N. Hagihara, *Tetrahedron Lett.*, 1975, **50**, 4467–4470.
- 27 M. Kitamura, S. Chiba, O. Saku and K. Narasaka, *Chem. Lett.*, 2002, **7**, 606–607.
- 28 Y. Koganemaru, M. Kitamura and K. Narasaka, *Chem. Lett.*, 2002, 784–785.
- 29 M. M. Heravi, T. Ahmadi, M. Ghavidel, B. Heidari and H. Hamidi, *RSC Adv.*, 2015, **5**, 101999–102075.
- 30 R. Yao, G. Rong, B. Yan, L. Qiu and X. Xu, *ACS Catal.*, 2016, **6**, 1024–1027.
- 31 Q. Zeng, K. Dong, J. Huang, L. Qiu and X. Xu, *Org. Biomol. Chem.*, 2019, **17**, 2326–2330.
- 32 Y. Liu and J. P. Wan, *Org. Biomol. Chem.*, 2011, **9**, 6873–6894.
- 33 S. Ashida and M. Murakami, *Bull. Chem. Soc. Jpn.*, 2008, **81**, 885–893.
- 34 C. D. Smith and M. F. Greaney, *Org. Lett.*, 2013, **15**, 3–6.
- 35 S. K. Yousuf, D. Mukherjee, B. Singh, S. Maity and S. Chandra Taneja, *Green Chem.*, 2010, **12**, 1568–1572.
- 36 K. R. Rohit, S. Radhika, S. Saranya and G. Anilkumar, *Adv. Synth. Catal.*, 2020, **362**, 1602–1650.
- 37 M. Zhou, L. A. Wolzak, Z. Li, F. J. De Zwart, S. Mathew and B. De Bruin, *J. Am. Chem. Soc.*, 2021, **143**, 20501–20512.
- 38 J. Li, W. Xu, R. Wang, Y. Li, G. Yin and M. Ye, *Nat. Commun.*, 1–9.
- 39 M. Murakami, S. Ashida and T. Matsuda, *Journal Am. Chem. Soc.*, 2006, **128**, 2166–2167.
- 40 M. Beller, C. Bolm, B. Blocks and F. Chemicals, *Transit. Met. Org. Synth.*
- 41 B. Cornils, W. A. Herrmann, T. I. Horváth, W. Leitner, S. Mecking, H. Olivier-Bourbigou and D. Vogt,

- Multiphase homogeneous catalysis*, Wiley-VCH Verlag, Weinheim, 2005.
- 42 B. C. Gates, *Catalytic Chemistry*, John Wiley & Sons, New York, 1992.
- 43 M. Liu and O. Reiser, *Org. Lett.*, 2011, **13**, 1102–1105.
- 44 J. A. Moulijn, P. W. . M. van Leeuwen and R. A. van Santen, *Catalysis - An Integrated Approach to Homogeneous, Heterogeneous and Industrial Catalysis*, Elsevier, Amsterdam, 1993.
- 45 J. M. Fraile, J. I. García and J. A. Mayoral, *Chem. Rev.*, 2009, **109**, 360–417.
- 46 J. Fairsoosa, M. Neetha and G. Anilkumar, *RSC Adv.*, 2021, **11**, 3452–3469.
- 47 Y. Monguchi, K. Nozaki, T. Maejima, Y. Shimoda, Y. Sawama, Y. Kitamura, Y. Kitade and H. Sajiki, *Green Chem.*, 2013, **15**, 490–495.
- 48 A. Anubhav, R. N. Rao, S. Das, S. Jena, S. Rej, B. Maiti and K. Chanda, *Tetrahedron Lett.*, 2020, **61**, 152273.
- 49 S. Aghigh, H. Jamshid, R. Seyedeh and M. Mousavi, 2018, 1–12.
- 50 K. Mullick, S. Biswas, A. M. Angeles-Boza and S. L. Suib, *Chem. Commun.*, 2017, **53**, 2256–2259.
- 51 X. Meng, J. Zhang, B. Chen, Z. Jing and P. Zhao, *Catal. Sci. Technol.*, 2016, **6**, 890–896.
- 52 H. Ahmadian, H. Veisi, C. Karami, A. Sedrpoushan, M. Nouri, F. Jamshidi and I. Alavioon, *Appl. Organomet. Chem.*, 2015, **29**, 266–269.
- 53 P. McMorn and G. J. Hutchings, *Chem. Soc. Rev.*, 2004, **33**, 108–122.
- 54 G. A. E. Oxford, D. Dubbeldam, L. J. Broadbelt and R. Q. Snurr, *J. Mol. Catal. A Chem.*, 2011, **334**, 89–97.
- 55 K. Sun, D. Li, G. Lu and C. Cai, 2021, 373–381.
- 56 C. Liao, X. Li, K. Yao, Z. Yuan, Q. Chi and Z. Zhang, .
- 57 M. Janani, M. A. Senejani and T. M. Isfahani, *Curr. Org. Synth.*, 2020, **17**, 109–116.
- 58 S. R. Chaurasia, A. R. Tiwari and B. M. Bhanage, *Mol. Catal.*, 2019, **478**, 110565.
- 59 R. G. Kalishomi and S. Rostamizadeh, *Russ. J. Gen. Chem.*, 2021, **91**, 1140–1146.
- 60 B. C. Hillol Khatua, Sandip Kumar Das, Satyajit Roy, *Angew. Chemie Int. Ed.*, 2020, **60**, 304–312.
- 61 V. Zubar, A. Brzozowska, J. Sklyaruk and M. Rueping, *Organometallics*.
- 62 M. Mastalir, M. Glatz, E. Pittenauer, G. Allmaier and K. Kirchner, *J. Am. Chem. Soc.*, 2016, **138**, 15543–15546.
- 63 A. Thakur and J. Louie, *Acc. Chem. Res.*, 2015, **48**, 2354–2365.
- 64 N. Kaur, *J. Iran. Chem. Soc.*, 2019, **16**, 2525–2553.
- 65 J. L. G. Fierro, Ed., *Metal Oxides: Chemistry an Applications*, CRC Press, New York, 2006.
- 66 Y. A. Titova, O. V Fedorova, G. L. Rusinov and V. N. Charushin, *Russ. Chem. Rev.*, 2015, **84**, 1294–1315.
- 67 Q. Cai, Y. Yang, D.-K. Li, F.-C. Jia, C. Xu and A.-X. Wu, *RSC Adv.*, 2015, **5**, 89427–89430.
- 68 Q.-H. Pd, I. I. Intramolecular, B. Ma, Y. Wang, J. Peng and Q. Zhu, 2011, **4**, 6362–6366.
- 69 K. Tanabo, *Solid Acids and Bases: their catalytic properties*, New york, Academic P., 1970.
- 70 Q. Zhang and F. Saito, *Adv. Powder Technol.*, 2012, **23**, 523–531.
- 71 M. Parashar, V. K. Shukla and R. Singh, *J. Mater. Sci. Mater. Electron.*, 2020, **31**, 3729–3749.
- 72 M. L. Occelli and R. J. Rennard, *Catal. Today*, 1988, **2**, 309–319.
- 73 G. N. Lewis, *J. Chem. Educ.*
- 74 R. G. Pearson, *J. Am. Chem. Soc.*, 1963, **85**, 3533–3539.
- 75 A. Corma, H. García, A. Leyva and A. Primo, *Appl. Catal. A Gen.*, 2003, **247**, 41–49.
- 76 B. D. Rowsell, R. J. Gillespie and G. L. Heard, *Inorg. Chem.*, 1999, **38**, 4659–4662.
- 77 A. Corma and H. Garci, *Chem. Rev.*, 2003, **103**, 4307–4365.
- 78 S. Kobayashi and K. Manabe, *Pure Appl. Chem.*, 2000, **72**, 1373–1380.
- 79 A. Corma, M. E. Domine and S. Valencia, *J. Catal.*, 2003, **215**, 294–304.
- 80 A. Lubineau and E. Meyer, *Tetrahedron*, 1988, **44**, 6065–6070.
- 81 D. C. Sherrington, A. P. Kybett, J. H. Clark, A. Lambert, D. J. Macquarrie, D. J. Nightingale, P. M. Price, J. K. Shorrocks and K. Wilson, in *Supported Catalysts and Their Applications*, ed. A. P. K. David C Sherrington, Royal Society of Chemistry, 2001, pp. 48–54.

- 82 G. A. Olah, G. K. Surya Prakash, R. Molnr and J. Sommer, *Superacid Chem.*
- 83 A. Krzywicki and M. Marczewski, *J.C.S. Faraday I*, 1980, **76**, 1311–1322.
- 84 A. Corma and V. Fornés, *Appl. Catal.*, 1990, **61**, 175–185.
- 85 B. A. T. Mehrabadi, S. Eskandari, U. Khan, R. D. White and J. R. Regalbuto, *A Review of Preparation Methods for Supported Metal Catalysts*, Elsevier Inc., 1st edn., 2017, vol. 61.
- 86 A. D. McNaught and A. Wilkinson., Eds., *IUPAC. Compendium of Chemical Terminology, 2nd ed. (the 'Gold Book')*, Blackwell Scientific Publications, Oxford, 1997.
- 87 A. E. Allen and D. W. C. MacMillan, *Chem. Sci.*, 2012, **3**, 633–658.
- 88 G. M. Sammis, H. Danjo and E. N. Jacobsen, *J. Am. Chem. Soc.*, 2004, **126**, 9928–9929.
- 89 B. M. Trost and X. Luan, *J. Am. Chem. Soc.*, 2011, **133**, 1706–1709.
- 90 M. Pang, J. Y. Chen, S. Zhang, R. Z. Liao, C. H. Tung and W. Wang, *Nat. Commun.*, 2020, **11**, 1–9.
- 91 N. Yamagiwa, H. Qin, S. Matsunaga and M. Shibasaki, *J. Am. Chem. Soc.*, 2005, **127**, 13419–13427.
- 92 J. A. Kalow and A. G. Doyle, *Tetrahedron*, 2013, **69**, 5702–5709.
- 93 J. Hou, A. Ee, W. Feng, J. H. Xu, Y. Zhao and J. Wu, *J. Am. Chem. Soc.*, 2018, **140**, 5257–5263.
- 94 Z. Chen, L. Gao, S. Ye, Q. Ding and J. Wu, *Chem. Commun.*, 2012, **48**, 3975–3977.
- 95 S. E. Denmark and M. T. Burk, *Chirality*, 2014, **26**, 344–355.
- 96 T. Yang, A. Ferrali, F. Sladojevich, L. Campbell and D. J. Dixon, *J. Am. Chem. Soc.*, 2009, **131**, 9140–9141.
- 97 K. Kaneda and T. Mitsudome, *Chem. Rec.*, 2017, **17**, 4–26.
- 98 K. D. Parghi and R. V. Jayaram, *Catal. Commun.*, 2010, **11**, 1205–1210.
- 99 P. Barbaro, F. Liguori, N. Linares and C. M. Marrodan, *Eur. J. Inorg. Chem.*, 2012, 3807–3823.
- 100 H. Gao, L. Hu, Y. Hu, X. Lv, Y. B. Wu and G. Lu, *Catal. Sci. Technol.*, 2021, **11**, 4417–4428.
- 101 M. I. Bugreev, E. I. Efimov, S. V. Ignatiev, D. V. Pankratov and V. I. Tchitaykin, in *Mat. Res. Soc. Symp. Proc.*, 2002, vol. 713, pp. 1–8.
- 102 F. Yang, A. Wang, S. Yue, W. Du, S. Wang, X. Zhang and X. Liu, *Sci. China Mater.*, 2021, **64**, 2989–2914.
- 103 S. Liu, J. Sun, G. Ren and X. Meng, *Mater. Sci. Semicond. Process.*, 2022, **137**, 106230.
- 104 X. Yang, S. Sun, J. Cui, M. Yang, Y. Luo and S. Liang, *Cryst. Growth Des.*, 2021, **21**, 6576–6618.
- 105 D. M. Griffith, H. Li, M. V. Werrett, P. C. Andrews and H. Sun, *Chem. Soc. Rev.*, 2021, **50**, 12037–12069.
- 106 T. Ollevier, *Org. Biomol. Chem.*, 2013, **11**, 2740.
- 107 A. E. Reed and P. v. R. Schleyer, *J. Am. Chem. Soc.*, 1990, **112**, 1434.
- 108 S. S. Garje and V. K. Jain, *Main Gr. Met. Chem.*, 1999, **22**, 45–58.
- 109 A. Michaelis and A. Polis, *Berichte der Dtsch. Chem. Gesellschaft*, 1887, **20**, 1516.
- 110 H. Gilman, H. L. Yablunky and A. C. Svigoon, *J. Am. Chem. Soc.*, 1939, **61**, 1170–1172.
- 111 V. G. Wittig and K. Clauss, *Justus Liebigs Ann. Chem.*, 1952, **578**, 136–146.
- 112 Y. Matano and H. Suzuki, *Bull. Chem. Soc. Jpn.*, 1996, **69**, 2673–2681.
- 113 T. Mukaiyama, N. Sakurai and K. Ikegai, *Chem. Lett.*, 2006, **35**, 1140–1141.
- 114 J. R. Desmurs, M. Labrouill, C. Le Roux, H. Gaspard, A. Laporterie and J. Dubac, *Tetrahedron*, 1997, **38**, 8871–8874.
- 115 M. Wada, E. Takeichi and T. Matsumoto, *Bull. Chem. Soc. Jpn.*, 1991, **64**, 990–994.
- 116 M. Wada, T. Takahashi, T. Domae, T. Fukuma, N. Miyoshi and K. Smith, *Tetrahedron*, 1997, **8**, 3939–3946.
- 117 P. A. Evans, J. Cui, S. J. Gharpure and R. J. Hinkle, *J. Am. Chem. Soc.*, 2003, **125**, 11456–11457.
- 118 S. Gmouh, H. Yang and M. Vaultier, *Org. Lett.*, 2003, **5**, 2219–2222.
- 119 J. A. R. Salvador, S. M. Silvestre and R. M. A. Pinto, *Molecules*, 2011, **16**, 2884–2913.
- 120 P. Malik and D. Chakraborty, *Tetrahedron Lett.*, 2010, **51**, 3521–3523.
- 121 T. H. El-Sayed, A. Aboelnaga, M. A. El-atawy and M. Hagar, *Molecules*, 2018, **23**, 1348–1369.
- 122 M. Wu, B. Xu, Y. Zhang, S. Qi, W. Ni and J. Hu, *Chem. Eng. J.*, 2020, **381**, 122558.
- 123 J. Di, J. Xia, H. Li, S. Guo and S. Dai, *Nano Energy*, 2017, **41**, 172–192.

- 124 R. He, D. Xu, B. Cheng, J. Yu and W. Ho, *Nanoscale Horizons*, 2018, **3**, 464–504.
- 125 H. Feng, Y. Du, C. Wang and W. Hao, *Curr. Opin. Green Sustain. Chem.*, 2017, **6**, 93–100.
- 126 S. Zhang, M. Xie, F. Li, Z. Yan, Y. Li, E. Kan, W. Liu, Z. Chen and H. Zeng, *Angew. Chemie Int. Ed.*, 2016, **55**, 1666–1669.
- 127 R. Mohan, *Nat. Publ. Gr.*, 2010, **2**, 2010.
- 128 K. Xu, L. Wang, X. Xu, S. X. Dou, W. Hao and Y. Du, *Energy Storage Mater.*, 2019, **19**, 446–463.
- 129 G. N. Subbanna, L. Ganapathi, C. N. R. Rao and D. A. Jefferson, *Mater. Res. Bull.*, 1987, **22**, 205–209.
- 130 M. Guilloux-Viry, J. R. Duclere, V. Bouquet and A. Perrin, in *Piezoelectric Materials for Macro/Micro Systems*, ed. D. Remiens, 2003, pp. 159–181.
- 131 X. Tao, Y. Zhao, L. Mu, S. Wang, R. Li and C. Li, *Adv. Energy Mater.*, 2018, **8**, 1–7.
- 132 D. Kato, K. Hongo, R. Maezono, M. Higashi, H. Kunioku, M. Yabuuchi, H. Suzuki, H. Okajima, C. Zhong, K. Nakano, R. Abe and H. Kageyama, *J. Am. Chem. Soc.*, 2017, **139**, 18725–18731.
- 133 H. Hu and C. Xiao, *Open J. Phys. Chem.*, 2017, **07**, 1–8.
- 134 S. B. Ötvös, R. Mészáros, G. Varga, M. Kocsis, Z. Kónya, Á. Kukovecz, P. Pusztai, P. Sipos, I. Pálkó and F. Fülöp, *Green Chem.*, 2018, **20**, 1007–1019.
- 135 R. Mészáros, S. B. Ötvös, G. Varga, É. Böszörményi, M. Kocsis, K. Karádi, Z. Kónya, Á. Kukovecz, I. Pálkó and F. Fülöp, *Mol. Catal.*
- 136 R. Mészáros, A. Márton, M. Szabados, G. Varga, Z. Kónya, Á. Kukovecz, F. Fülöp, I. Pálkó and S. B. Ötvös, *Green Chem.*, 2021, **23**, 4685–4696.
- 137 R. I. Mészáros, 2021.
- 138 K. Matsuo and T. Yasuda, *Chem. Sci.*, 2019, **10**, 10687–10697.
- 139 S. Lohar, K. Dhara, P. Roy, S. P. Sinha Babu and P. Chattopadhyay, *ACS Omega*, 2018, **3**, 10145–10153.
- 140 E. A. Weiss, M. J. Tauber, R. F. Kelley, M. J. Ahrens, M. A. Ratner and M. R. Wasielewski, *J. Am. Chem. Soc.*, 2005, **127**, 11842–11850.
- 141 S. W. Woods, *J. Clin. Psychiatry*, 2003, **64**, 663–667.
- 142 A. J. Warman, T. S. Rito, N. E. Fisher, D. M. Moss, N. G. Berry, P. M. O'Neill, S. A. Ward and G. A. Biagini, *J. Antimicrob. Chemother.*, 2013, **68**, 869–880.
- 143 M. C. Montoya, L. Didone, R. F. Heier, M. J. Meyers and D. J. Krysan, *ACS Infect. Dis.*, 2018, **4**, 499–507.
- 144 X. Liu and X.-J. Wang, *J. Genet. Genomics*, 2020, **47**, 119–121.
- 145 M. Mayer, P. T. Lang, S. Gerber, P. B. Madrid, I. G. Pinto, R. K. Guy and T. L. James, *Chem. Biol.*, 2006, **13**, 993–1000.
- 146 N. Sharma, R. Gupta, M. Kumar and R. R. Gupta, *J. Fluor. Chem.*, 1999, **98**, 153–157.
- 147 C. Dai, X. Sun, X. Tu, L. Wu, D. Zhan and Q. Zeng, *Chem. Commun.*, 2012, **48**, 5367–5369.
- 148 M. Dawei, Q. Geng, H. Zhang and Y. Jiang, *Angew. Chemie Int. Ed.*, 2010, **49**, 1291–1294.
- 149 D. Mahesh, P. Sadhu and T. Punniyamurthy, *J. Org. Chem.*, 2016, **81**, 3227–3234.
- 150 P. S. Salunkhe, Y. S. Patil, I. A. Dhole, B. S. Kalshetti, V. B. Patil, S. R. Mane and A. A. Ghanwat, *New J. Chem.*, 2019, **43**, 14806–14817.
- 151 S. Anbu, A. Paul, K. Surendranath, N. S. Solaiman and A. J. L. Pombeiro, *Sensors Actuators, B Chem.*, 2021, **337**, 129785.
- 152 Y. Chen, L. Qian, W. Zhang and B. Han, *Angew. Chemie Int. Ed.*, 2008, **47**, 9330–9333.
- 153 D. K. Maiti, S. Halder, P. Pandit, N. Chatterjee, D. De Joarder, N. Pramanik, Y. Saima, A. Patra and P. K. Maiti, *J. Org. Chem.*, 2009, **74**, 8086–8097.
- 154 T. B. Nguyen, J. Le Bescont, L. Ermolenko and A. Al-Mourabit, *Org. Lett.*, 2013, **15**, 6218–6221.
- 155 K. Gopalaiah and S. N. Chandrudu, *RSC Adv.*, 2015, **5**, 5015.
- 156 A. A.-M. T.B. Nguyen, J. Le Bescont, L. Ermolenko, *Org. Lett.*, 2013, **15**, 6218–6221.
- 157 R. D. Patil and S. Adimurthy, *Adv. Synth. Catal.*, 2011, **353**, 1695–1700.
- 158 T. P. D. Mahesh, P. Sadhu, *J. Org. Chem.*, 2016, **81**, 3227–3234.
- 159 K. Junge, V. Papa and M. Beller, *Chem. - A Eur. J.*, 2019, **25**, 122–143.
- 160 J. Yang, M. A. Uddin, Y. Tang, Y. Wang, Y. Wang, H. Su, R. Gao, Z. K. Chen, J. Dai, H. Y. Woo and X. Guo, *ACS Appl. Mater. Interfaces*, 2018, **10**, 23235–23246.

- 161 X. Li, L. P. Zhang, L. Kang and Y. Zhao, *Chem. Commun.*, 2019, **55**, 11390–11393.
- 162 K. Murugan, C. Panneerselvam, J. Subramaniam, M. Paulpandi, R. Rajaganesh, M. Vasanthakumaran, J. Madhavan, S. S. Shafi, M. Roni, J. S. Portilla-Pulido, S. C. Mendez, J. E. Duque, L. Wang, A. T. Aziz, B. Chandramohan, D. Dinesh, S. Piramanayagam and J. S. Hwang, *Sci. Rep.*, 2022, **12**, 1–11.
- 163 W. Wang, S. Zhang, J. Wang, F. Wu, T. Wang and G. Xu, *J. Agric. Food Chem.*, 2021, **69**, 491–500.
- 164 Y. S. Higasio and T. Shoji, *Appl. Catal. A Gen.*, 2001, **221**, 197–207.
- 165 Z. H. Skraup, *Monatshefte für Chemie*, 1881, **2**, 139–170.
- 166 M. J. Climent, A. Corma, J. C. Hernández, A. B. Hungria, S. Iborra and S. Martínez-Silvestre, *J. Catal.*, 2012, **292**, 118–129.
- 167 D. Wei, V. Dorcet, C. Darcel and J. B. Sortais, *ChemSusChem*, 2019, **12**, 3078–3082.
- 168 H. Vander Mierde, P. Van Der Voort, D. De Vos and F. Verpoort, *European J. Org. Chem.*, 2008, **2008**, 1625–1631.
- 169 C. S. Cho and S. G. Oh, *Tetrahedron Lett.*, 2006, **47**, 5633–5636.
- 170 A. Mondal, M. K. Sahoo, M. Subaramanian and E. Balaraman, *J. Org. Chem.*, 2020, **85**, 7181–7191.
- 171 S. A. Raw, C. D. Wilfred and R. J. K. Taylor, *Org. Biomol. Chem.*, 2004, **2**, 788.
- 172 S. Antoniotti and E. Duñach, *Tetrahedron Lett.*, 2002, **43**, 3971–3973.
- 173 T. Mallat and A. Baiker, *Catal. Today*, 1994, **19**, 247–283.
- 174 P. Chandra, T. Ghosh, N. Choudhary, A. Mohammad and S. M. Mobin, *Coord. Chem. Rev.*, 2020, **411**, 213241.
- 175 J. L. Lábár, M. Adamik, B. P. Barna, Z. Czigány, Z. Fogarassy, Z. E. Horváth, O. Geszti, F. Misják, J. Morgiel, G. Radnóczy, G. Sáfrán, L. Székely and T. Szűts, *Microsc. Microanal.*, 2012, **18**, 406–420.
- 176 M. Kocsis, S. B. Ötvös, G. F. Samu, Z. Fogarassy, B. Pécz, Á. Kukovecz, Z. Kónya, P. Sipos, I. Pálkó and G. Varga, *ACS Appl. Mater. Interfaces*, 2021, **13**, 42650–42661.
- 177 Y. Zhang, X. Zhang, Y. Ling, F. Li, A. M. Bond and J. Zhang, *Angew. Chemie Int. Ed.*, 2018, **130**, 13467–13471.
- 178 H. Huang, X. Li, J. Wang, F. Dong, P. K. Chu, T. Zhang and Y. Zhang, *ACS Catal.*, 2015, **5**, 4094–4103.
- 179 H. Naatz, S. Lin, R. Li, W. Jiang, Z. Ji, C. H. Chang, J. Köser, J. Thöming, T. Xia, A. E. Nel, L. Mädler and S. Pokhrel, *ACS Nano*, 2017, **11**, 501–515.
- 180 P. Wu, S. Dai, G. Chen, S. Zhao, Z. Xu, M. Fu, P. Chen, Q. Chen, X. Jin, Y. Qiu, S. Yang and D. Ye, *Appl. Catal. B Environ.*
- 181 L. Miao, X. Tang, S. Zhao, X. Xie, C. Du, T. Tang and H. Yi, *Nano Res.*, 2022, **15**, 1660–1671.
- 182 P. F. Zhang, J. Y. Zhang, T. Sheng, Y. Q. Lu, Z. W. Yin, Y. Y. Li, X. X. Peng, Y. Zhou, J. T. Li, Y. J. Wu, J. X. Lin, B. Bin Xu, X. M. Qu, L. Huang and S. G. Sun, *ACS Catal.*, 2020, **10**, 1640–1651.
- 183 M. Szabados, A. Adél Ádám, P. Traj, S. Muráth, K. Baán, P. Béteky, Z. Kónya, Á. Kukovecz, P. Sipos and I. Pálkó, *J. Catal.*, 2020, **391**, 282–297.
- 184 R. L. Frost, Z. Ding, J. T. Klopogge and W. N. Martens, *Thermochim. Acta*, 2002, **390**, 133–144.
- 185 C.-F. Tsang, J. K. Meen and D. Elthon, *J. Am. Ceram. Soc.*, 1994, **77**, 3119–3124.
- 186 G. E. Tobon-Zapata, S. B. Etcheverry and E. J. Baran, *J. Mater. Sci. Lett.*, 1997, **16**, 656–657.
- 187 R. L. Frost, W. N. Martens, L. Rintoul, E. Mahmutagic and J. T. Klopogge, *J. Raman Spectrosc.*, 2002, **33**, 252–259.
- 188 C. Xu, P. Qiu, L. Li, H. Chen, F. Jiang and X. Wang, *ACS Appl. Mater. Interfaces*, 2018, **10**, 25321–25328.
- 189 K. Coenen, F. Gallucci, B. Mezari, E. Hensen and M. van Sint Annaland, *J. CO<sub>2</sub> Util.*, 2018, **24**, 228–239.
- 190 D. Stoilova, V. Koleva and V. Vassileva, *Spectrochim. Acta - Part A Mol. Biomol. Spectrosc.*, 2002, **58**, 2051–2059.
- 191 R. L. Frost, B. J. Reddy, D. L. Wain and W. N. Martens, *Spectrochim. Acta - Part A Mol. Biomol. Spectrosc.*, 2007, **66**, 1075–1081.
- 192 F. Dong, Y. Sun, W. K. Ho and Z. Wu, *Dalt. Trans.*, 2012, **41**, 8270–8284.
- 193 Y. Huai, Y. Qian and Y. Peng, *Appl. Surf. Sci.*, 2020, **531**, 147334.
- 194 M. Kocsis, M. Szabados, S. B. Ötvös, G. F. Samu, Z. Fogarassy, B. Pécz, Á. Kukovecz, Z. Kónya, P. Sipos, I. Pálkó and G. Varga, *J. Catal.*, 2022, **414**, 163–178.



- 195 R. J. Jia, J. T. Han, X. J. Wu, C. L. Wu, Y. H. Huang and W. Huang, *Mater. Res. Bull.*, 2008, **43**, 1702–1708.
- 196 M. Bernard, A. Hugot-Le Goff, B. V. Thi and S. Cordoba de Torresi, *J. Electrochem. Soc.*, 1993, **140**, 3065–3070.
- 197 C. Murli, S. M. Sharma, S. K. Kulshreshtha and S. K. Sikka, *Phys. B Condens. Matter*, 2001, **307**, 111–116.
- 198 B. Rivas-Murias and V. Salgueiriño, *J. Raman Spectrosc.*, 2017, **48**, 837–841.
- 199 J. L. Ortiz-Quiñonez, I. Zumeta-Dubé, D. Díaz, N. Nava-Etzana, E. Cruz-Zaragoza and P. Santiago-Jacinto, *Inorg. Chem.*, 2017, **56**, 3394–3403.
- 200 Y. Yang, S. Wu, Y. Li, Q. Zhang and X. Zhao, *J. Mater. Chem. A*, 2020, **8**, 1254–1264.
- 201 M. G. Uytterhoeven and R. A. Schoonheydt, *Microporous Mater.*, 1994, **3**, 265–279.
- 202 H. Y. Xu, S. Le Xu, X. D. Li, H. Wang and H. Yan, *Appl. Surf. Sci.*, 2006, **252**, 4091–4096.
- 203 J. Park, X. Shen and G. Wang, *Sensors Actuators, B Chem.*, 2009, **136**, 494–498.
- 204 M. K. Carpenter and D. A. Corrigan, *J. Electrochem. Soc.*, 1989, **136**, 1022–1026.
- 205 M. C. Biesinger, B. P. Payne, A. P. Grosvenor, L. W. M. Lau, A. R. Gerson and R. S. C. Smart, *Appl. Surf. Sci.*, 2011, **257**, 2717–2730.
- 206 M. C. Biesinger, B. P. Payne, L. W. M. Lau, A. Gerson and R. S. C. Smart, *Surf. Interface Anal.*, 2009, **41**, 324–332.
- 207 J. M. Bothwell, W. Krabbe and R. S. Mohan, *Chem. Soc. Rev.*, 2011, **40**, 4649–4707.
- 208 B. Ritschel and C. Lichtenberg, *Synlett*, 2018, **29**, 2213–2217.
- 209 M. Huang, J. Hou, R. Yang, L. Zhang, X. Zhu and Y. Wan, *Synth.*, 2014, **46**, 3356–3364.
- 210 D. Prat, A. Wells, J. Hayler, H. Sneddon, C. R. McElroy, S. Abou-Shehada and P. J. Dunn, *Green Chem.*, 2016, **18**, 288–296.
- 211 M. Fan, W. Zhou, Y. Jiang and D. Ma, *Org. Lett.*, 2015, **17**, 5934–5937.
- 212 T. Garnier, M. Danel, V. Magné, A. Pujol, V. Bénétteau, P. Pale and S. Chassaing, *J. Org. Chem.*, 2018, **83**, 6408–6422.
- 213 A. C. Mantovani, T. A. C. Goulart, D. F. Back and G. Zeni, *Chem. - A Eur. J.*, 2014, **20**, 12663–12668.
- 214 L. Wang, J. Zhang, J. Sun, L. Zhu, H. Zhang, F. Liu, D. Zheng, X. Meng, X. Shi and F.-S. Xiao, *ChemCatChem*, 2013, **5**, 1606–1613.
- 215 M. Li, X. Xing, Z. Ma, J. Lv, P. Fu and Z. Li, *ACS Sustain. Chem. Eng.*, 2018, **6**, 5495–5503.
- 216 L. Orha, J. M. Tukacs, B. Gyarmati, A. Szilágyi, L. Kollár and L. T. Mika, *ACS Sustain. Chem. Eng.*, 2018, **6**, 5097–5104.
- 217 M. Rovira, M. Soler, I. Güell, M. Z. Wang, L. Gómez and X. Ribas, *J. Org. Chem.*, 2016, **81**, 7315–7325.
- 218 S. Kozuch and J. M. L. Martin, *ACS Catal.*, 2012, **2**, 2787–2794.
- 219 D. Ventura-Espinosa, S. Martín and J. A. Mata, *J. Catal.*, 2019, **375**, 419–426.
- 220 A. Melli, S. Potenti, M. Melosso, S. Herbers, L. Spada, A. Gualandi, K. G. Lengsfeld, L. Dore, P. Buschmann, P. G. Cozzi, J. U. Grabow, V. Barone and C. Pizzarini, *Chem. - A Eur. J.*, 2020, **26**, 15016–15022.
- 221 B. Dutta, S. Biswas, V. Sharma, N. O. Savage, S. P. Alpay and S. L. Suib, *Angew. Chemie Int. Ed.*, 2016, **128**, 2211–2215.
- 222 M. Kocsis, K. Baán, S. B. Ötvös, Á. Kukovecz, Z. Kónya, P. Sipos, I. Pálkó and G. Varga, *Catal. Sci. Technol.*, 2023, 3069–3083.
- 223 C. Zhang and N. Jiao, *Angew. Chemie Int. Ed.*, 2010, **49**, 6174–6177.
- 224 D. Bellezza, R. J. Zaragozá, M. José Aurell, R. Ballesteros and R. Ballesteros-Garrido, *Org. Biomol. Chem.*, 2021, **19**, 677–683.
- 225 J. Ramler and C. Lichtenberg, *Chem. - A Eur. J.*, 2020, **26**, 10250–10258.
- 226 M. Vellakkaran, K. Singh and D. Banerjee, *ACS Catal.*, 2017, **7**, 8152–8158.
- 227 S. Elangovan, J. Neumann, J. B. Sortais, K. Junge, C. Darcel and M. Beller, *Nat. Commun.*, 2016, **7**, 1–8.
- 228 Y. Tsuji, K. T. Huh and Y. Watanabe, *J. Org. Chem.*, 1987, **52**, 1673–1680.
- 229 Y. Tsuji, H. Nishimura, K.-T. Huh and Y. Watanabe, *J. Organomet. Chem.*, 1985, **286**, c44–c46.
- 230 J. Li, J. Zhang, H. Yang and G. Jiang, *J. Org. Chem.*, 2017, **82**, 3284–3290.

- 231 R. N. Monrad and R. Madsen, *Org. Biomol. Chem.*, 2011, **9**, 610–615.
- 232 D. Panja, B. Paul, B. Balasubramaniam, R. K. Gupta and S. Kundu, *Catal. Commun.*, 2020, **137**, 105927.
- 233 S. Shee, K. Ganguli, K. Jana and S. Kundu, *Chem. Commun.*, 2018, **54**, 6883–6886.
- 234 R. Poreddy, C. Engelbrekt and A. Riisager, *Catal. Sci. Technol.*, 2015, **5**, 2467–2477.
- 235 H. Yan, S. Yao, J. Wang, S. Zhao, Y. Sun, M. Liu, X. Zhou, G. Zhang, X. Jin, X. Feng, Y. Liu, X. Chen, D. Chen and C. Yang, *Appl. Catal. B Environ.*, 2021, **284**, 119803.
- 236 J. S. Yadav, B. V. Subba Reddy, K. Premalatha and K. S. Shankar, *Synthesis (Stuttg.)*, 2008, 3787–3792.
- 237 P. Daw, A. Kumar, N. A. Espinosa-jalapa, Y. Diskin-posner, Y. Ben-david and D. Milstein, .
- 238 I. J. Casely, J. W. Ziller, B. J. Mincher and W. J. Evans, *Inorg. Chem.*, 2011, **50**, 1513–1520.

## MAGYAR NYELVŰ ÖSSZEFOGLALÓ (SUMMARY IN HUNGARIAN)

A Scifinder adatbázison (<https://scifinder.cas.org>) 2023. január 2-án végzett általános keresés alapján az elmúlt 10 évben a katalízis területen megjelent körülbelül 260 000 új publikáció egynegyede heterociklusos vegyületek előállításával és/vagy átalakításával foglalkozott.\* Legtöbbjük valamilyen katalitikus rendszert ír le (átmenetifém katalízis, Lewis-sav katalízis, organokatalízis, biokatalízis, fázistranszfer katalízis, elektrokatalízis), mivel az általuk biztosított alternatív reakcióút vagy mechanizmus sokkal gazdaságosabb és versenyképesebb, mint a sztöchiometrikus eljárások.

Annak ellenére, hogy a szintetikus szerves kémia területén a homogén nemesfém-katalízis dominál, a nem nemesfém-centrumot tartalmazó heterogenizált katalizátoroknak is számos előnyük lehet. Nemcsak az újrahasznosíthatóság és a robusztusság előnyeit biztosíthatják, ami önmagában is gazdaságos és környezetbarát alternatívát jelenthet a katalizátorválasztásban, de akár sokkal hatékonyabb jelöltek is lehetnek monofémes társaikhoz képest (fokozott szelektivitás és/vagy hozam, enyhébb reakciókörülmények, zöldebb oldószeresek), ha a különböző fémcentrumok képesek az egymással való együttműködésre.

Ezt a lehetőséget megcélózva elsődleges hipotézisünk az volt, hogy a Lewis savas bizmutit ( $\text{Bi}_2\text{O}_2\text{CO}_3$ ) vázszerkezet réz-, kobalt-, mangán- vagy nikkelkationokkal vagy oxidokkal történő módosításával hatékony multifunkciós katalizátorok állíthatók elő, amelyek heterogén módon képesek többlépéses ciklizációs reakciókat promótni. Ezen túlmenően azt is feltételeztük, hogy hatékonyságukat még tovább lehet növelni, ha meghatározzuk azokat a szerkezeti tényezőket, amelyek a döntően befolyásolhatják a katalitikus viselkedést. Így a módosított szerkezeteket alaposan tanulmányoztuk mind szerkezetileg (XRD, Raman, XPS stb.), mind katalitikusan, számos katalitikus ciklizációs reakcióban tesztelve őket.

Kezdetben a bizmutitváz átmenetifém ionokkal történő módosítása a karbamid-hidrolízis módszerével történt, amely során a karbamid szabályozott hidrolízise biztosítja a lecsapáshoz szükséges mennyiségű hidroxid- és karbonátanion jelenlétét a rendszerben. A sikeres előkísérletek után azonban a bizmutit szerkezetek közvetlenül is szintetizálhatók voltak egy módosított együttes lecsapásos módszerrel, amelyben a megfelelő koncentrációjú (3,75 mmol) bizmut- és átmenetifém nitrát oldatokhoz megfelelő koncentrációjú (0,6 M) ammónia és nátrium-karbonát oldatot adagoltunk. Ezt követően, a  $\text{CuBi}_2\text{O}_2\text{CO}_3$  esetében 80 °C-on, a Co-,

---

\* A Scifinder (<https://scifinder.cas.org>) általános keresése 2023. január 2-án 265839 "katalízissel" kapcsolatos angol nyelvű folyóiratot talált 2012 és 2023 januárja közötti időszakban, amelyek közül 71525 heterociklusok előállítására és/vagy átalakítására irányult.

Mn-,  $\text{NiBi}_2\text{O}_2\text{CO}_3$  esetén 100 °C-on 24 órás folyamatos keverés következett, majd a kapott, színes termékeket szűrtük, mostuk (desztillált vízzel) és szárítottuk (60 °C, egy éjszakán át). A réz-bizmutit kivételével a finoman porított szilárd anyagokat további hőkezelésnek vetettük alá 3 órán keresztül 290 °C-on, hogy eltávolítsuk a visszamaradt víznyomokat

Röntgen-diffraktometriás mérések alapján minden módosított bizmutitrendszert a Sillén-típusú bizmut szerkezeti analójaként lehetett azonosítani, amelyben a kationok beépülése izomorf módon történt meg. A SEM-EDX elemterképek rögzítése után azonban ezt az állítást részben felül kellett vizsgálni, mivel a réztartalmú rendszer homogén kationeloszlást mutatott, azonban a Mn-, Co- és Ni-tartalmú bizmutokban az eloszlás heterogénnek bizonyult. Az összetételek meghatározása során (ICP-MS, TG és XPS) nem volt különbség a rézzel módosított bizmutit tömbi- és felületi összetételében, míg a többi átmenetifém tartalmú rendszerben az átmenetifémek felületi feldúsulása volt megfigyelhető. A nagy felbontású transzmissziós elektronmikroszkópos felvételek alapján morfológiai különbségek is mutatkoztak: míg a réz-bizmutit Sillén-típusú lamelláris morfológia jellemezte, addig a többi átmenetifém tartalmú bizmutit két különböző morfológiájú részecskéből állt. A TEM-EDX mérések ezen túlmenően azt is kimutatták, hogy ezek a részecskék összetételükben is különböztek. Ez alapján a felületen különböző átmenetifém oxidok megkötődése volt feltételezhető.

Az anyagtudományi jellemzés során további lényeges különbségeket is találtunk a katalizátorjelöltekkel kapcsolatban. Míg a rézionokkal történő módosítás után az infravörös, Raman, UV-DR és XP spektroszkópiai mérések egy azurit típusú komplex interkalálódását erősítették meg a bizmutit váz rétegek közti terében, addig a Co- és  $\text{MnBi}_2\text{O}_2\text{CO}_3$  analízise határfelületi helyek kialakulását mutatta ki a bizmutit hordozó felülete és az átmenetifém oxidok között. A nikkeltartalmú katalizátor nem interkalálódott, és nem tartalmazott határfelületi helyeket. Ezen megállapítások alapján a katalitikus képességekben is különbségekre lehetett számítani.

A réztartalmú rendszer katalitikus képességeit a 2-jód-anilin és 2-bróm-tiofenol kapcsolási reakciójában vizsgáltuk. Ez a reakció azért is érdekes, mert a  $\text{Bi}^{3+}$ , bár Lewis-sav katalizátorként ismert, legjobb tudásunk szerint még soha nem használták hasonló reakcióban. A módosított rendszer nemcsak a fenotiazinok szintézisében bizonyult aktívnak, hanem sokkal környezetbarátabb és egyszerűbb körülmények között is kiváló szelektivitással és konverzióval tudott működni összehasonlítva a legjobb elérhető technológiával. Ezenkívül az irodalomban nincs példa arra, hogy hasonlóan alacsony koncentrációjú bázis alkalmazása elegendő lenne fenotiazin szelektív előállításához ilyen típusú kapcsolásokban. A kinetikai vizsgálatok

bebizonyították, hogy a  $\text{CuBi}_2\text{O}_2\text{CO}_3$  kooperatív katalizátorként módon képes katalizálni a fenotiazin szintézisét, elősegítve egy koncertikus reakció lejátszódását. A forrón szűrési- és újrafelhasználhatósági tesztek emellett megmutatták, hogy a katalizátor heterogén módon képes katalizálni a reakciót, illetve, hogy aktivitása és szelektivitása 5 egymást követő ciklus után sem csökken. A reakció kiterjeshetőségét vizsgáló tesztek eredményeit figyelembe véve megállapítható, hogy az optimalizált reakciókörülmények között számos származék esetében magas hozamok és szelektivitások érhetők el, és a katalizátor nagyfokú robusztusságot mutat a reakciók (ex situ XRD, TEM és XPS) által okozott szerkezeti degradációval szemben.

A mangán-, kobalt- és nikkellionokkal módosított bizmutit szerkezetek katalitikus teljesítményét számos modellreakcióban teszteltünk. Először a 2-fenilbenzimidazol szintézis többlépcsős reakciókaszkádjában. Az előkísérleteket DMSO oldószerben végeztük bizmutvegyületeket jelenlétében. Csak a  $\text{Bi}_2\text{O}_3$  és a  $\text{Bi}_2\text{O}_3\text{CO}_3$  bizonyult kismértékben aktívnak az imin intermedierekhez vezető oxidatív kapcsolásban és/vagy a gyűrűzárási lépésben. A kezdeti szerény teljesítmény ellenére bizakodásra adott okot az a tény, hogy csak a reakcióközeg víztartalmának növelésével növekedtek mind a konverzió, mind pedig a szelektivitás értékek. Az összehasonlíthatóság érdekében a reakciót tiszta átmenetifém oxidok jelenlétében is végrehajtottuk, és egy kivétellel hasonló eredményeket kaptunk, kivéve a nikkellel módosított rendszer esetében, amikor is érdemi aktivitás nem volt megfigyelhető, így az optimalizálási lépések során ezzel a katalizátorjelöléssel nem folytattunk kísérleteket.

Az optimalizálás során sikerült meghatározni az optimális kísérleti körülményeket a kobalt- és mangántartalmú bizmutit esetében, valamint azt is megállapítottuk, hogy a helyesen megválasztott oldószer/oldószer keverék alkalmas a termékkeverék összetételének szabályozására. Az egyes komponensek lehetséges hozzájárulásait is vizsgáltuk az optimális reakciókörülményeken. Kimutattuk, hogy még a hordozóhoz impregnálással rögzített átmeneti fém-oxidok teljesítménye is meghaladja az egyes komponensek önálló teljesítményeit, de az együttes lecsapással szintetizált minták bizonyultak a legaktívabbnak. Ez indirekt bizonyíték a határfelületi helyek jelenlétére.

Az kinetikai kísérletek is megerősítették ezt az állítást. Ráadásul a kobalttartalmú rendszer sokkal aktívabbnak bizonyult, mint a mangántartalmú megfelelője. A kobalttartalmú rendszer esetében meghatároztuk az egyes komponensek hozzájárulásait is a reakciósorozat egyes reakcióihoz. Emellett a heterogenitási és újrafelhasználhatósági vizsgálatok kimutatták, hogy a katalizátorok heterogénen működnek, és katalitikus teljesítményük nem csökken jelentősen 5 egymást követő ciklus után sem. A reakció kiterjeshetőségét tekintve megállapítható, hogy az optimalizált reakciókörülmények között mindkét katalizátor nem csak

közvetlen származékképzésre, hanem izoszterek képzésére is alkalmas. Végül az ex situ XRD, TEM és XPS mérések azt mutatták, hogy a katalizátorok szerkezeti integritása változatlan marad a reakcióciklusok után is.

Végül a Mn-, Co-, Ni-tartalmú bizmutok katalitikus képességét vizsgáltuk oxidatív dehidrogénező kapcsolási reakciókban. Az anilin és származékai homo- és hetero-azokapcsolásaiban tapasztalt biztató eredményeket követően kinolin és kinoxalin vegyületek szintézisét optimalizáltuk. Különböző anilin és o-fenilén-diamin származékok 1,3-propándiollal, illetve etilénlikollal történő reakcióját vizsgáltuk a megfelelő kinolinok vagy kinoxalinok előállítására. Mindkét reakcióban a diol egyszerre szolgált reakciópartnerként és oldószerként, és oxidálószerként a levegő oxigéntartalmát hasznosítottuk, ami nagyon egyszerű módszereket eredményezett. Általánosságban elmondható, hogy a katalizátorok nagymértékben szelektívek a kinolinokra és kinoxalinokra, közepes vagy jó konverzióval. A forró szűrési teszt és az újratermelhetőségi reakciósorozat alapján sikeresen igazoltuk a kinoxalin szintézis heterogén jellegét  $\text{CoBi}_2\text{O}_2\text{CO}_3$  jelenlétében, illetve kontrollkísérletekben kimutattuk az o-fenilén-diamin és az etilénlikol  $\text{CoBi}_2\text{O}_2\text{CO}_3$  által katalizált oxidatív dehidrogénező mechanizmusát.

Összefoglalva, a szerkezeti jellemzés és a katalitikus vizsgálatok eredményei azt mutatták, hogy a módosított együttes lecsapás módszerével előállított átmenetifém ionokkal módosított bizmutitok nagy aktivitású és szelektív, robusztus és heterogén katalizátornak bizonyultak számos heterociklusokat eredményező szintézisben. A réztartalmú rendszer a Sillén-típusú beyerit új szerkezeti analógjának tekinthető, illetve a mangán- és kobalttartalmú rendszerekben sikeresen mutattuk ki a váz és az átmenetifémek/átmenetifém oxidok között kialakult határfelületek jelenlétét. A nikkellionokkal módosított rendszer nem tartalmazott egyéb speciális helyeket a  $\text{Bi}^{3+}$  és  $\text{Ni}^{2+/3+}$  aktív centrumokon kívül. Ennek megfelelően a réz-, mangán- és kobaltionokat tartalmazó rendszerek kiváló katalitikus teljesítményt mutattak, meghaladva az egyes átmeneti fém oxidok vagy a bizmutit katalitikus teljesítményét. Mivel egyértelmű összefüggéseket sikerült megállapítani a kompozitok szerkezete és az elért aktivitási és szelektivitási értékek között, kijelenthető, hogy kiindulópontunk, hogy hatékony, heterogén, kooperatív katalizátorok állíthatók elő egy katalitikusan aktív hordozó ( $\text{Bi}_2\text{O}_2\text{CO}_3$ ), és átmenetifém ionok/oxidok (Cu, Mn, Co) kombinálásával, helyesnek bizonyult.

## APPENDIX

### S1. Identification of phenothiazines by NMR spectroscopy

#### 10H-phenothiazine:

<sup>1</sup>H NMR (500 MHz, DMSO-d<sub>6</sub>) δ 7.20-7.16 (m, 4H), 7.13-7.09 (m, 2H), 7.00-6.97 (m, 2H).

<sup>13</sup>C NMR (500 MHz, DMSO-d<sub>6</sub>) δ 127.33, 126.77, 121.48, 114.44, 114.24.

#### 10H-phenothiazine-2-carbonitrile:

<sup>1</sup>H NMR (500 MHz, DMSO-d<sub>6</sub>) δ 7.57-7.53 (m, 2H), 7.42-7.41 (d, 1H), 7.20-7.16 (m, 2H), 7.13-7.09 (m, 1H), 7.01—6.99 (d, 1H).

<sup>13</sup>C NMR (125 MHz, DMSO-d<sub>6</sub>) δ 127.43, 127.33, 127.32, 125.34, 121.48, 117.30, 114.56.

#### 2,4-dichloro-10H-phenothiazine:

<sup>1</sup>H NMR (500 MHz, DMSO-d<sub>6</sub>) δ 7.64-7.63 (d, 2H), 7.33-7.31 (d, 2H), 7.22-7.20 (d, 2H), 7.19-7.16 (m, 2H), 7.13-7.09 (m, 2H), 7.01-6.99 (d, 2H).

<sup>13</sup>C NMR (125 MHz, DMSO-d<sub>6</sub>) δ 127.42, 127.19, 123.21, 122.31, 115.65, 114.38.

#### 2,4-dimethyl-10H-phenothiazine:

<sup>1</sup>H NMR (500 MHz, DMSO-d<sub>6</sub>) δ 7.31-7.30 (d, 1H), 7.20-7.16 (t, 1H), 7.13-7.09 (t, 1H), 7.01-6.99 (m, 1H), 6.92-6.91 (m, 1H), 2.30 (s, 3H).

<sup>13</sup>C NMR (125 MHz, DMSO-d<sub>6</sub>) δ 138.10, 125.52, 127.13, 123.98, 121.87, 115.62, 113.27, 21.06, 20.70.

#### 2-chloro-10H-phenothiazine:

<sup>1</sup>H NMR (500 MHz, DMSO-d<sub>6</sub>) δ 7.37-7.36 (d, 1H), 7.33-7.31 (d, 1H), 7.26 (d, 1H), 7.20-7.16 (m, 2H), 7.13-7.09 (m, 1H), 7.01-6.99 (d, 1H).

<sup>13</sup>C NMR (125 MHz, DMSO-d<sub>6</sub>) δ 127.43, 127.33, 127.11, 121.48, 113.98, 113.88.

#### 2-nitro-10H-phenothiazine:

<sup>1</sup>H NMR (500 MHz, DMSO-d<sub>6</sub>) δ 8.14-8.10 (m, 2H), 7.69-7.68 (d, 1H), 7.20-7.16 (m, 2H), 7.13-7.09 (m, 1H), 7.01-7.00 (d, 1H).

<sup>13</sup>C NMR (125 MHz, DMSO-d<sub>6</sub>) δ 128.29, 127.57, 127.33, 115.81, 114.62, 108.69.

#### 2-chloro-4-fluoro-10H-phenothiazine:

<sup>1</sup>H NMR (500 MHz, DMSO-d<sub>6</sub>) δ 7.41-7.40 (d, 1H), 7.23-7.18 (m, 1H), 7.17-7.13 (m, 1H), 7.12-7.10 (m, 1H), 7.01-7.00 (d, 1H).

<sup>13</sup>C NMR (125 MHz, DMSO-d<sub>6</sub>) δ 134.09, 127.24, 127.13, 122.19, 115.80, 113.00, 112.96, 110.43, 110.25.

### S2. Identification of 2-phenylbenzimidazoles/oxazoles/thiazoles by NMR spectroscopy

#### 2-Phenyl-1H-benzo[d]imidazole:

<sup>1</sup>H NMR (500 MHz, DMSO-d<sub>6</sub>) δ 8.19-8.14 (m, 2H), 7.59-7.50 (m, 5H), 7.25-7.23 (m, 2H);

<sup>13</sup>C NMR (100 MHz, DMSO-d<sub>6</sub>) δ 151.97, 140.41, 137.09, 130.06, 129.61, 128.92, 126.99, 123.55, 122.68, 117.63, 113.36.

#### 2-(4-Methoxyphenyl)-1H-benzo[d]imidazole:

<sup>1</sup>H NMR (500 MHz, DMSO-d<sub>6</sub>) δ 8.16-8.10 (m, 2H), 7.56 (br s, 2H), 7.17-7.09 (m, 4H), 3.83 (s, 3H);

<sup>13</sup>C NMR (100 MHz, DMSO-d<sub>6</sub>) δ 161.39, 153.02, 140.42, 137.06, 128.10, 123.55, 122.68, 121.90, 117.63, 113.36, 112.88, 55.33.

**2-(2-Methoxyphenyl)-1H-benzo[d]imidazole:**

<sup>1</sup>H NMR (500 MHz, DMSO-*d*<sub>6</sub>) δ 8.26 (d, 1H), 7.63 (d, 2H), 7.46 (t, 1H), 7.14-7.08 (m, 3H), 6.98 (t, 1H), 3.96 (s, 3H);

<sup>13</sup>C NMR (100 MHz, DMSO-*d*<sub>6</sub>) δ 157.60, 150.92, 138.68, 136.85, 130.86, 130.00, 123.54, 122.75, 120.38, 116.35, 115.39, 113.25, 110.70, 55.75.

**2-(4-Chlorophenyl)-1H-benzo[d]imidazole:**

<sup>1</sup>H NMR (500 MHz, DMSO-*d*<sub>6</sub>) δ 8.01 (d, 2H), 7.79 (d, 2H), 7.54 (d, 1H), 7.50 (d, 2H), 7.43-7.29 (m, 2H);

<sup>13</sup>C NMR (100 MHz, DMSO-*d*<sub>6</sub>) δ 152.97, 140.41, 137.06, 135.07, 128.40, 128.13, 127.32, 123.55, 122.68, 117.63, 113.36.

**2-(2-Chlorophenyl)-1H-benzo[d]imidazole:**

<sup>1</sup>H NMR (500 MHz, DMSO-*d*<sub>6</sub>) δ 8.03-8.00 (m, 1H), 7.65-7.62 (m, S3 3H), 7.55-7.48 (m, 2H), 7.20-7.17 (m, 2H);

<sup>13</sup>C NMR (100 MHz, DMSO-*d*<sub>6</sub>) δ 152.34, 139.07, 137.43, 133.68, 131.29, 129.66, 128.27, 126.53, 125.77, 123.49, 122.72, 116.03, 113.28.

**2-(3-Nitrophenyl)-1H-benzo[d]imidazole:**

<sup>1</sup>H NMR (500 MHz, DMSO-*d*<sub>6</sub>) δ 9.02 (t, 1H), 8.23 (d, 1H), 8.07 (d, 1H), 7.79-7.74 (m, 2H), 7.54 (d, 1H), 7.29-7.22 (m, 2H);

<sup>13</sup>C NMR (100 MHz, DMSO-*d*<sub>6</sub>) δ 153.00, 147.43, 139.50, 136.75, 132.59, 128.26, 127.57, 124.56, 124.49, 123.55, 122.68, 117.38, 113.80.

**2-Phenylbenzo[d]oxazole:**

<sup>1</sup>H NMR (500 MHz, DMSO-*d*<sub>6</sub>) δ 8.05-8.00 (m, 2H), 7.78 (d, 1H), 7.64 (d, 1H), 7.55-7.30 (m, 3H), 7.29-7.16 (m, 2H);

<sup>13</sup>C NMR (100 MHz, DMSO-*d*<sub>6</sub>) δ 162.56, 150.34, 141.62, 131.76, 128.64, 127.10, 125.29, 124.64, 119.07, 110.63.

**2-(4-Methoxyphenyl)benzo[d]oxazole:**

<sup>1</sup>H NMR (500 MHz, DMSO-*d*<sub>6</sub>) δ 7.79 (d, 2H), 7.78-7.75 (m, 1H), 7.61-7.59 (m, 1H), 7.42-7.35 (m, 2H), 7.00-6.97 (d, 2H), 3.76 (s, 3H);

<sup>13</sup>C NMR (100 MHz, DMSO-*d*<sub>6</sub>) δ 163.26, 162.21, 150.60, 141.82, 128.60, 125.29, 124.64, 120.78, 119.07, 113.87, 110.63, 55.33.

**2-(2-Methoxyphenyl)benzo[d]oxazole:**

<sup>1</sup>H NMR (500 MHz, DMSO-*d*<sub>6</sub>) δ 7.80-7.74 (m, 2H), 7.61, 7.61-7.59 (m, 1H), 7.52-7.35 (m, 2H) 7.32, 7.28-7.20 (m, 2H), 7.07 (d, 1H), 3.84 (s, 3H);

<sup>13</sup>C NMR (100 MHz, DMSO-*d*<sub>6</sub>) δ 162.39, 157.69, 150.26, 141.05, 130.89, 129.50, 125.24, 125.11, 121.42, 119.24, 115.19, 113.46, 110.50, 55.83.

**2-(4-Chlorophenyl)benzo[d]oxazole:**

<sup>1</sup>H NMR (500 MHz, DMSO-*d*<sub>6</sub>) δ 7.93 (d, 2H) m 7.80 (d, 1H), 7.58 (d, 1H) 7.43-7.30 (m, 4H);

<sup>13</sup>C NMR (100 MHz, DMSO-*d*<sub>6</sub>) δ 163.49, 150.60, 141.82, 137.78, 129.02, 128.91, 125.79, 125.29, 124.64, 119.07, 110.63.

**2-(2-Chlorophenyl)benzo[d]oxazole:**

<sup>1</sup>H NMR (500 MHz, DMSO-*d*<sub>6</sub>) δ 7.84 (d, 1H), 7.6-7.57 (m, 1H), 7.43-7.29 (m, 5H)

<sup>13</sup>C NMR (DMSO-*d*<sub>6</sub>) δ 161.31, 150.72, 141.36, 133.28, 130.82, 129.21, 128.62, 126.03, 125.23, 125.08, 123.13, 118.93, 110.49.



**2-(3-Nitrophenyl)benzo[d]oxazole:**

<sup>1</sup>H NMR (500 MHz, DMSO-*d*<sub>6</sub>) δ 8.68 (t, 1H), 8.24-8.14 (m, 2H), 7.85 (d, 1H), 7.66 (d, 1H), 7.69-7.54 (m, 1H), 7.48-7.39 (m, 2H);

<sup>13</sup>C NMR (100 MHz, DMSO-*d*<sub>6</sub>) δ: 163.51, 150.23, 149.23, 141.42, 133.87, 129.06, 125.29, 125.21, 124.92, 124.65, 124.08, 119.20, 110.56.

**2-Phenylbenzo[d]thiazole:**

<sup>1</sup>H NMR (500 MHz, DMSO-*d*<sub>6</sub>) δ 8.09-8.06 (m, 2H), 7.90-7.88 (m, 1H), 7.50-7.46 (m, 4H), 7.39-7.37 (m, 1H);

<sup>13</sup>C NMR (100 MHz, DMSO-*d*<sub>6</sub>) δ: 167.23, 153.39, 134.15, 134.01, 130.63, 128.53, 127.20, 126.16, 125.23, 122.96, 122.02.

**2-(4-Methoxyphenyl)benzo[d]thiazole:**

<sup>1</sup>H NMR (500 MHz, DMSO-*d*<sub>6</sub>) δ 7.93-7.83 (m, 2H), 7.70 (d 1 H), 7.57- 7.48 (m, 1H), 7.30-7.25 (m, 1H), 7.05-6.96 (m, 2H), 3.85 (s, 3H);

<sup>13</sup>C NMR (100 MHz, DMSO-*d*<sub>6</sub>) δ 166.15, 160.93, 153.71, 135.04, 128.54, 126.90, 126.16, 125.23, 122.96, 122.02, 114.36, 55.33.

**2-(2-Methoxyphenyl)benzo[d]thiazole**

<sup>1</sup>H NMR (500 MHz, DMSO-*d*<sub>6</sub>) δ 8.04-8.00 (m, 2H), 7.68 (d, 1H), 7.55-7.42 (m, 3H), 7.32 (t, 1H), 7.21 (t, 1H, 7.06 (d, 1H), 3.92 (s, 3H);

<sup>13</sup>C NMR (100 MHz, DMSO-*d*<sub>6</sub>) δ 165.17, 156.25, 152.74, 136.04, 129.99, 128.59, 126.56, 125.19, 122.32, 122.00, 121.55, 121.48, 113.90, 55.75.

**2-(2-Chlorophenyl)benzo[d]thiazole**

<sup>1</sup>H NMR (500MHz, DMSO-*d*<sub>6</sub>) δ 8.04-7.87 (m, 3H), 7.97-7.51(m, 3H), 7.45-7.20 (m, 2H);

<sup>13</sup>C NMR (100 MHz, DMSO-*d*<sub>6</sub>) δ 165.46, 153.31, 135.93, 134.02, 130.26, 130.13, 129.24, 128.63, 126.77, 126.56, 125.20, 122.30, 122.02.

**2-(4-Chlorophenyl)benzo[d]thiazole**

<sup>1</sup>H NMR (500MHz, DMSO-*d*<sub>6</sub>) δ 8.06-7.95 (m, 2H), 7.91 (d, 2H), 7.58-7.42 (m, 4H);

<sup>13</sup>C NMR (100 MHz, DMSO-*d*<sub>6</sub>) δ 166.94, 153.71, 136.45, 135.02, 131.78, 129.25, 128.81, 126.16, 125.23, 122.96, 122.02.

**2-(3-Nitrophenyl)benzo[d]thiazole**

<sup>1</sup>H NMR (500 MHz, DMSO-*d*<sub>6</sub>) δ 8,60 (t, 1H), 8.24 (d, 1H), 8,11-8.04 (m, 3H), 7.65 – 7.59 (m, 1H), 7.58-7.49 (m, 2H);

<sup>13</sup>C NMR (100 MHz, DMSO-*d*<sub>6</sub>) δ 166.35, 153.12, 147.37, 135.42, 132.78, 132.36, 129.54, 126.16, 125.23, 124.45, 123.09, 122.44, 122.24.

**S3. Identification of azobenzenes by NMR spectroscopy****Azobenzene**

<sup>1</sup>H NMR (500 MHz, DMSO-*d*<sub>6</sub>) δ 7.63-7.57 (m, 1H), 7.52-7.45 (m, 1H), 7.45-7.38 (m, 1H);

<sup>13</sup>C NMR (125 MHz, DMSO-*d*<sub>6</sub>) δ 153.03, 129.94, 129.12, 122.06.

**1,2-bis(4-methoxyphenyl)diazene**

<sup>1</sup>H NMR (500 MHz, DMSO-*d*<sub>6</sub>) δ 7.66-7.60 (m, 1H), 7.04-6.98 (m, 1H), 3.76 (s, 6H);

<sup>13</sup>C NMR (100 MHz, DMSO-*d*<sub>6</sub>) δ 160.73, 147.10, 124.02, 114.57, 55.33.

**1-(4-methoxyphenyl)-2-phenyldiazene**

<sup>1</sup>H NMR (500 MHz, DMSO-*d*<sub>6</sub>) δ 7.66-7.57 (m, 4H), 7.52-7.45 (m, 2H), 7.45-7.38 (m, 1H), 7.04 – 6.98 (m, 2H), 3.76 (s, 3H);

<sup>13</sup>C NMR (100 MHz, DMSO-*d*<sub>6</sub>) δ 160.73, 152.32, 147.10, 129.94, 129.12, 124.02, 122.09, 114.57, 55.33.

**1,2-bis(2-methoxyphenyl)diazene**

<sup>1</sup>H NMR (500 MHz, DMSO-*d*<sub>6</sub>) δ 7.73 (dd, 1H), 7.35 (dd, 1H), 7.13 (q, 2H), 3.85 (s, 3H);

<sup>13</sup>C NMR (100 MHz, DMSO-*d*<sub>6</sub>) δ 153.01, 143.50, 128.22, 125.05, 122.30, 114.39, 56.15.

**1-(2-methoxyphenyl)-2-phenyldiazene**

<sup>1</sup>H NMR (500 MHz, DMSO-*d*<sub>6</sub>) δ 7.77 (dd, 1H), 7.63-7.57 (m, 2H), 7.52-7.45 (m, 2H), 7.45-7.38 (m, 1H), 7.33 (t, 1H), 7.14 (t, 1H), 7.10 (dd, 1H), 3.85 (s, 3H);

<sup>13</sup>C NMR (100 MHz, DMSO-*d*<sub>6</sub>) δ 152.92, 151.96, 143.22, 129.94, 129.55, 128.22, 124.08, 122.30, 122.18, 114.39, 56.15.

**1,2-bis(3-nitrophenyl)diazene**

<sup>1</sup>H NMR (500 MHz, DMSO-*d*<sub>6</sub>) δ 8.64 (t, 1H), 8.32-8.26 (m, 1H), 7.81-7.75 (m, 1H), 7.69 (dd, 1H);

<sup>13</sup>C NMR (100 MHz, DMSO-*d*<sub>6</sub>) δ 152.16, 147.25, 129.06, 127.30, 123.00, 116.59.

**1-(3-nitrophenyl)-2-phenyldiazene**

<sup>1</sup>H NMR (500 MHz, DMSO-*d*<sub>6</sub>) δ 8.63 (t, 1H), 8.32-8.26 (m, 1H), 7.80-7.75 (m, 1H), 7.72-7.65 (m, 1H), 7.63-7.57 (m, 2H), 7.52-7.45 (m, 2H), 7.45-7.38 (m, 1H);

<sup>13</sup>C NMR (100 MHz, DMSO-*d*<sub>6</sub>) δ 152.60, 152.13, 147.25, 129.94, 129.12, 129.06, 127.30, 123.00, 122.65, 116.58.

**1,2-bis(4-bromophenyl)diazene**

<sup>1</sup>H NMR (500 MHz, DMSO-*d*<sub>6</sub>) δ 7.73-7.67 (m, 1H), 7.63-7.57 (m, 1H);

<sup>13</sup>C NMR (125 MHz, DMSO-*d*<sub>6</sub>) δ 151.90, 132.06, 123.25, 122.26.

**1-(4-bromophenyl)-2-phenyldiazene**

<sup>1</sup>H NMR (500 MHz, DMSO-*d*<sub>6</sub>) δ 7.73-7.67 (m, 2H), 7.63-7.57 (m, 4H), 7.52-7.45 (m, 2H), 7.45-7.38 (m, 1H);

<sup>13</sup>C NMR (125 MHz, DMSO-*d*<sub>6</sub>) δ 152.32, 151.90, 132.06, 129.94, 129.12, 123.25, 122.26, 122.06.

**1,2-bis(4-chlorophenyl)diazene**

<sup>1</sup>H NMR (500 MHz, DMSO-*d*<sub>6</sub>) δ 7.79-7.73 (m, 1H), 7.50-7.44 (m, 1H);

<sup>13</sup>C NMR (100 MHz, DMSO-*d*<sub>6</sub>) δ 151.15, 133.73, 128.90, 122.63.

**1-(4-chlorophenyl)-2-phenyldiazene**

<sup>1</sup>H NMR (500 MHz, DMSO-*d*<sub>6</sub>) δ 7.79-7.73 (m, 1H), 7.63-7.57 (m, 1H), 7.52-7.38 (m, 2H);

<sup>13</sup>C NMR (100 MHz, DMSO-*d*<sub>6</sub>) δ 152.32, 151.15, 133.73, 129.94, 129.12, 128.90, 122.60, 122.09.

**1,2-di-p-tolyldiazene**

<sup>1</sup>H NMR (500 MHz, DMSO-*d*<sub>6</sub>) δ 7.61-7.55 (m, 1H), 7.28-7.22 (m, 1H), 2.36 (s, 6H);

<sup>13</sup>C NMR (100 MHz, DMSO-*d*<sub>6</sub>) δ 149.94, 138.49, 131.06, 116.25, 21.18.

**1-phenyl-2-(p-tolyl)diazene**

<sup>1</sup>H NMR (500 MHz, DMSO-*d*<sub>6</sub>) δ 7.59 (t, 4H), 7.52-7.45 (m, 2H), 7.45-7.38 (m, 1H), 7.28-7.22 (m, 2H), 2.36 (s, 3H);

<sup>13</sup>C NMR (100 MHz, DMSO-*d*<sub>6</sub>) δ 152.32, 149.94, 138.49, 131.06, 129.94, 129.12, 122.06, 116.25, 21.18.

**4,4'-(diazene-1,2-diyl)dibenzonitrile**

<sup>1</sup>H NMR (500 MHz, DMSO-*d*<sub>6</sub>) δ 7.85-7.76 (m, 1H);

<sup>13</sup>C NMR (100 MHz, DMSO-*d*<sub>6</sub>) δ 155.72, 133.54, 123.23, 118.45, 112.27.

**4-(phenyldiazenyl)benzonitrile**

$^1\text{H}$  NMR (500 MHz, DMSO- $d_6$ )  $\delta$  7.85 – 7.76 (m, 4H), 7.63 – 7.57 (m, 2H), 7.52 – 7.45 (m, 2H), 7.45 – 7.38 (m, 1H);

$^{13}\text{C}$  NMR (100 MHz, DMSO- $d_6$ )  $\delta$  155.72, 152.32, 133.54, 129.94, 129.12, 123.23, 122.09, 118.45, 112.27.

**S4. Identification of quinolines by NMR spectroscopy****Quinoline:**

$^1\text{H}$  NMR (500 MHz, DMSO- $d_6$ )  $\delta$ : 8.90 (dd, 1H), 8.36 (dd, 1H), 8.02-7.99 (d, 1H), 7.98-7.97 (d, 1H), 7.63-7.61 (t, 1H), 7.63, 7.52- 7.49 (m, 2H);

$^{13}\text{C}$  NMR (100 MHz, DMSO- $d_6$ )  $\delta$ : 148.77, 148.05, 131.52, 130.14, 129.36, 128.58, 127.43, 126.15, 121.32.

**8-methoxyquinoline:**

$^1\text{H}$  NMR (500 MHz, DMSO- $d_6$ )  $\delta$  8.83 (dd, 2H), 8.29 (dd, 2H), 7.97 – 7.91 (m, 2H), 7.51 (dd, 2H), 7.32 (t, 2H), 7.18 (dd, 2H), 3.83 (s, 3H);

$^{13}\text{C}$  NMR (100 MHz, DMSO- $d_6$ )  $\delta$  154.53, 148.72, 139.39, 130.00, 129.75, 128.73, 126.29, 122.48, 113.75, 55.69.

**6-methoxyquinoline:**

$^1\text{H}$  NMR (500 MHz, DMSO- $d_6$ )  $\delta$  8.73 (dd, 2H), 8.24 (d, 2H), 7.91 (d, 2H), 7.51 – 7.43 (m, 2H), 7.38 (t, 2H), 7.11 (dd, 2H), 3.79 (s, 3H);

$^{13}\text{C}$  NMR (100 MHz, DMSO- $d_6$ )  $\delta$  157.52, 148.24, 143.70, 130.13, 129.96, 128.26, 122.15, 115.12, 105.51, 55.28.

**7-nitroquinoline:**

$^1\text{H}$  NMR (500 MHz, DMSO- $d_6$ )  $\delta$  8.87 (d, 1H), 8.61 (dd, 1H), 8.20 (dd, 1H), 8.16 – 8.07 (m, 2H), 7.51 (dd, 1H);

$^{13}\text{C}$  NMR (100 MHz, DMSO- $d_6$ )  $\delta$  151.01, 148.14, 148.05, 131.61, 128.54, 127.26, 124.39, 122.52, 120.70.

**6-chloroquinoline:**

$^1\text{H}$  NMR (500 MHz, DMSO- $d_6$ )  $\delta$  8.93 (dd, 1H), 8.36 (d, 1H), 8.04 (d, 1H), 7.78 (dd, 1H), 7.63 – 7.7.56 (m, 2H);

$^{13}\text{C}$  NMR (100 MHz, DMSO- $d_6$ )  $\delta$  147.83, 146.61, 131.83, 129.90, 129.72, 129.42, 126.34, 123.91, 121.68.

**8-methylquinoline:**

$^1\text{H}$  NMR (500 MHz, DMSO- $d_6$ )  $\delta$  8.93 (dd, 1H), 8.33 (dd, 1H), 7.80 (d, 1H), 7.63 (dd, 2H), 7.50 (t, 1H), 2.73 (s, 3H);

$^{13}\text{C}$  NMR (100 MHz, DMSO- $d_6$ )  $\delta$  148.24, 147.03, 132.78, 130.63, 130.30, 129.90, 128.42, 125.74, 121.07, 17.02.

**6-methylquinoline:**

$^1\text{H}$  NMR (500 MHz, DMSO- $d_6$ )  $\delta$  8.82 (dd, 1H), 8.23 (dt, 1H), 7.94 (d, 1H), 7.73 (t, 1H), 7.50 – 7.43 (m, 2H), 2.47 (s, 3H);

$^{13}\text{C}$  NMR (100 MHz, DMSO- $d_6$ )  $\delta$  149.29, 147.07, 135.26, 130.63, 130.03, 128.52, 128.05, 127.97, 121.11, 21.55.

## S5. Identification of quinoxalines by NMR spectroscopy

### Quinoxaline:

$^1\text{H}$  NMR (500 MHz,  $\text{DMSO}-d_6$ )  $\delta$ : 8.96 (s, 2H), 8.11-8.10 (dd, 2H), 7.88-7.86 (dd, 2H);

$^{13}\text{C}$  NMR (100 MHz,  $\text{DMSO}-d_6$ )  $\delta$ : 145.55, 144.04, 130.05, 127.01.

### 6-bromoquinoxaline:

$^1\text{H}$  NMR (500 MHz,  $\text{DMSO}-d_6$ )  $\delta$  8.98 (d, 1H), 8.34 (d, 1H), 8.20 (d, 1H), 8.06-8.04, (m 1H), 8.00 (dd, 1H);

$^{13}\text{C}$  NMR (100 MHz,  $\text{DMSO}-d_6$ )  $\delta$  145.88, 145.33, 142.40, 141.34, 133.71, 129.10, 128.66, 122.32.

### 6-chloroquinoxaline:

$^1\text{H}$  NMR (500 MHz,  $\text{DMSO}-d_6$ )  $\delta$  8.98 (d, 1H), 8.20 (d, 1H), 7.92 (m, 2H), 6.9 (d, 1H);

$^{13}\text{C}$  NMR (100 MHz,  $\text{DMSO}-d_6$ )  $\delta$ : 145.52, 144.95, 143.61, 142.30, 134.30, 130.36, 130.32, 125.51.

### 6-nitroquinoxaline:

$^1\text{H}$  NMR (500 MHz,  $\text{DMSO}-d_6$ )  $\delta$  9.16 (d, 1H), 8.97, (d, 1H), 8.93 (d, 1H), 8.42-8.27 (m, 2H);

$^{13}\text{C}$  NMR (100 MHz,  $\text{DMSO}-d_6$ )  $\delta$ : 147.50, 147.08, 146.90, 144.71, 142.41, 130.89, 123.85, 123.79.

### quinoxaline-6-carboxylic acid:

$^1\text{H}$  NMR (500 MHz,  $\text{DMSO}-d_6$ )  $\delta$ : 9.34 (d, 1H), 8.88 (d, 1H), 8.38 (m, 1H), 8.18-8.12 (m, 2H);

$^{13}\text{C}$  NMR (100 MHz,  $\text{DMSO}-d_6$ )  $\delta$ : 167.26, 146.12, 145.33, 145.05, 140.72, 131.47, 128.28, 127.18, 124.81.

### 6-methylquinoxaline:

$^1\text{H}$  NMR (500 MHz,  $\text{DMSO}-d_6$ )  $\delta$  9.00 (d, 1H), 8.87 (d, 1H), 7.97 (d, 1H), 7.87 (d, 1H), 7.71 (d, 1H), 2.56. (s, 3H);

$^{13}\text{C}$  NMR (100 MHz,  $\text{DMSO}-d_6$ )  $\delta$ : 144.75, 144.08, 142.32, 141.92, 138.45, 130.48, 127.68, 126.70, 21.05.